NASA's Space Lidar Measurements of the Earth and Planets

"A brief overview"

James B. Abshire

NASA - Goddard Space Flight Center
Solar System Exploration Division
Greenbelt MD 20771 USA

Presentation to:
IEEE Photonics Society Meeting
University of Maryland

April 5, 2011

Acknowledgements:

Instrument and Science Teams of:

MOLA, ICESat/GLAS, Calipso, MLA, LOLA, LIST SDT

James.Abshire@gsfc.nasa.gov

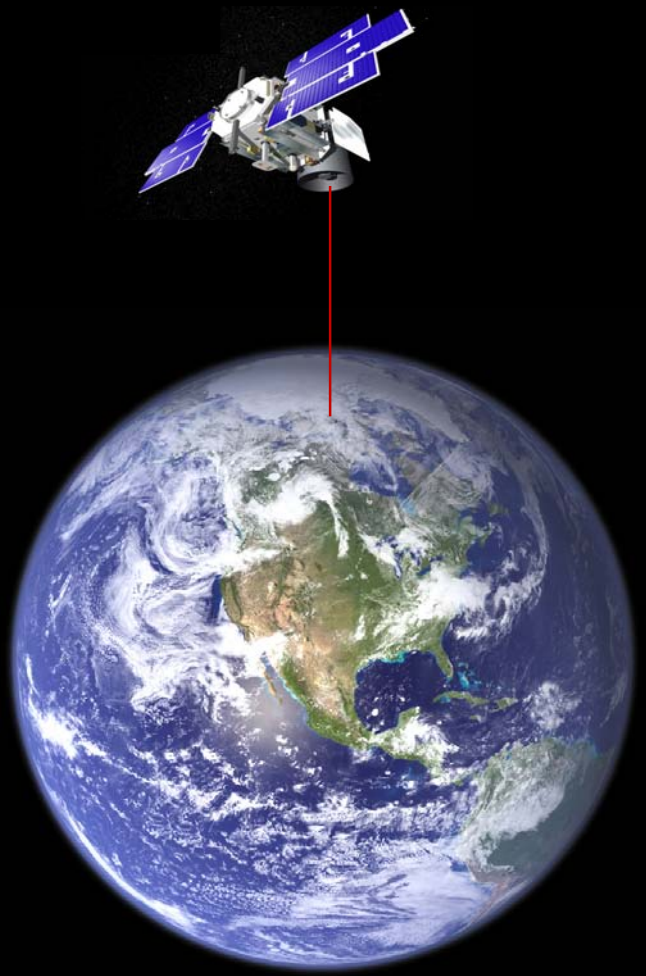

Outline:

- Early space lidar
- Start of Diode pumped laser era:
  - MOLA & SLA
- Recent space lidar missions:
  - Example measurements of:
  - Ice sheets, ice processes, trees
  - The moon, Mercury
- Applications for the future
  - Imaging lidar
  - Greenhouse gas measurements
- Summary

The vertical dimensio

The Geoscience Laser Altimeter System – 200

Aerosol and Cloud Laser Measurements from Spac

J. Spinhirne/ NASA GSFC

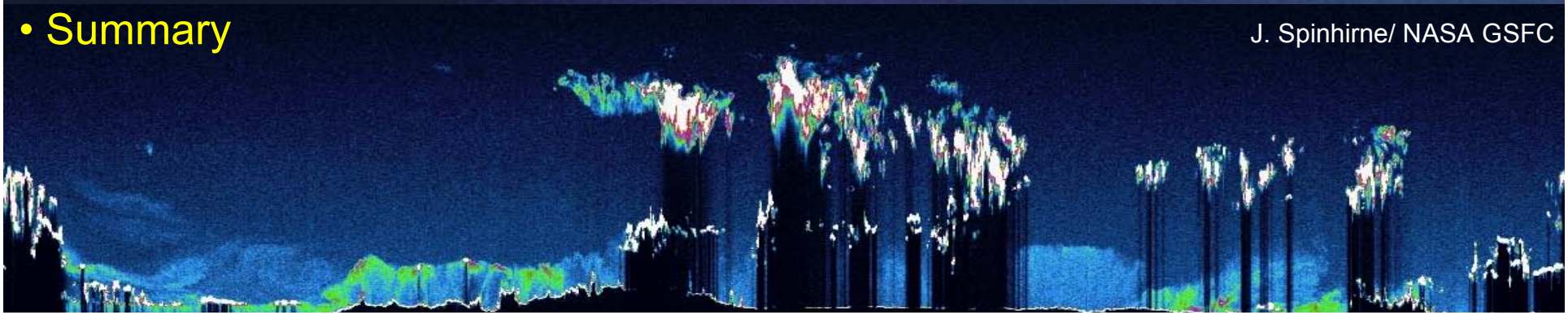

Ground-based Satellite Laser Ranging (SLR): NASA- Goddard, October, 1964

SATELLITE LASER RANGING - 1964

Code 524 SLR Team
Dr. Henry Plotkin
Tom Johnson
Paul Spadin
John Moye
Walt Carrion
Nelson McAvoy
Howard Genatt
Louis Caudill
John Degnan
Ed Reid
Charles Peruso

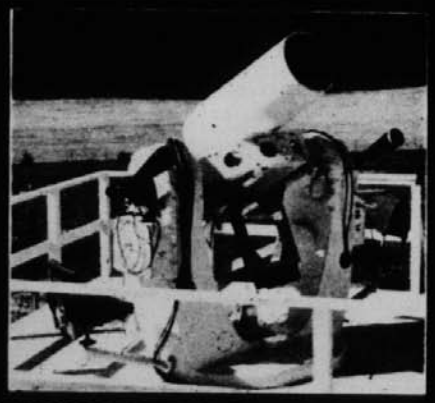

TRANSMITTING LASER AND RECEIVING TELESCOPE, MOUNTED ON A MODIFIED NIKE-AJAX RADAR PEDESTAL.

GODdard LASer (GODLAS)

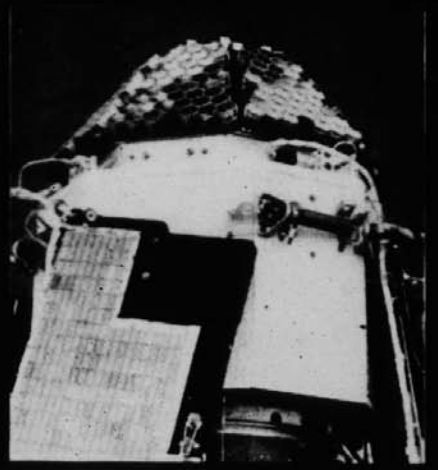

THE BEACON EXPLORER-B SATELLITE WITH ARRAY OF CUBE-CORNER REFLECTORS.

BE-B: first satellite with retro-reflectors

First Lidar in Space (1971) Apollo Laser Altimeters (Lunar orbit)

GSFC

AS15-88-11966

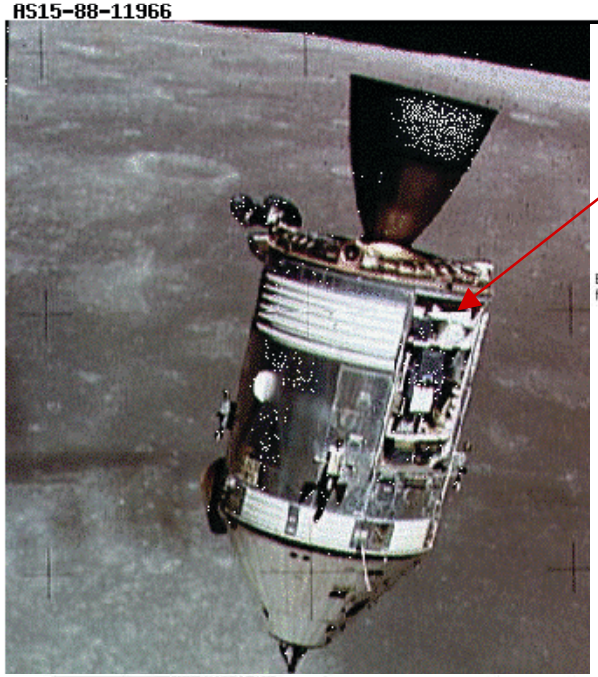

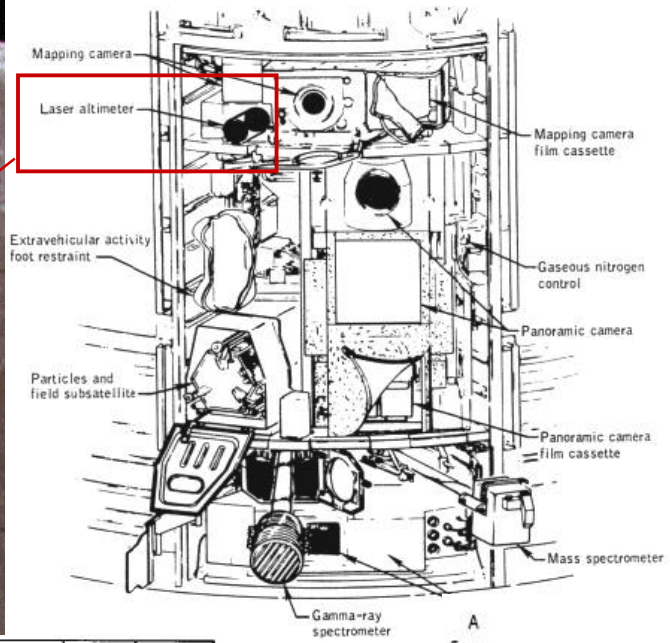

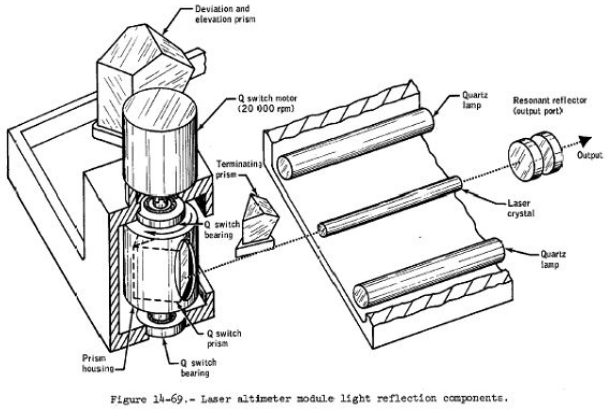

Figure 14-69.- Laser altimeter module light reflection components.

RCA Aerospace built <u>flash lamp pumped, mechanically Q-switched</u> ruby lasers for Apollos 15, 16 & 17

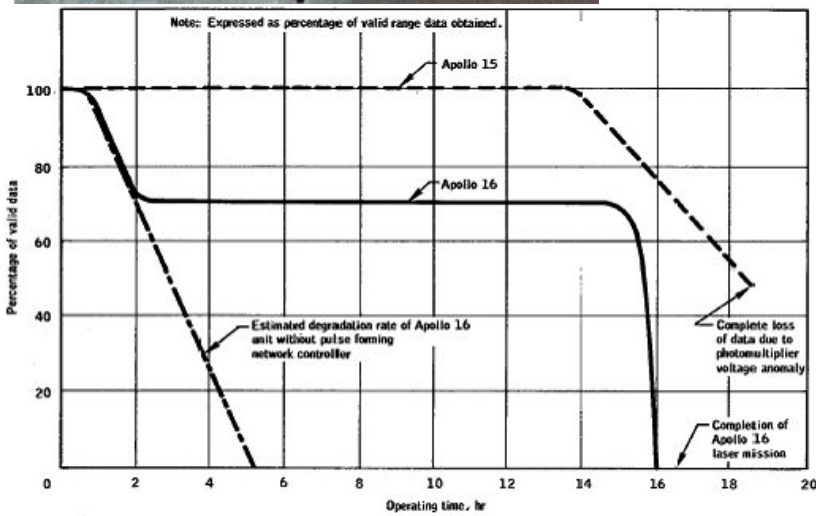

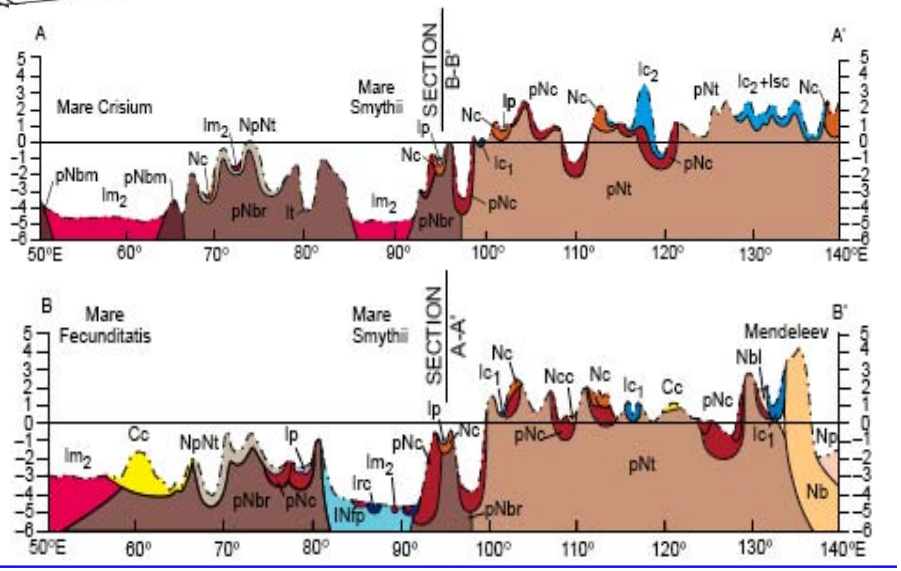

First Space Lidar: Apollo Laser Altimeter (1971)

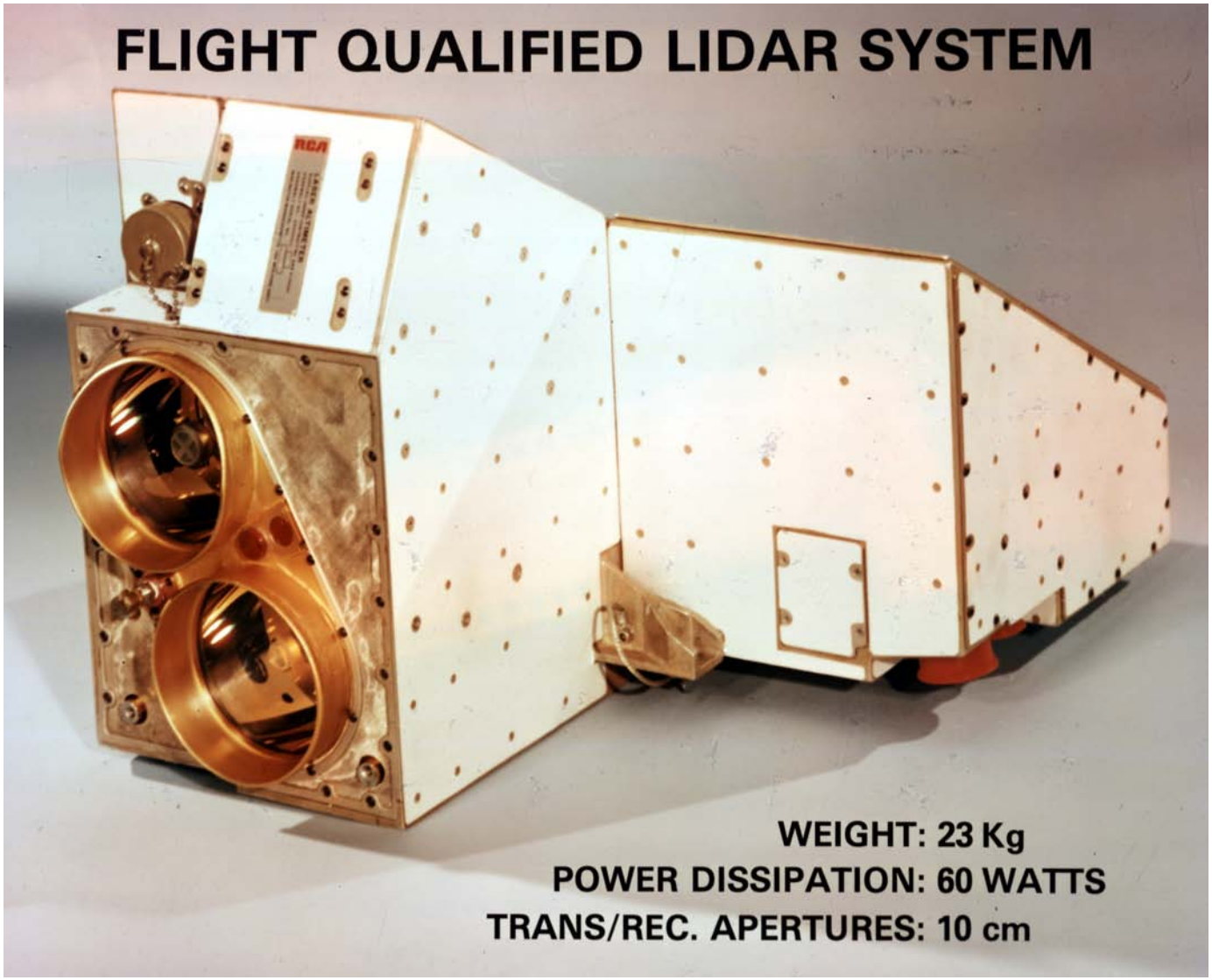

Laser transmitter:

- Mechanically Q- switched ruby laser
- Flashlamp pumped
- Based on mil-qualified rangefinder for tank
- 0.05 Hz laser firing rate
- RCA Astronautics
- Flown on Apollo 15-17

LITE Experiment on Space Shuttle (1994, LaRC)
Earth Orbit

An Overview of LITE: NASA's Lidar In-space Technology Experiment

DAVID M. WINKER, RICHARD H. COUCH, AND M. PATRICK McCORMICK

The Lidar In-space Technology Experiment (LITE) is a three-wavelength backscatter lidar developed by NASA Langley Research Center to fly on the Space Shuttle. LITE flew on Discovery in September 1994 as part of the STS-64 mission. The goals of the LITE mission were to validate key lidar technologies for spaceborne applications, to explore the applications of space lidar, and to gain operational experience which will benefit the development of future systems on free-flying satellite platforms. The performance of the LITE instrument was excellent, resulting in the collection of over 40 GBytes of data. These data present us with our first highly detailed global view of the vertical structure of cloud and aerosol from the Earth's surface through the middle stratosphere. This paper will discuss the LITE instrument, the LITE mission, and briefly present some results from the experiment. These preliminary results highlight the benefits to be obtained from long duration satellite lidars.

Table 1 LITE Science Steering Group Members

Dr. M. P. McCormick	NASA Langley Research Center
Dr. D. M. Winker	NASA Langley Research Center
Dr. E. V. Browell	NASA Langley Research Center
Dr. J. A. Coakley	Oregon State University
Dr. C. S. Gardner	University of Illinois
Dr. R. M. Hoff	AES (Canada)
Dr. G. S. Kent	Science and Technology Corp.
Dr. S. H. Melfi	University of Maryland
Dr. R. T. Menzies	Jet Propulsion Laboratory
Dr. C. M. R. Platt	CSIRO (Australia)
Dr. D. A. Randall	Colorado State University
Dr. J. A. Reagan	University of Arizona

I. Introduction

Since the launch of TIROS-1 in 1960, most of the satellite instruments placed into orbit for study of the Earth's atmosphere and surface have been passive imagers and sounders operating in the visible, infrared, and microwave spectral regions. Technology developments over the last three decades have allowed the capabilities of the current generation of passive satellites to advance far beyond those of that first instrument. The first *active* orbital sensors used for Earth science were radar systems flown on Skylab in the early 1970's. Radar technology has also steadily improved since then, resulting in today's imaging radars and scatterometers flown on operational platforms such as ERS-2 and Radarsat.

Notwithstanding the many advances made over the years in active microwave sensors and various passive remote interest in radiation studies. The small footprint of a lidar avoids most of the beamfilling problems faced by both passive and active microwave instruments.

NASA Langley Research Center has developed a number of ground-based and airborne lidar systems over the last 25 years for the study of clouds, aerosols, water vapor, and ozone. Several studies were performed in the 1970's and early 1980's showing the benefits to atmospheric studies of operational orbital lidar systems. The development of such operational systems first requires the validation of key enabling technologies. Toward this end, LITE was initiated in 1985 to demonstrate operation of a lidar in space and the maturity of lidar technology. It was decided the most convincing demonstration was within the context of actual atmospheric investigations and toward this end a LITE Science Steering Group (Table 1) was formed in 1988 to develop instrument performance requirements, guide the development of the LITE experiment plan, and utilize the

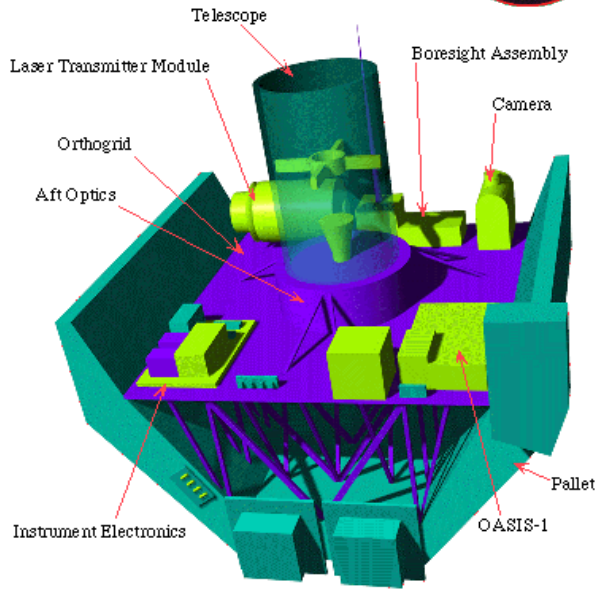

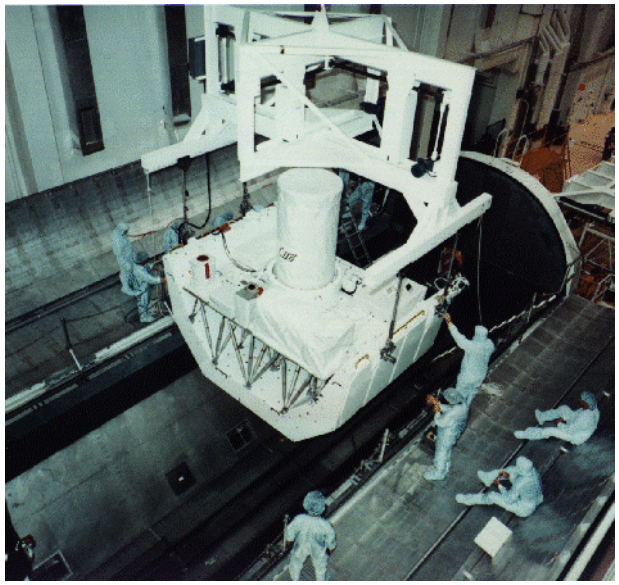

- The LITE instrument was flown aboard Space Shuttle Discovery on mission STS-64 in September 1994.
- Three measurement wavelengths: 355, 532, and 1064 nm.
- During its 11-day operation LITE accumulated 53 h of 10-sec averaged backscatter profiles within a few degrees of nadir
- **First lidar profiles of the Earth's atmosphere from space !**

LITE Laser & measurement example

Flashlamp-pumped
Water-cooled
Pressurized canister

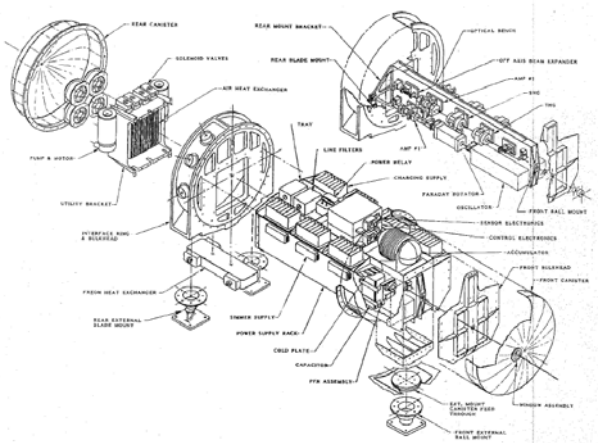

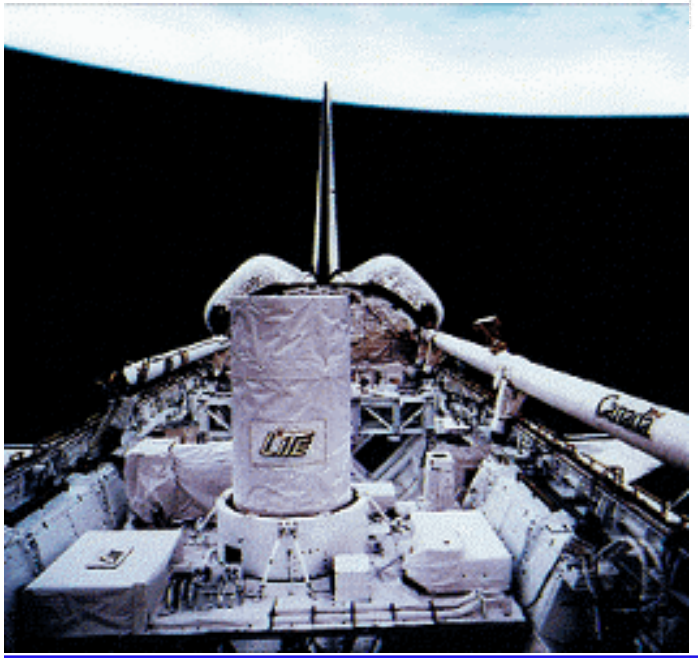

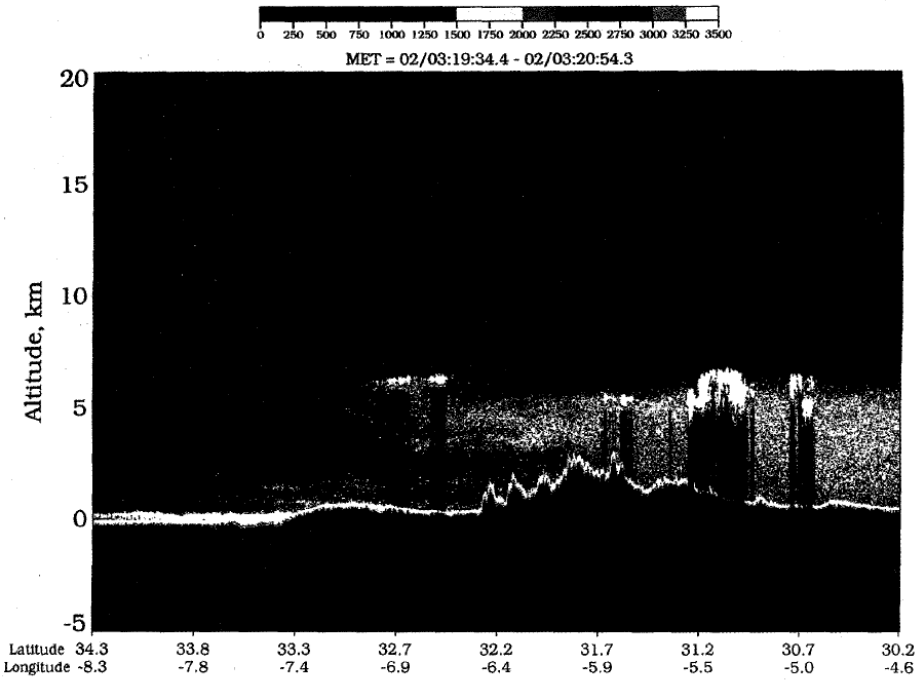

Fig. 13. Offset-subtracted LITE return signal at 532 nm showing aerosol structure in the vicinity of the Atlas Mountains and the Atlantic coast of Morocco.

Mars Orbiter Laser Altimeter (1996, GSFC)

(initially on Mars Observer Mission, launched Sept., 1992)

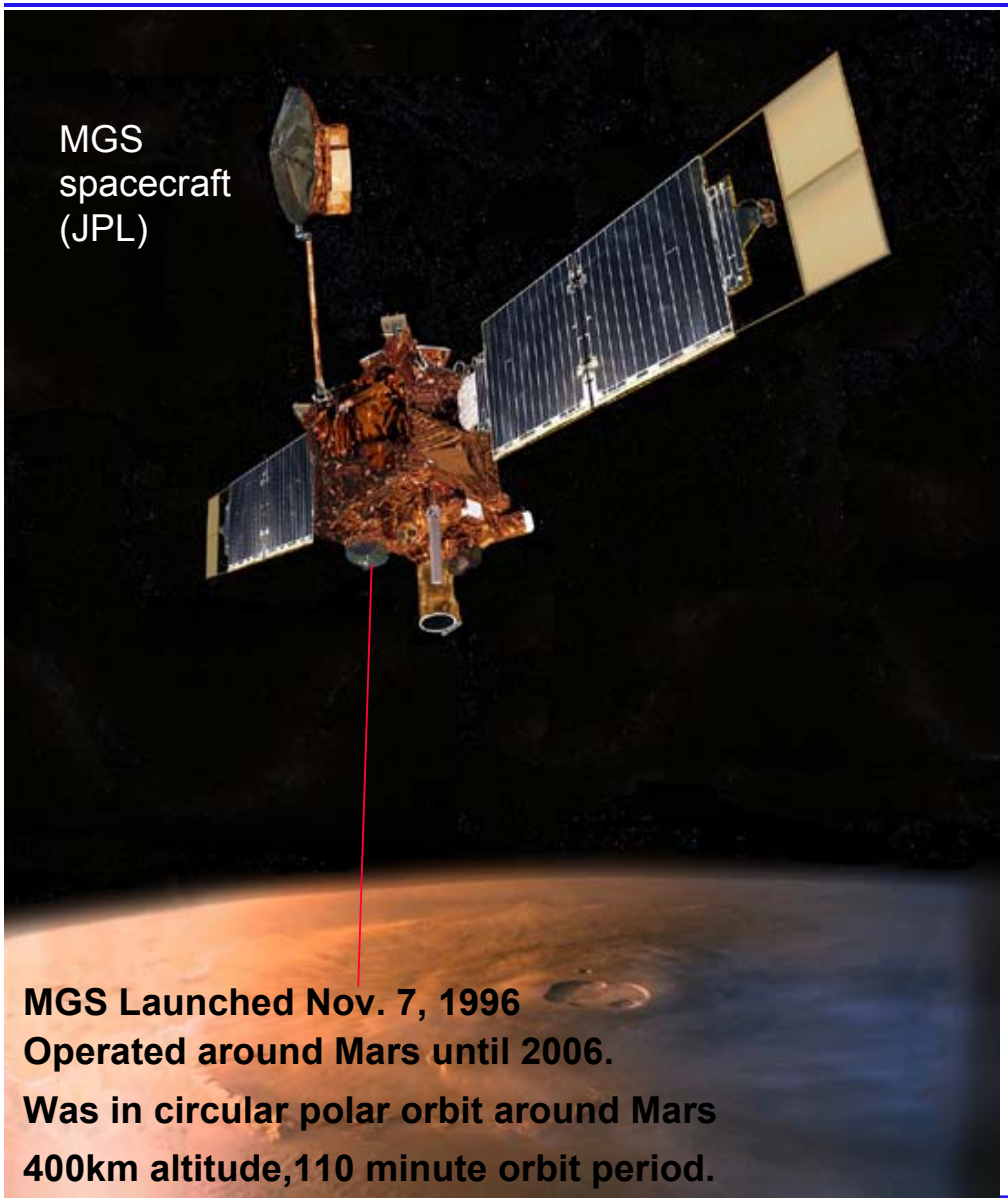

- Radial orbit quality depends on gravity field, atmospheric drag, solar radiation pressure, spacecraft maneuvers.
- Range accuracy depends on pulse timing resolution, surface roughness, off-nadir angle, atmospheric refraction.
- MOLA measured pulse spreading and echo pulse energy; permit estimates of pulse spreading, surface reflectivity and atmospheric extinction

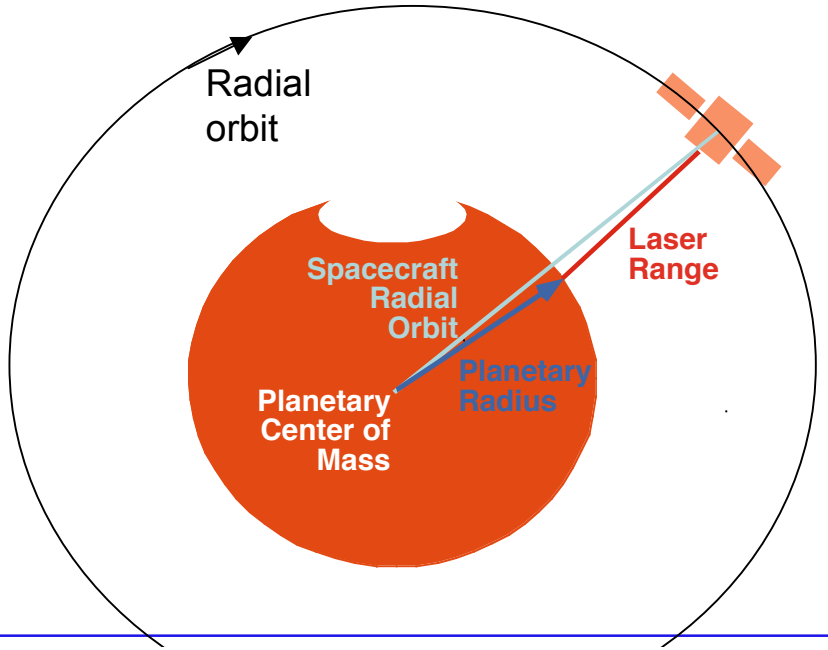

Mars Observer Laser Altimeter (MOLA)

Laser Transmitter:

McDonnell Douglas Electronics Systems Division

Q-switched **Diode-Pumped ND:YAG laser**

"Power oscillator" (single stage, zig-zag slab)

Based on airborne target designator design

10 Hz, 40 mJ/pulse, 8 nsec pulse width

400 urad, multimode spatial pattern

In-vacuum operation

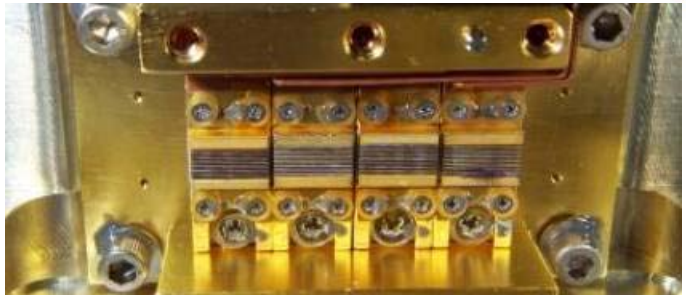

Laser's AlGaAs laser diode pump arrays:

- ~x5 improved laser efficiency (no water cooling)
- ~x100 to x200 improved lifetime

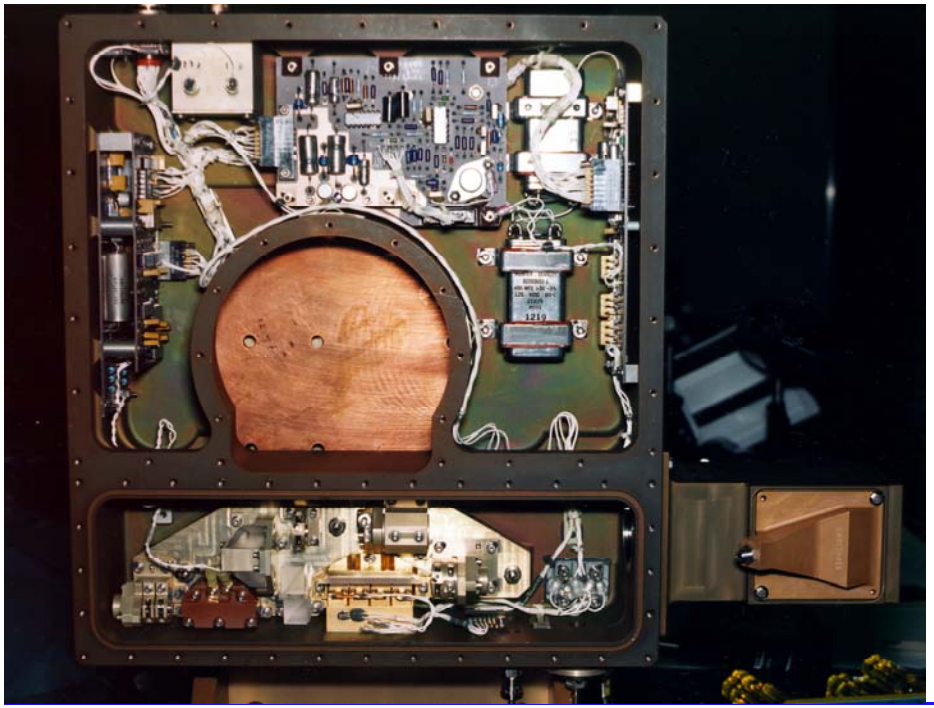

Telescope:

Space FTIR spectrometer (Voyager IRIS)

Detector:

Si Avalanche Photodiode

Perkin Elmer Opto-electronics (then RCA)

Analog Detection

QE~30%, Gain ~150

Min detect. signal ~230 photons

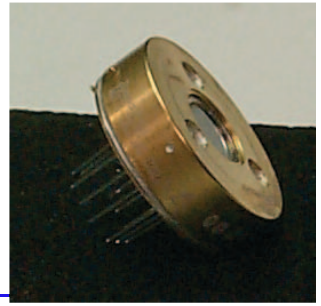

MOLA Instrument & Mapping Parameters

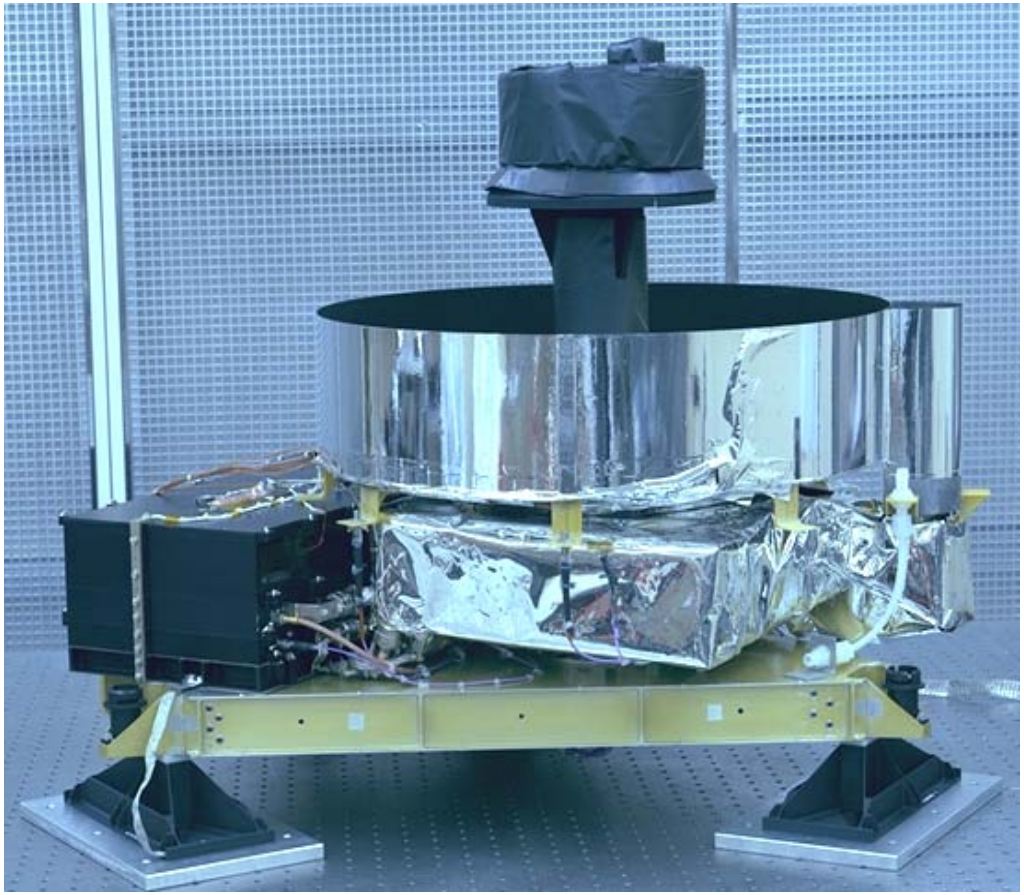

- Laser Wavelength: 1064 ± 0.2 nm
- Laser Pulsewidth: 8 nsec
- Pulse energy (start of mapping): 48 mJ
- Pulse repetition frequency: 10 Hz
- Range resolution: 38 cm
- Return pulses detected: ~99%
- Maximum range (hardware limit): 786 km
- Surface spot size in mapping orbit: ~168 m
- Along-track shot spacing: ~330 m
- Vertical accuracy (radial orbit error): <1 m
- Number of laser firings: 671,121,600
- Operated in lidar & radiometer modes

David Smith, NASA Goddard, PI; Maria Zuber, Deputy PI

MOLA Measurements

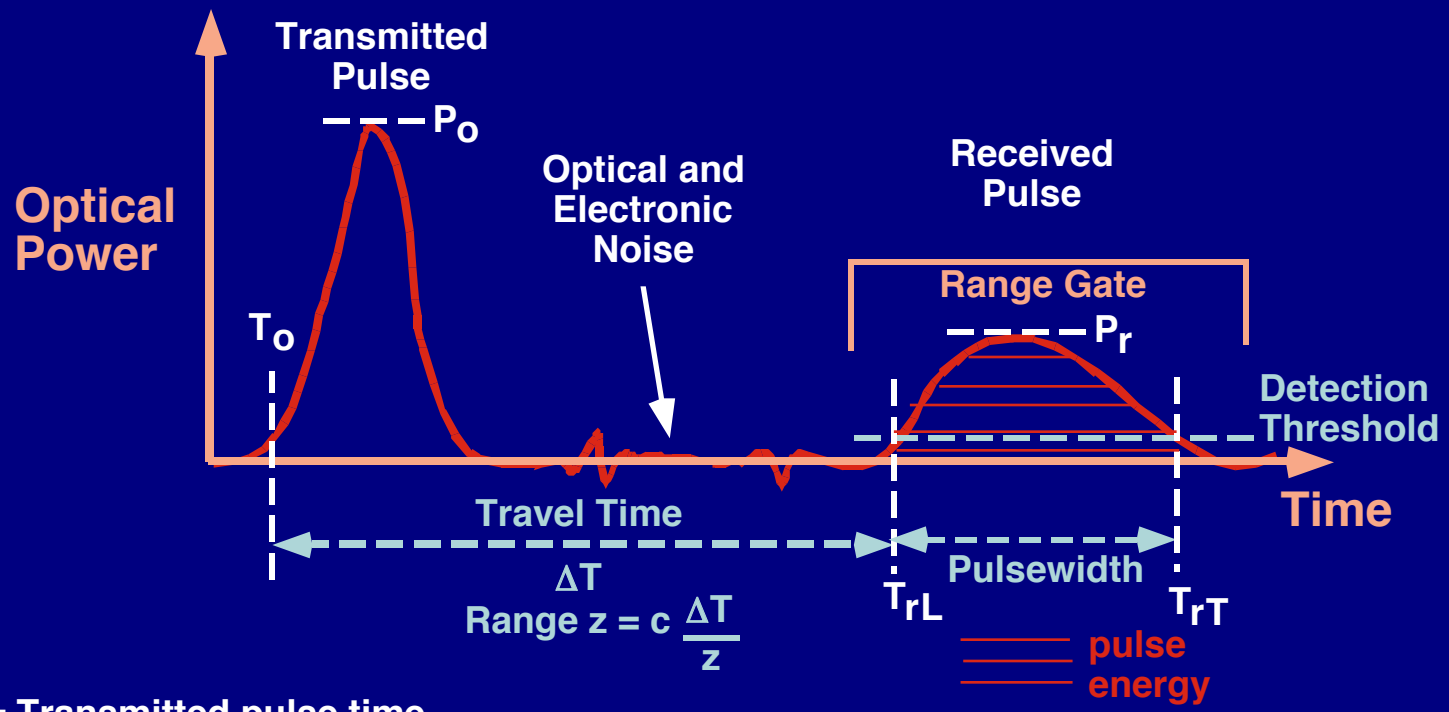

T_o = Transmitted pulse time
P_o = Transmitted pulse power
T_{rL} = Leading edge received pulse time
T_{rT} = Trailing edge received pulse time
P_r = Received pulse power

Range -> Elevation
Pulsewidth -> Surface roughness
Received/Transmitted Pulse Energy ->Surface reflectivity

Olympus Mons Aureole from MOLA

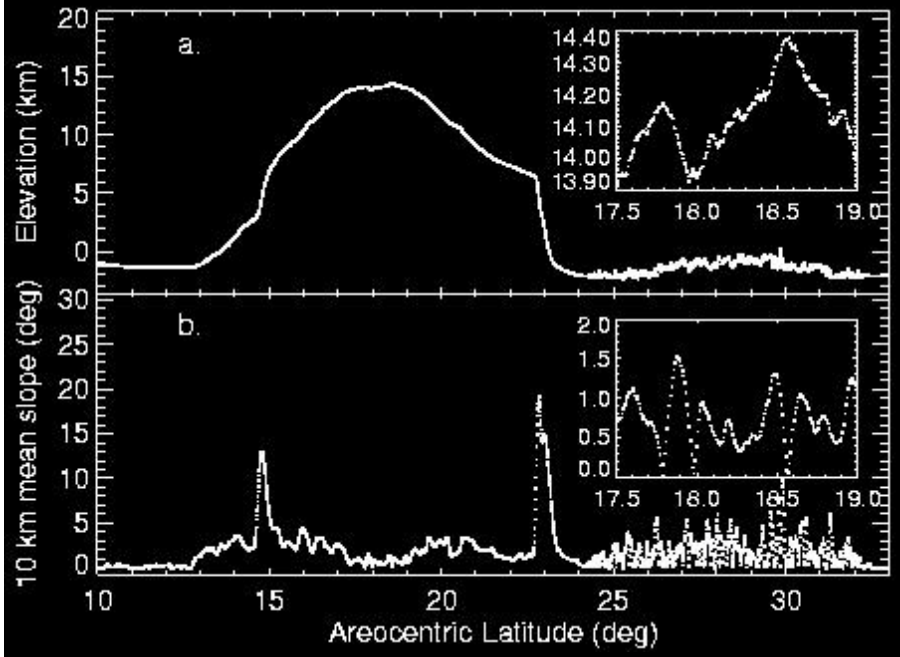

Aharonson et al. [1998]

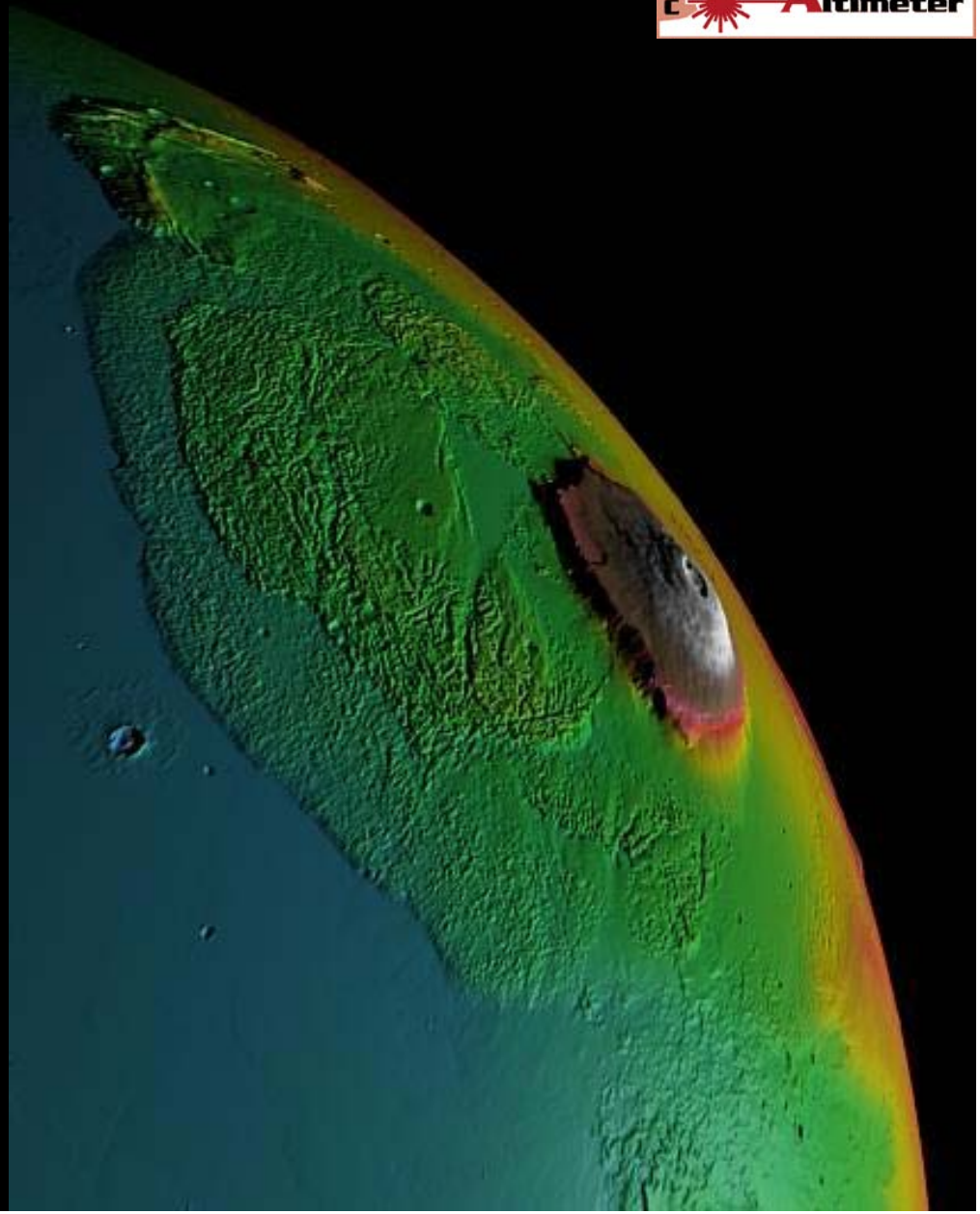

NASA GSFC Mars Orbiter Laser Altimeter

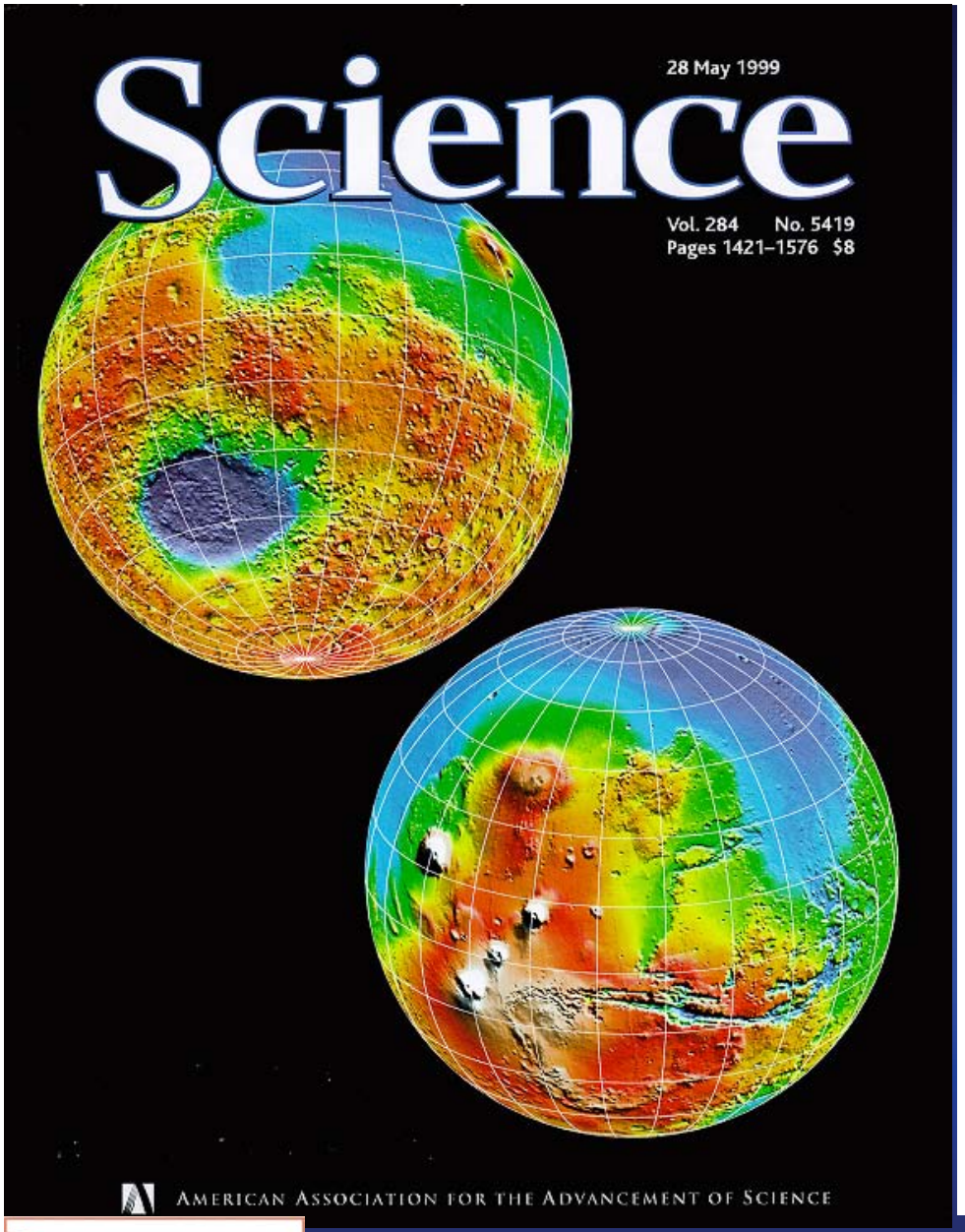

RESEARCH ARTICLE

Observations of the North Polar Region of Mars from the Mars Orbiter Laser Altimeter

Maria T. Zuber*, David E. Smith, Sean C. Solomon, James B. Abshire, Robert S. Afzal, Oded Aharonson, Kathryn Fishbaugh, Peter G. Ford, Herbert V. Frey, James B. Garvin, James W. Head, Anton B. Ivanov, Catherine L. Johnson, Duane O. Muhleman, Gregory A. Neumann, Gordon H. Pettengill, Roger J. Phillips, Xiaoli Sun, H. Jay Zwally, W. Bruce Banerdt, Thomas C. Duxbury

Elevations from the Mars Orbiter Laser Altimeter (MOLA) have been used to construct a precise topographic map of the martian north polar region. The northern ice cap has a maximum elevation of 3 kilometers above its surroundings but lies within a 5-kilometer-deep hemispheric depression that is contiguous with the area into which most outflow channels emptied. Polar cap topography displays evidence of modification by ablation, flow, and wind and is consistent with a primarily H_2O composition. Correlation of topography with images suggests that the cap was more spatially extensive in the past. The cap volume of 1.2×10^6 to 1.7×10^6 cubic kilometers is about half that of the Greenland ice cap. Clouds observed over the polar cap are likely composed of CO_2 that condensed out of the atmosphere during northern hemisphere winter. Many clouds exhibit dynamical structure likely caused by the interaction of propagating wave fronts with surface topography.

The north polar ice cap of Mars is one of the largest present-day reservoirs of volatiles on that planet and preserves the record of seasonal cycles of carbon dioxide and dust (*1–4*). Measurements of polar cap topography furnish critical constraints on volatile abundance and composition and provide a quantitative basis for studying surface-atmosphere interactions relevant to present and past hydrological cycles. Since arrival at Mars on 12 September 1997, the Mars Orbiter laser altimeter (MOLA) (*5, 6*), an instrument on the Mars Global Surveyor (MGS) spacecraft (*7*), has collected ~2.6 million measurements of topography and cloud heights in the northern hemisphere of Mars (*8*). These observations afford a new view of martian polar processes that has broad implications for the planet's seasonal and climatic evolution.

MOLA coverage (Fig. 1) includes profiles across Mars's northern hemisphere collected during three spacecraft orbital phases (*9*): the aerobraking hiatus orbit (AHO; 18 profiles) and science phasing orbits (SPO) before and after Mars solar conjunction in May 1997 (SPO-1 and 2; 61 and 127 profiles). The MOLA instrument operates with maximum signal/noise ratio and minimum range error when oriented at a 0° incidence angle with respect to the martian surface. However, when ranging in this nadir-oriented configuration, the inclination of the MGS orbit (~93.7°) resulted in an ~450-km-diameter gap in coverage, centered on the pole. In order to obtain measurements of topography at latitudes above 86.3°N, the MGS spacecraft was pointed ~50° off-nadir on alternate passes during 2 weeks in June and July 1998. Ten profiles were collected in this mode, which enabled the maximum height of the ice cap to be measured.

Several major geologic units are located in the high-latitude northern hemisphere of Mars (Fig. 1A). Polar deposits consist of layered terrain and residual ice (Apl and Api); the residual ice constitutes the perennial ice deposits, which are distinguished from seasonal frosts. Circumpolar deposits consist of a variety of types of mantled plains (Hv), outliers of residual ice that may mark the former extent of polar ice (Api), and a range of surface dune deposits (Adl and Adc).

Previous regional topographic measurements of the martian north polar cap were based on stereo imaging and three Mariner 9 radio occultation measurements (*10, 11*). These results suggested that the northern cap rose 4 to 6 km above the surroundings and had two maxima in elevation located at approximately 88°N, 120°E and 83°N, 10°E. The MOLA observations have much higher spatial sampling and provide an increase in vertical accuracy of ~2 orders of magnitude over previous measurements. The new observations reveal a different topographic expression of the ice cap and surroundings.

Regional setting and the hydrological cycle. As shown in a 2-km grid (Fig. 1B) of northern hemisphere topography (*12*), the elevation of the north polar cap increases progressively toward the pole from its southern limit at ~80°N. The highest point of the polar cap is within a few kilometers of the rotation pole and has an elevation of –1950 ± 50 m with respect to the average elevation of the equator (*13*). The terrain that surrounds the ice cap lies between –4800 and –5200 m, leading to a cap relief of approximately 2950 ± 200 m. The root-mean-square misfit of elevations of the 10 profiles that cross the north pole is 28 m.

The martian surface outside the ice cap slopes gently downward toward the pole at all longitudes in the northern hemisphere (for example, Fig. 2) and most steeply in the vicinity of the Tharsis rise. Thus, except within the bounds of the 1500-km-diameter circular depression centered at 45°N, 110°E in Utopia Planitia (*14*), any liquid water will flow to high northern latitudes. Most previous studies have assumed that transport of water between the polar caps and crust occurs almost solely by insolation-driven exchange between the surface and the atmosphere (*15, 16*). However, the topography in Fig. 2 suggests that water could potentially have flowed overland or beneath the surface to the martian north pole.

Clifford (*17*) proposed that a global-scale sub-permafrost groundwater system may have facilitated transport of H_2O from the north pole to the equator on Mars. In this model, basal melting of the polar cap due to pressure loading and the local thermal gradient produces a downward percolation of groundwater into a global aquifer. For reasonable values of crustal permeability and for the assumed elevation based on earlier data, the hydrostatic head associated with the groundwater beneath the cap could have driven 10^8 km^3 of groundwater to the equator over martian history, a volume that would represent an important contribution to the

M. T. Zuber, O. Aharonson, G. A. Neumann, and G. H. Pettengill are in the Department of Earth, Atmospheric, and Planetary Sciences, Massachusetts Institute of Technology, Cambridge, MA 02139, USA. D. E. Smith, J. B. Abshire, R. S. Afzal, J. B. Garvin, H. V. Frey, G. A. Neumann, X. Sun, M. T. Zuber, and H. J. Zwally are at the Earth Sciences Directorate, NASA/Goddard Space Flight Center, Greenbelt, MD 20771, USA. P. G. Ford is at the Center for Space Research, Massachusetts Institute of Technology, Cambridge, MA 02139, USA. K. Fishbaugh and J. W. Head are in the Department of Geological Sciences, Brown University, Providence, RI 02912, USA. A. B. Ivanov and D. O. Muhleman are at the California Institute of Technology, Pasadena, CA 91125, USA. R. J. Phillips is in the Department of Earth and Planetary Sciences, Washington University, St. Louis, MO 63130, USA. C. L. Johnson and S. C. Solomon are in the Department of Terrestrial Magnetism, Carnegie Institution of Washington, Washington D.C. 20015, USA. W. B. Banerdt and T. C. Duxbury are at the Jet Propulsion Laboratory, Pasadena, CA 91109.

*To whom correspondence should be addressed: zuber@tharsis.gsfc.nasa.gov

NASA GSFC Mars Orbiter Laser Altimeter

- MOLA was first multi-year space lidar investigation
- > 666 million measurements during the Mars Global Surveyor mission
- Hundreds of papers published on the results

NEAR Laser Rangefinder (1998, JHU/APL)
(Asteroid 433 Eros)

GSFC

NEAR Laser Rangefinder

The NEAR Laser Rangefinder (NLR) is an altimeter that uses a solid-state pulsed laser to measure distance between the spacecraft and the surface of the asteroid 433 Eros. It is one of the five facility instruments onboard the NEAR spacecraft and will make highly accurate measurements of the asteroid's shape and detailed surface structure. The Laser Rangefinder is a diode-pumped neodymium–yttrium–aluminum–garnet (Nd-YAG) laser built by the McDonnell-Douglas Corporation. The receiver, built by the Johns Hopkins Applied Physics Laboratory, uses a compact reflecting telescope with baffle/door assembly, an enhanced hybrid silicon avalanche photodiode detector, a rad-hardened microprocessor controller

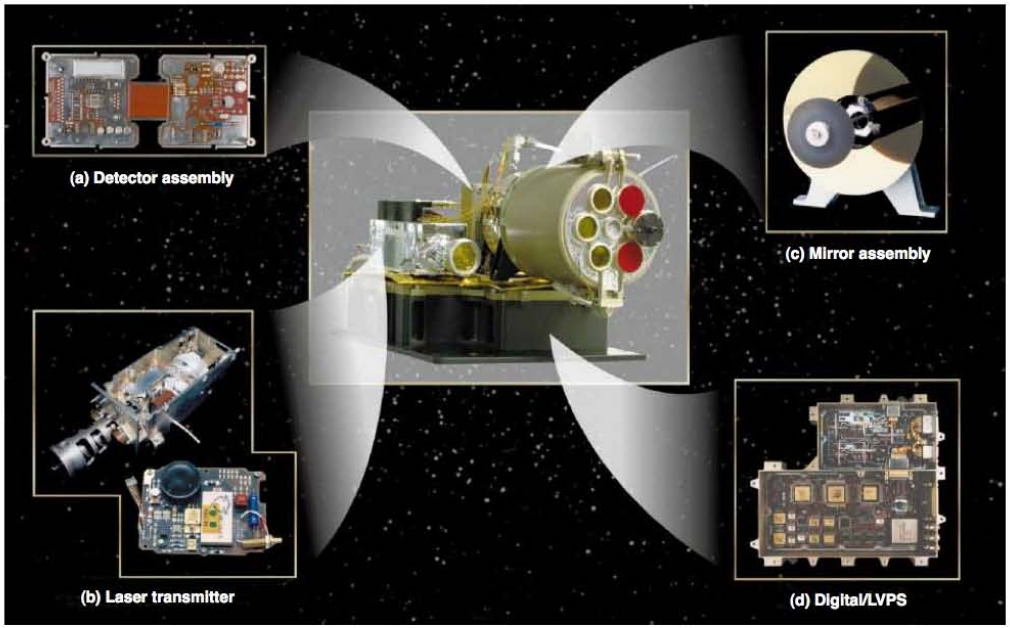

Figure 3. The integrated NLR instrument showing key subsystems. (a) The detector assembly uses an enhanced avalanche photodiode hybrid mounted at the receiver focal plane (the detector is on the opposite side as shown). (b) The laser resonator and associated laser power supply are based on previous designs. (c) Receiver optics (mirror assembly) consist of an all-reflective, lightweight Dall–Kirkham telescope made of aluminum (athermal design). (d) Receiver electronics are shown mounted in the NLR chassis; both the digital processing unit and the low-voltage power supply (LVPS) are shown. The calibration unit, a 109.5-m length of spooled optical fiber, is shown on top of the transmitter in the center photograph (black cylinder). Not shown is the avalanche photodiode power supply (+550 V DC) and the laser power supply; both were remotely located to minimize interference with the sensitive receiver electronics.

NEAR Laser Rangefinder: A Tool for the Mapping and Topologic Study of Asteroid 433 Eros

Timothy D. Cole

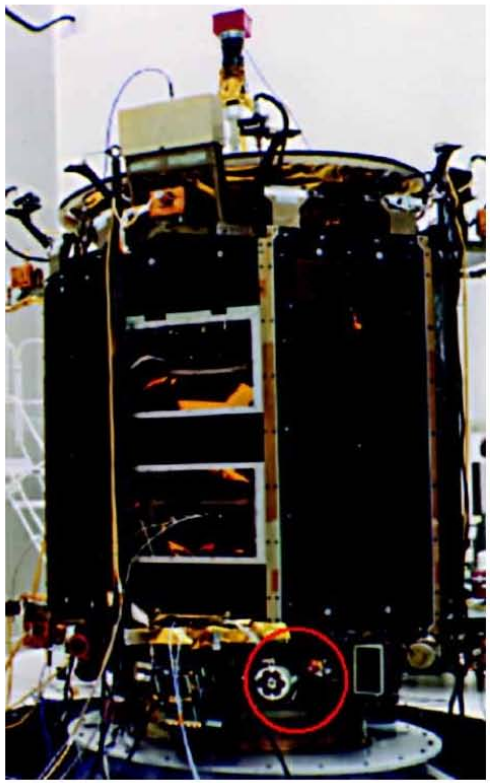

Figure 17. The NLR instrument (circled) as integrated into the NEAR spacecraft. Note the red-tag covers used to protect optics prior to launch. The total spacecraft mass was 816.5 kg (1800 pounds) (with propellant); the NLR weighed slightly less than 5 kg.

[10] Cole, T. D., and Davidson, F. M., "Performance Evaluation of the Near-Earth Asteroid Rendezvous (NEAR) Laser Rangefinder," *Proc. SPIE, Photonics for Space Environments IV* 2811, 156–168 (1996).

Near Laser Rangefinder (1998, APL)

GSFC

The Shape of 433 Eros from the NEAR-Shoemaker Laser Rangefinder

Maria T. Zuber,[1,2*] David E. Smith,[2] Andrew F. Cheng,[3] James B. Garvin,[2] Oded Aharonson,[1] Timothy D. Cole,[3] Peter J. Dunn,[4] Yanping Guo,[3] Frank G. Lemoine,[2] Gregory A. Neumann,[1,2] David D. Rowlands,[2] Mark H. Torrence[4]

oid (Fig. 1) (*15*). From these data we hav constructed a topographic model of Er (Fig. 2) with a spatial resolution of 960 m ar a radial accuracy of ~30 m (*16*) with respe to the asteroid's center of mass (*17*).

Eros has a mean radius of 7311 ± 10 (Table 1) and exhibits excursions in the equ torial plane that range from ~3500 m to ov 17,500 m. The maximum chord is 32.697 k (oriented along 3.96°N, 185.47°E to 0.31° 18.69°E), consistent with an orbital value

Specifications

General

Mass: 5 kg

Power: 20.7 W peak, 16.5 W average

Volume: overall TX/RX assembly 37.5 cm (deep) × 21.6 cm (high) × 22.9 cm (wide) inclusive of overhangs; 10.9 × 15.2 × 3.8 cm laser power supply; 7.6 × 2.5 × 14 cm medium voltage power supply

Data rates: commandable, 51 bps or 6.4 bps

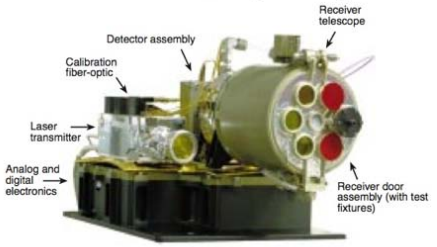

Technical

Laser wavelength: 1.064 μm

Range accuracy requirement: 6 m

Range requirement: 50 km

Inflight range calibration capability

Pulse repetition rate: commandable among 1/8, 1, 2, and 8 Hz

Pulse energy: 15 mJ

Pulse divergence: 235 μrad

Pulse duration: 12 ns

Range gates: two, commandable

Detector threshold: commandable, eight values

Receiver aperture: 7.6 cm (effective)

Range quantization level: 31 cm

Predicted range at asteroid acquisition: 150 km

www.sciencemag.org SCIENCE VOL 289 22 SEPTEMBER 2000

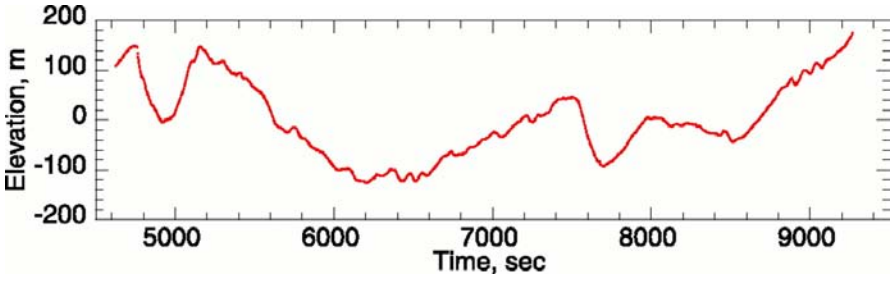

poorly constrained because the structure is situated within a regional low. Even given the depth uncertainty, Psyche is deeper relative to its size than simple (bowl-shaped) craters on the terrestrial planets, consistent with its formation in a low-gravity and perhaps a low-velocity regime.

A second, larger concavity, provisionally named Himeros, is centered at 0°N, 75°E. This structure spans a distance on the surface of slightly greater than Eros's mean radius and displays a saddle shape (Fig. 3), with the symmetry axis of its broad inflection in curvature [Web fig. 2 (*23*)] oriented approximately longitudinally. The structure also exhibits complex short-wavelength curvature variations to the east and west of the structure that trend approximately latitudinally. Himeros lacks topographic characteristics that are commonly associated with an impact origin such as a closed depression, rim, and ejecta blanket (*20*, *30*, *31*). If Himeros's present morphology was preserved since its time of formation, then this feature likely formed as a consequence of collision, i.e., contact between two bodies of roughly similar sizes. However, at the current resolution of the topographic model we cannot rule out the possibility that this structure formed as a result of impact when Eros was part of a larger parent body, or during the process of the asteroid's breakaway into a separate entity. In either of these scenarios, the morphology of an originally impact-generated Himeros would have been modified from its original configuration. We see no geophysical evidence that would suggest that Eros attained its present shape by accumulation or reaccumulation of smaller asteroidal bodies.

A mesh view of the shape of Eros (Fig. 4A) in the vicinity of Himeros includes superposed vectors of gravitational acceleration (*32*) that indicate directions of downslope movement. The highest slopes on the asteroid cluster to the southwest and northwest of Himeros, which are regions that have lower than average crater density (*18*), and collectively suggest that these are regions where regolith has been transported downward (with respect to the gravitational potential) by mass wasting.

The histogram in Fig. 4B shows that the average slope on a surface baseline of ~3° is about 10°, substantially higher than that on a comparable spatial scale on the terrestrial plan-

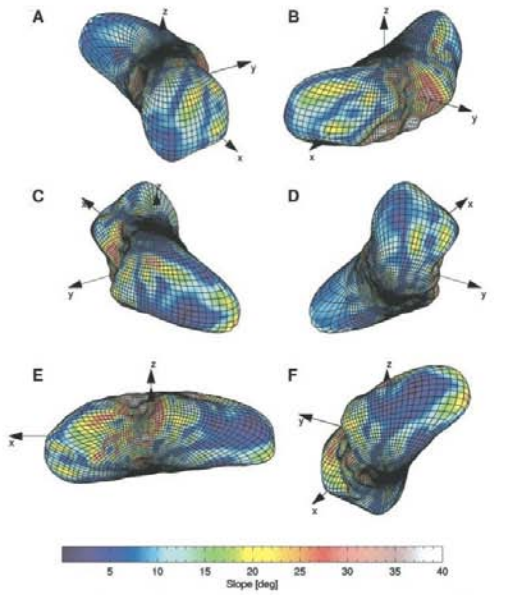

Fig. 3. Six perspective views of a three-dimensional shape model of 433 Eros from the NLR plotted to spherical harmonic degree and order 24. The mesh represents the scaled shape, and the surface facets are color-coded according to the surface slope with respect to a constant-density gravity field derived from the shape model (*32*). The asteroid is viewed at the following (elevation, azimuth) pairs: (**A**) 30°N, 60°E; (**B**) 30°N, 120°E; (**C**) 30°N, 0°E; (**D**) 30°S, 60°E; (**E**) 30°S, 300°E; and (**F**) 30°S, 0°E.

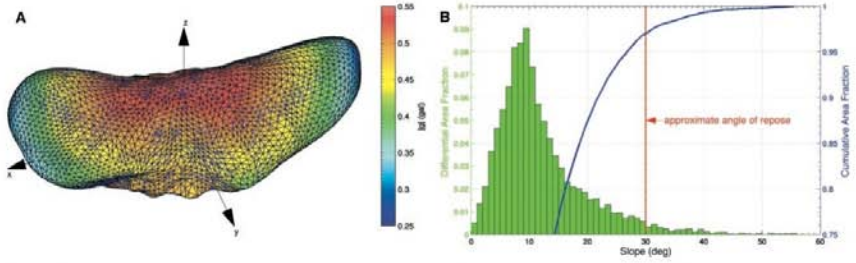

Fig. 4. (**A**) Vectors showing directions of gravitational acceleration ($\vec{g}$). Units are Gals, where 1 Gal = 1 cm s^{-2}. The asteroid is viewed from 30°N, 60°E. Colors represent the magnitude of $\vec{g}$ and arrows indicate the direction. (**B**) Histogram and cumulative frequency distribution of 3°-baseline surface slopes (*32*).

Downloaded from www.sciencemag.org on April 3, 2011

Shuttle Laser Altimeter (1996, 1997) Experiment Accomplishments

- Acquired waveforms from globally-distributed surfaces & vegetation
  ~3 million laser measurements per mission
- Demonstrated laser altimeter geo-location techniques (~1.5 m radial)
- Demonstrated simultaneous estimation of orbit and pointing parameters
- Improved waveform analysis techniques
  – basis for ICESat & Desdynl waveform processing & geolocation

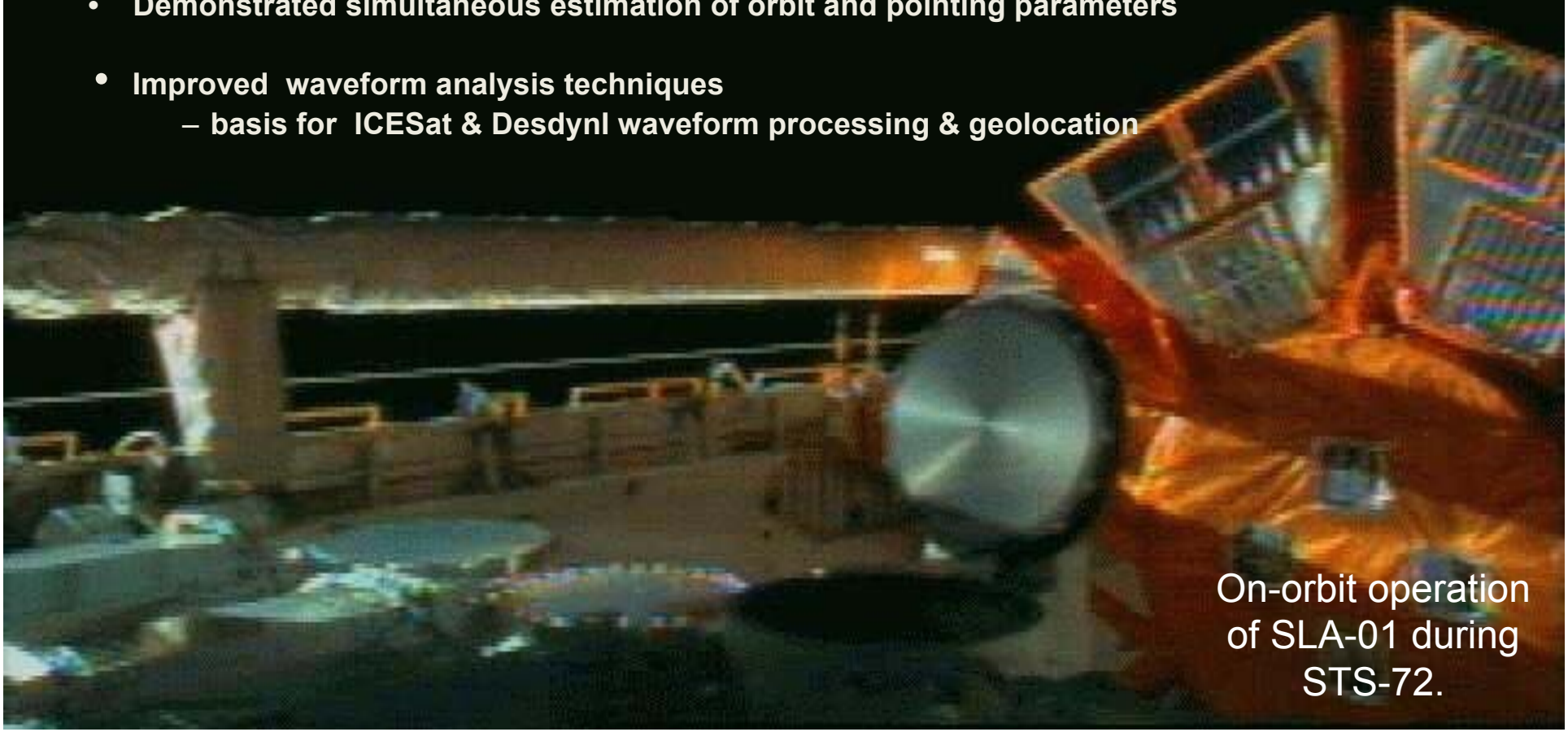

On-orbit operation of SLA-01 during STS-72.

Shuttle Laser Altimeter (SLA-1 & SLA-2)

GSFC Shuttle Hitchhiker Experiment

Jack Bufton, Jim Garvin, Bryan Blair, David Harding and others …

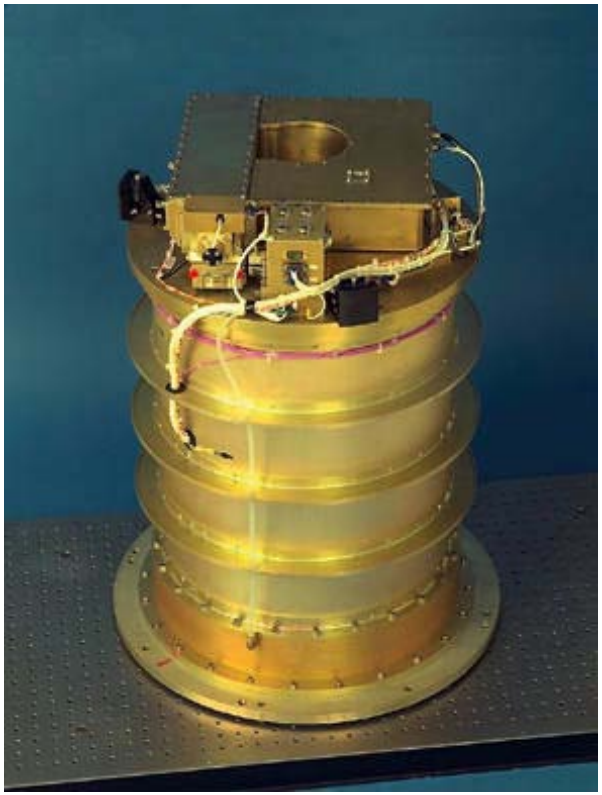

Laser Altimeter Canister

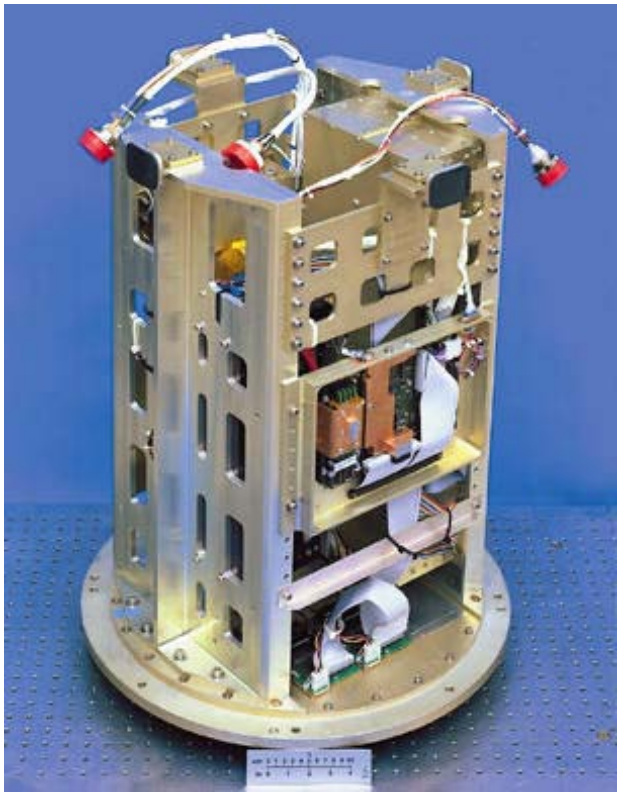

Altimeter Support Canister

Laser Altimeter Canister integration into HH canister prior to SLA-01 Mission

Shuttle Laser Altimeter (1996, 1997)

Shuttle Hitchhiker Experiments

- **A pathfinder for Earth science lidar/altimetry missions:**
  - SLA-01: Jan. 1996 flight, ± 28.5° orbit inclination, 80 hours operation
    - → 1st orbital surface lidar (backscatter waveform digitizing)
    - → assessed orbital SNR & instrument performance
  - SLA-02: August 1997 flight, ± 57° orbit inclination, 80 hours operation
    - → improved geographic coverage
    - → improved electronics for echo waveform measurements

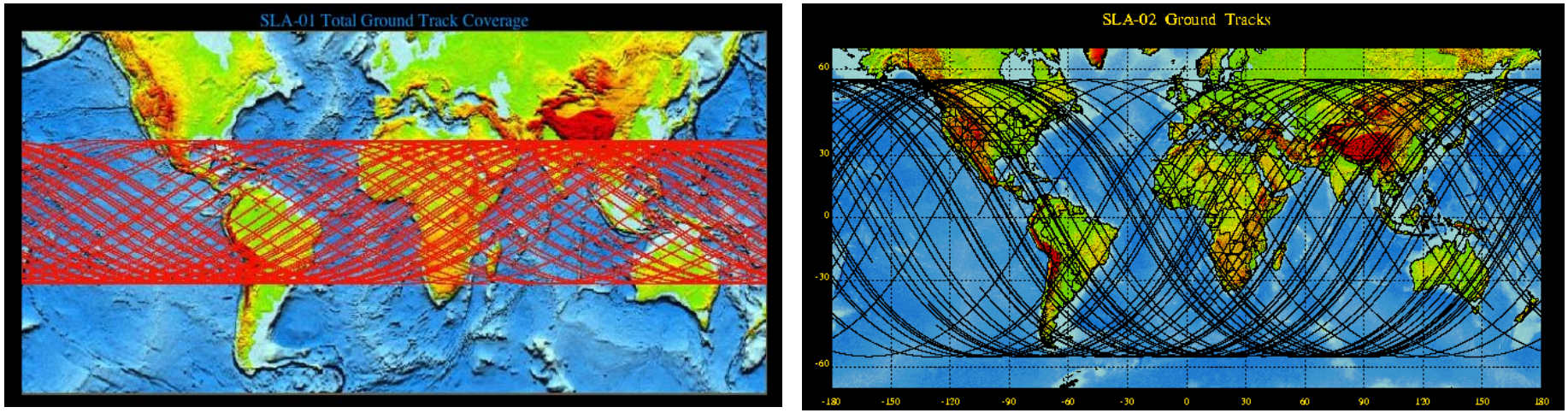

Ground tracks for geolocated SLA-01 and -02 data sets.

Shuttle Laser Altimeter-2

Examples of echo pulses from vegetation

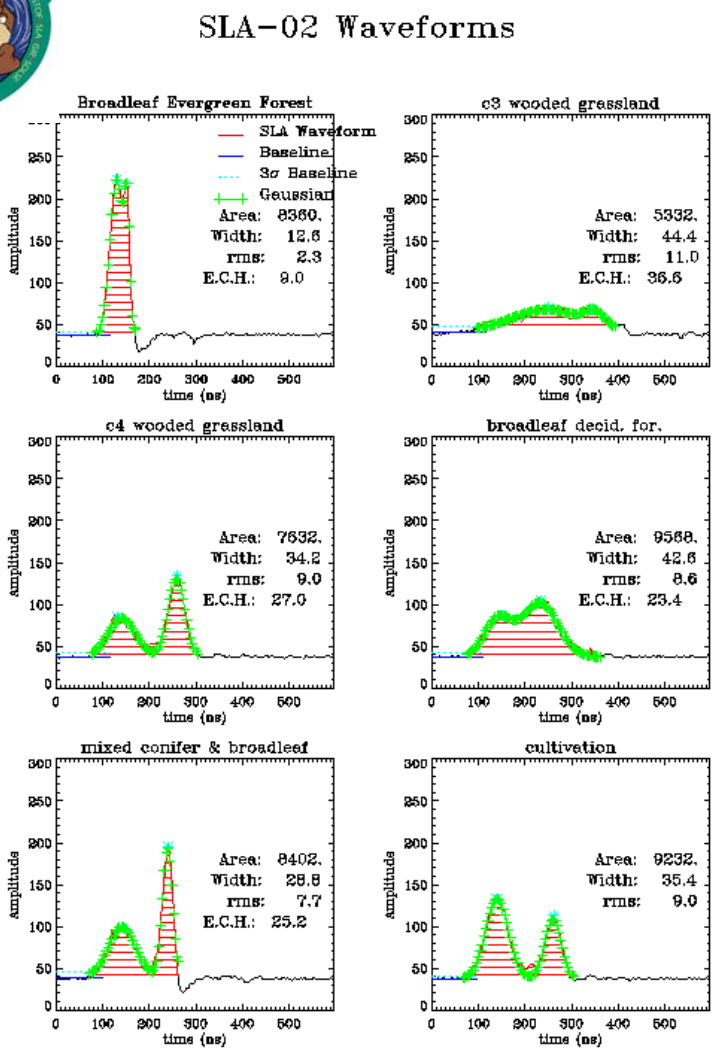

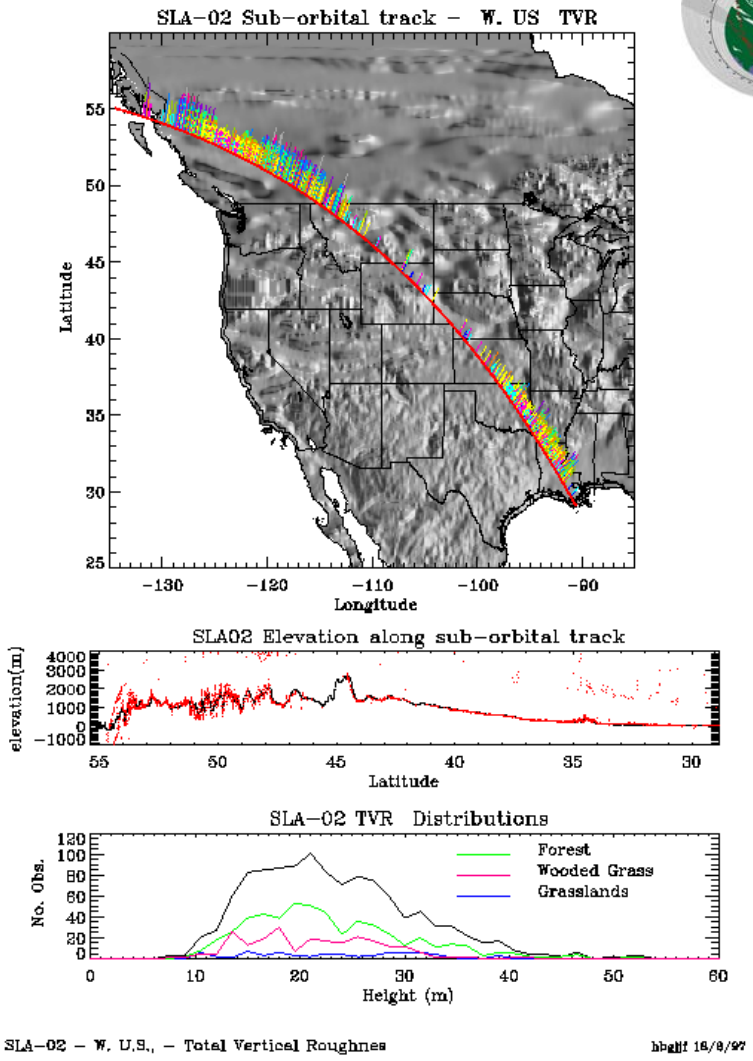

CALIPSO Mission

Earth Orbit, Atmospheric Structure

NASA LaRC

Dave Winker and Zhaoyan Liu
NASA Langley, Hampton, VA

Sun-synchronous orbit

Three co-aligned instruments:

CALIOP: polarization lidar

- 70-meter footprint
- 1/3 km footprint spacing

IIR: Imaging IR radiometer

WFC: Wide-Field Camera

Calipso First light: 7 June 2006

CALIOP First Light Observations
(all 3 channels)

June 9, 2006

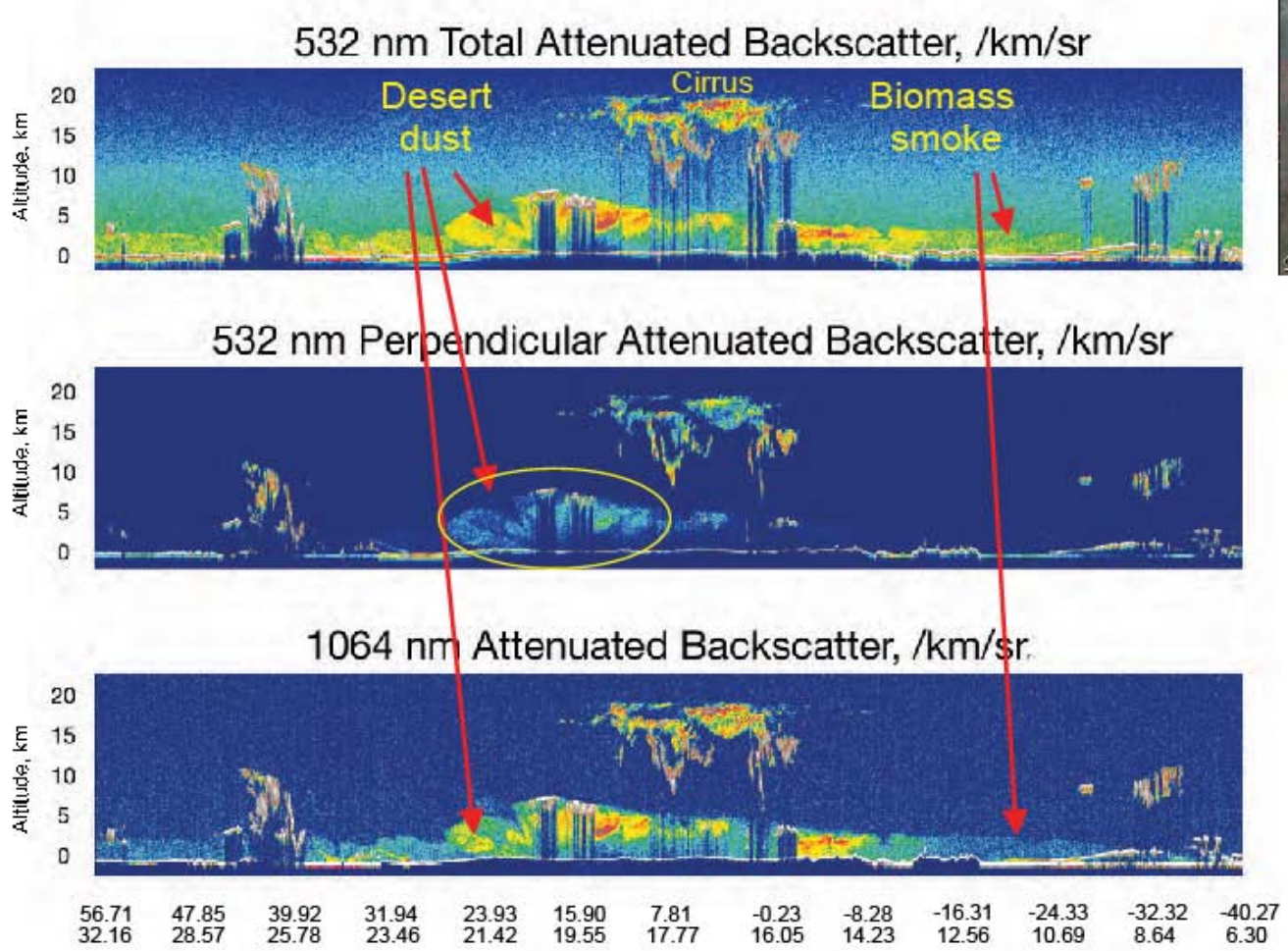

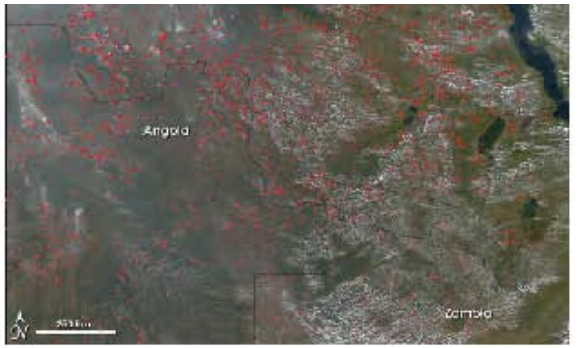

Fire locations in southern Africa from MODIS, 6/10/06

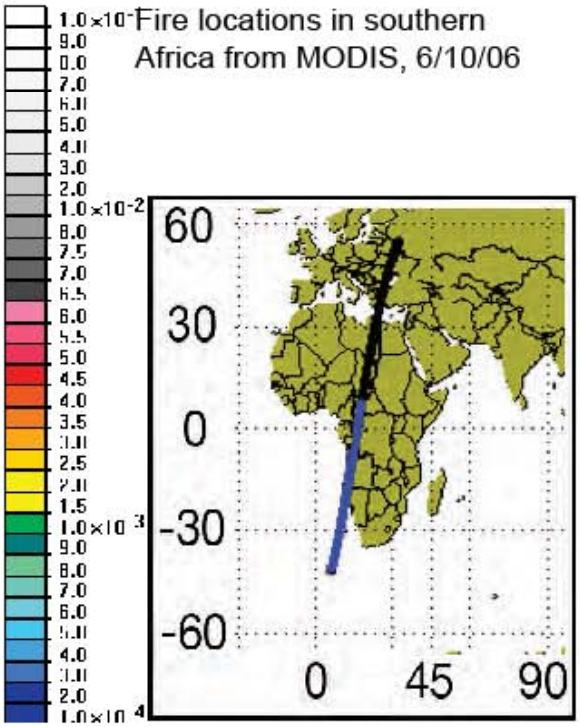

D. Winker/ NASA LaRC

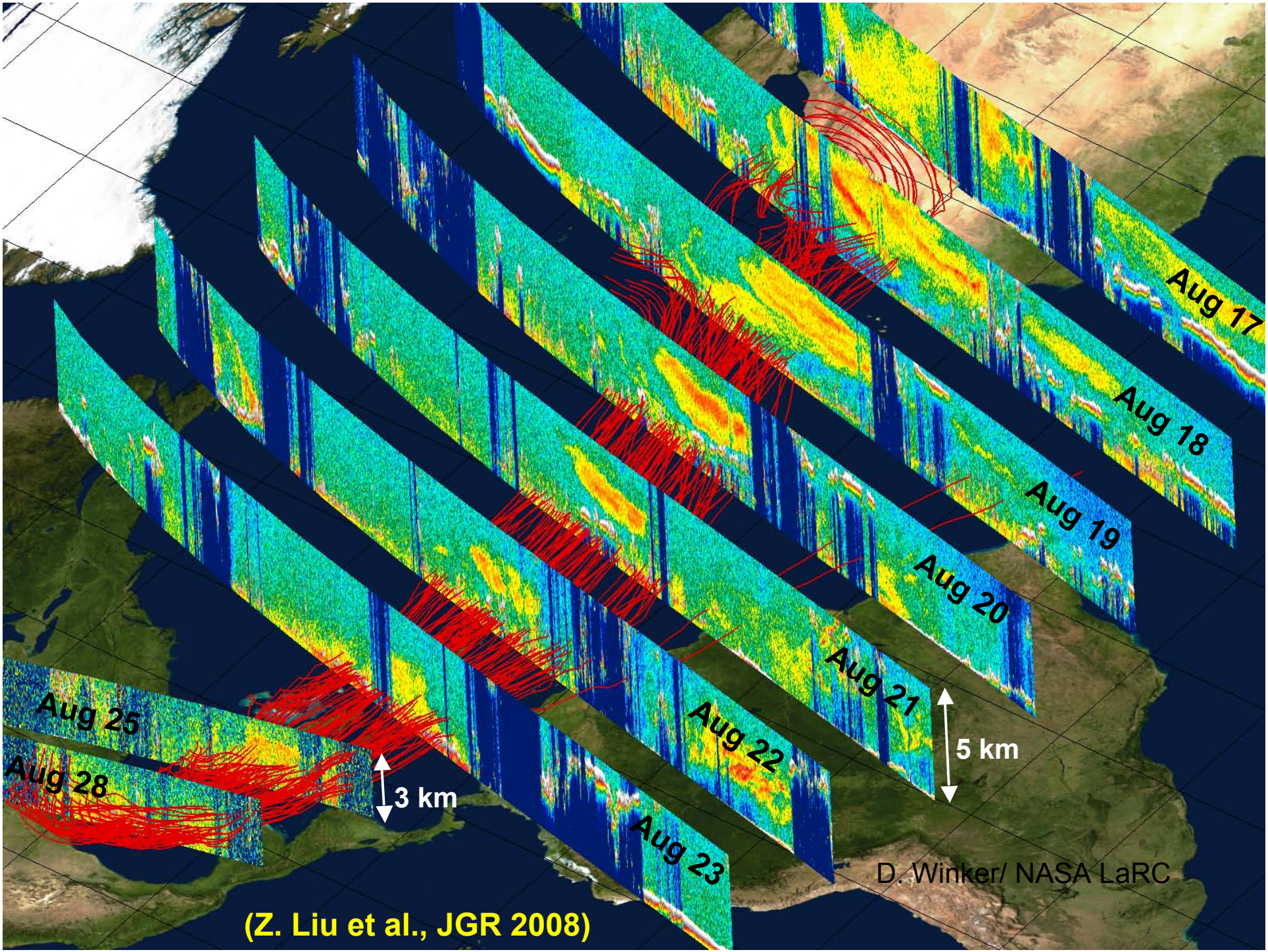
Aug 17
Aug 18
Aug 19
Aug 20
Aug 21
Aug 22
Aug 23
Aug 25
Aug 28
5 km
3 km
D. Winker/ NASA LaRC
(Z. Liu et al., JGR 2008)

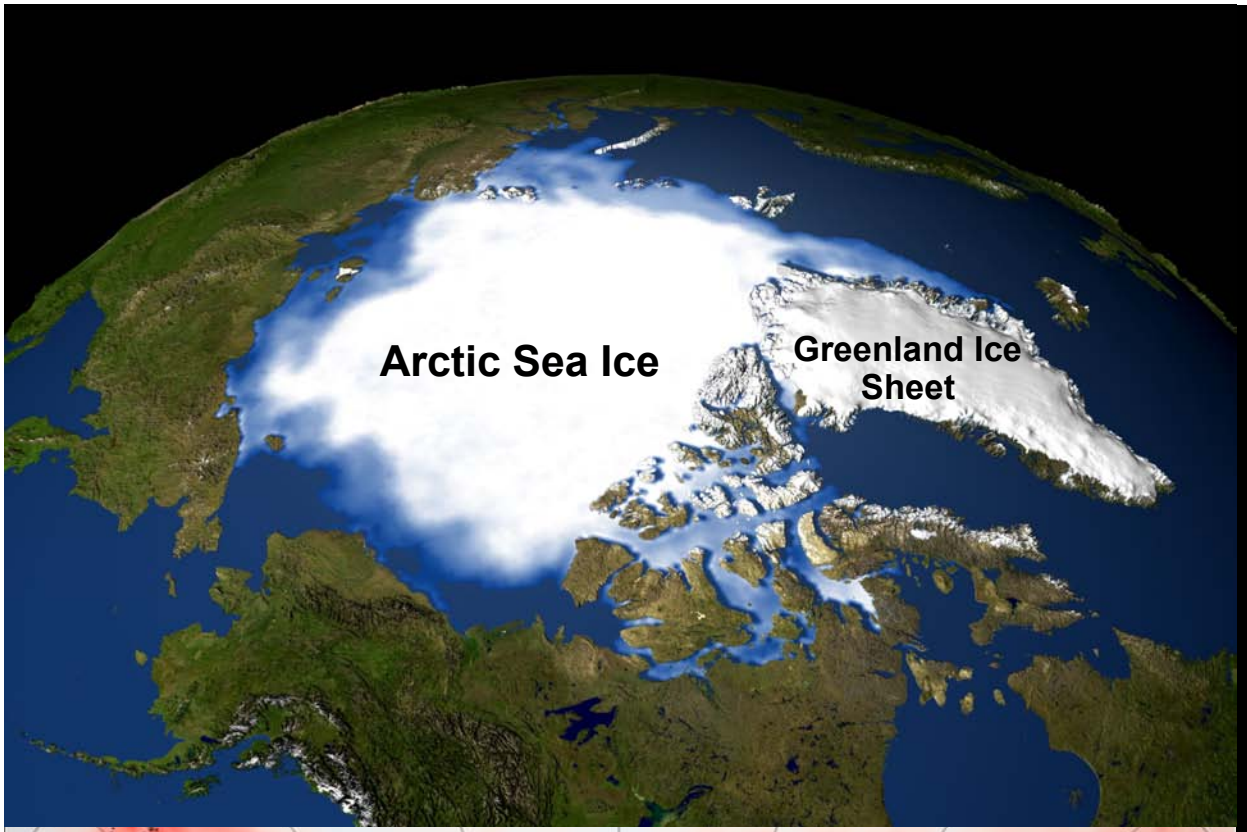

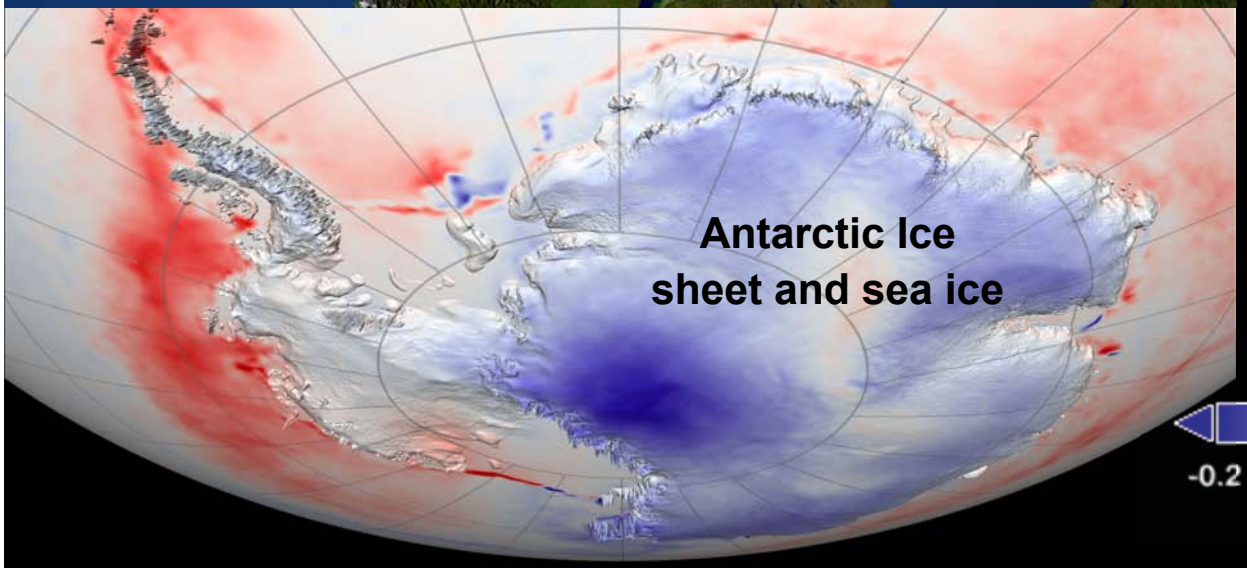

J. Comiso NASA GSFC

ICESat/GLAS

(GSFC/ Earth Orbit - precision altimetry)

Focus - Lidar measurements of the Cryosphere

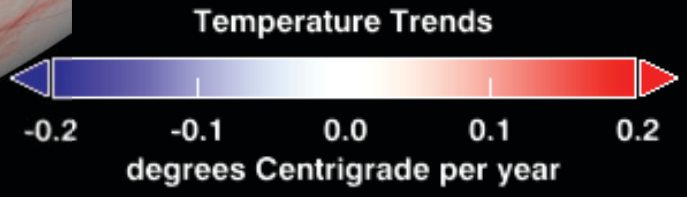

Abdalati/NASA GSFC

ICESat/GLAS - Launch Feb 2003
Measurement Approach

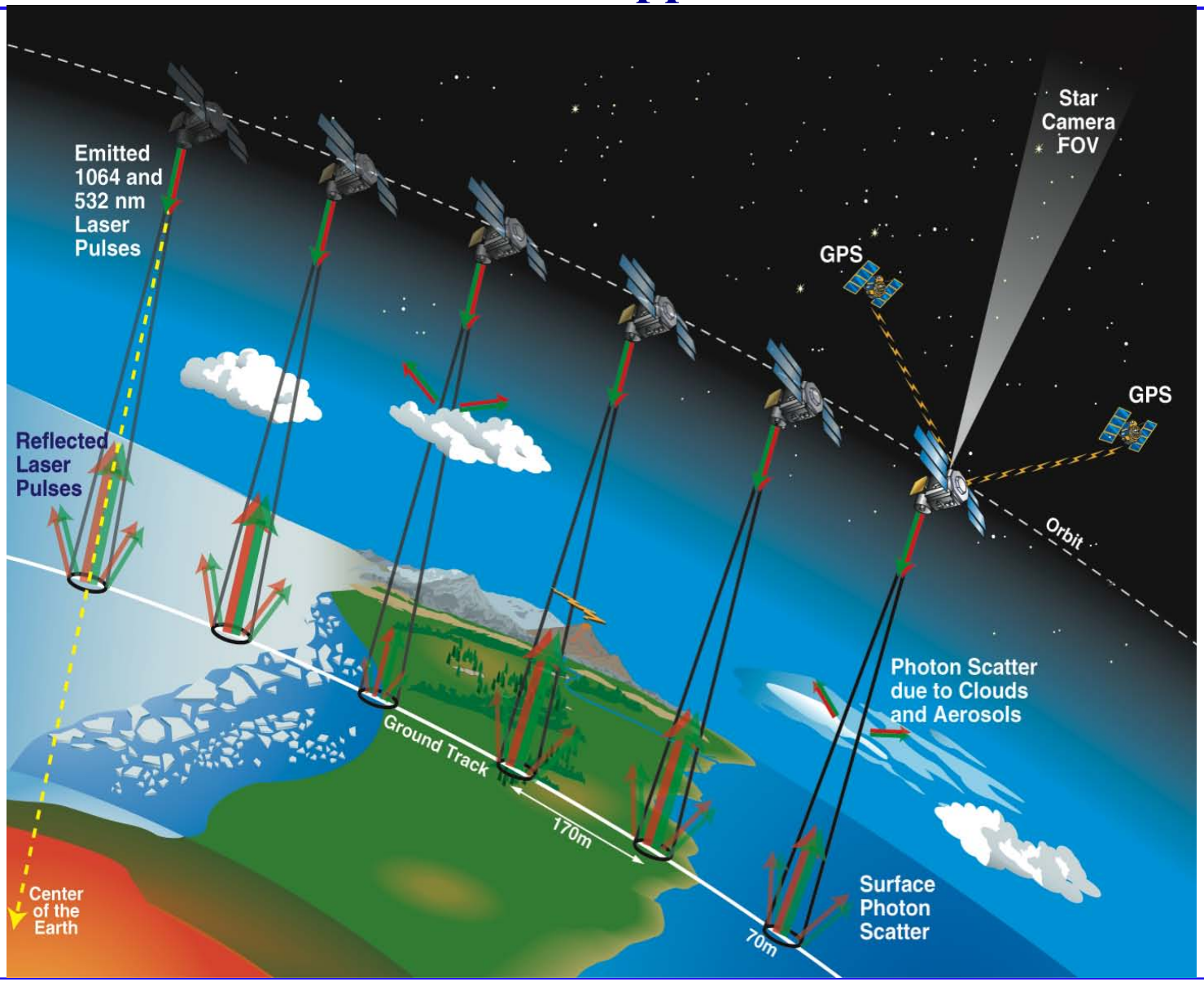

ICESat & GLAS Instrument

GPS antennas
JPL GPS receivers:
Precision orbital position
Precise time

Star trackers

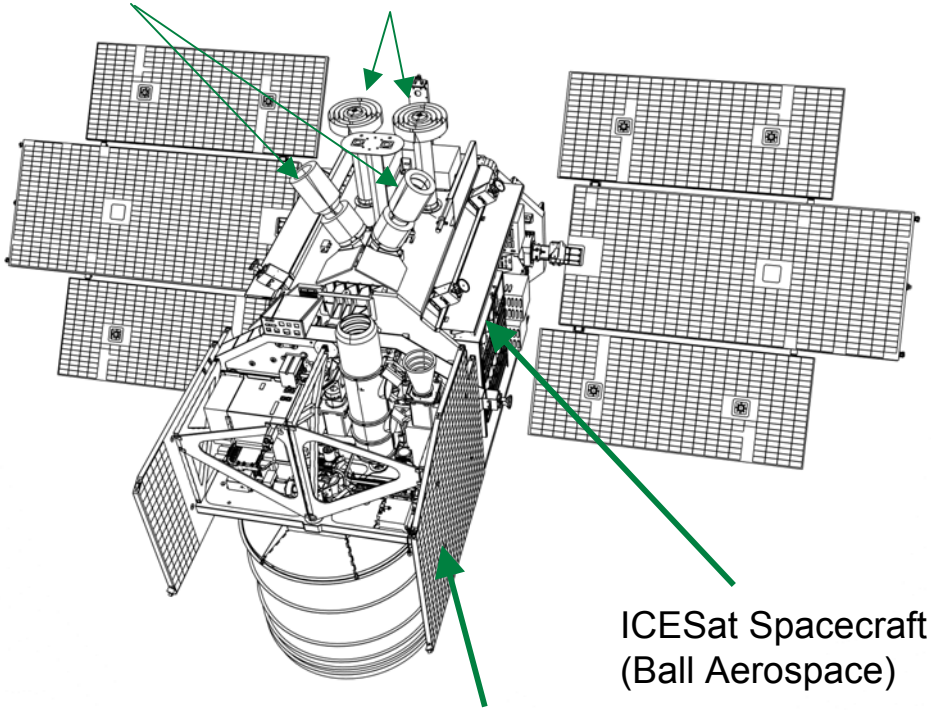

ICESat Spacecraft
(Ball Aerospace)

GLAS lidar
(NASA-Goddard)

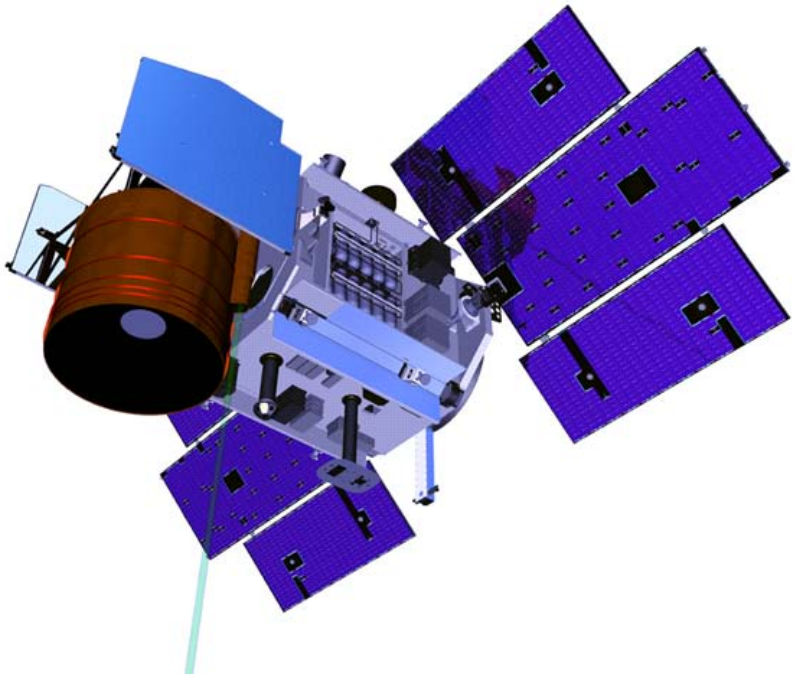

Laser Beams
(1064 & 532 nm)
toward Nadir

GLAS - Lasers & Detectors

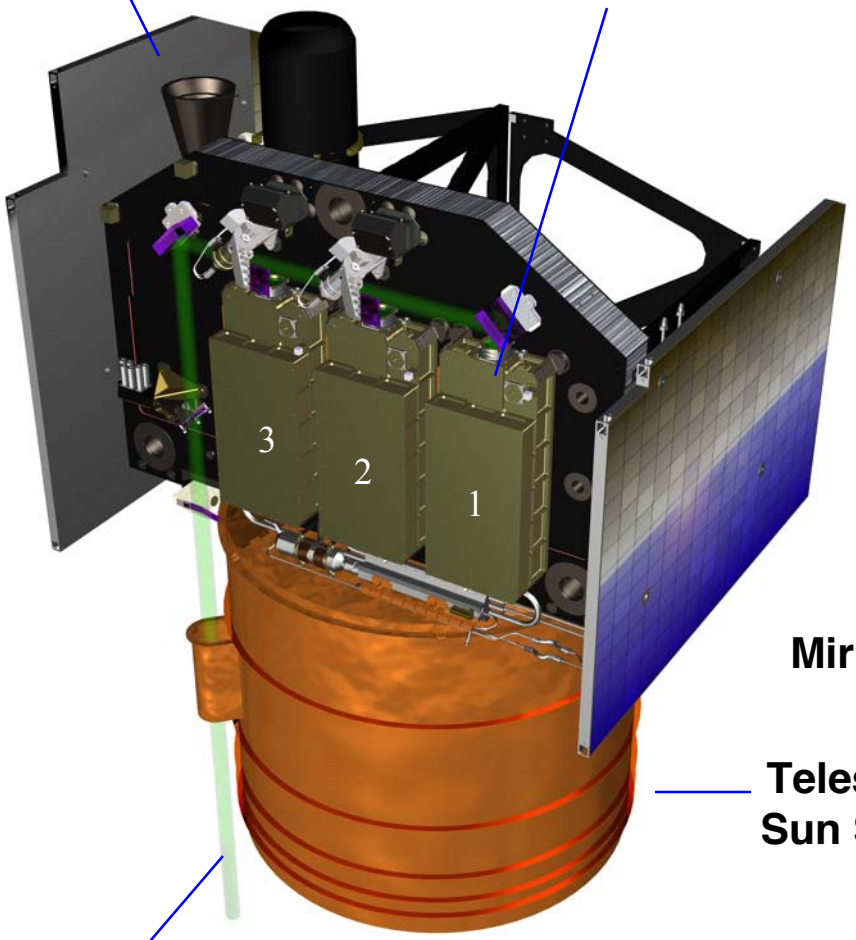

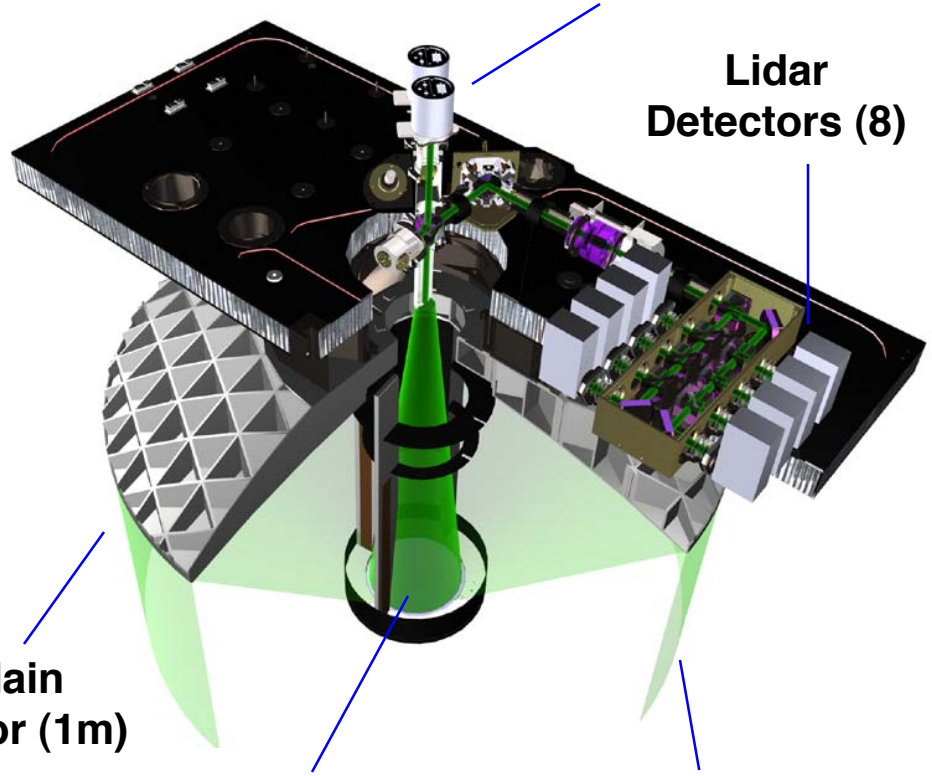

1064 nm Si APD detector
1 GHz rate waveform recorder
532 nm photon counting detectors
Photon counting/histogramming

Greenland Elevation Changes Since 2003

Lidar used to monitor thinning of Greenland ice, and height (-> flow rates) of major ice streams

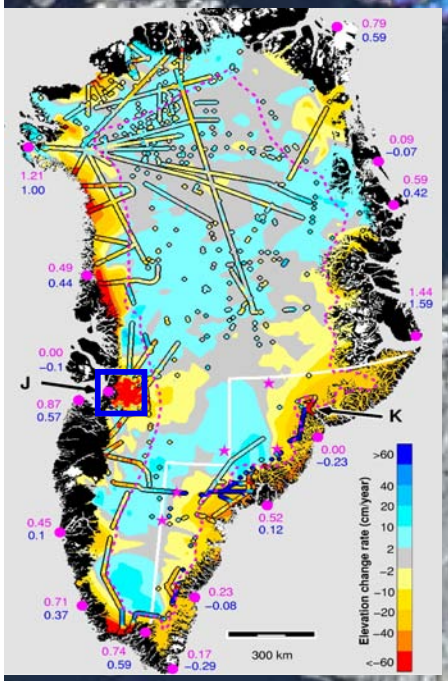

Airborne lidar mapping, Krabill et al.

Zwally et al., Preliminary Results

Thinning **No Change** **Thickening**

ICE, CLOUD, & LAND ELEVATION SATELLITE
ICESAT
NASA'S EARTH SCIENCE ENTERPRISE

Altimetry Resolution:
Ice elevations above Lake Vostok, Antarctica

On orbit measurements match pre-launch testing. Original Requirement < 10 cm.

ICESat elevation height & rms deviation across icesheet above Lake Vostok.

Rms value of **< 2.5 cm** for individual elevation measurements is GLAS range precision.

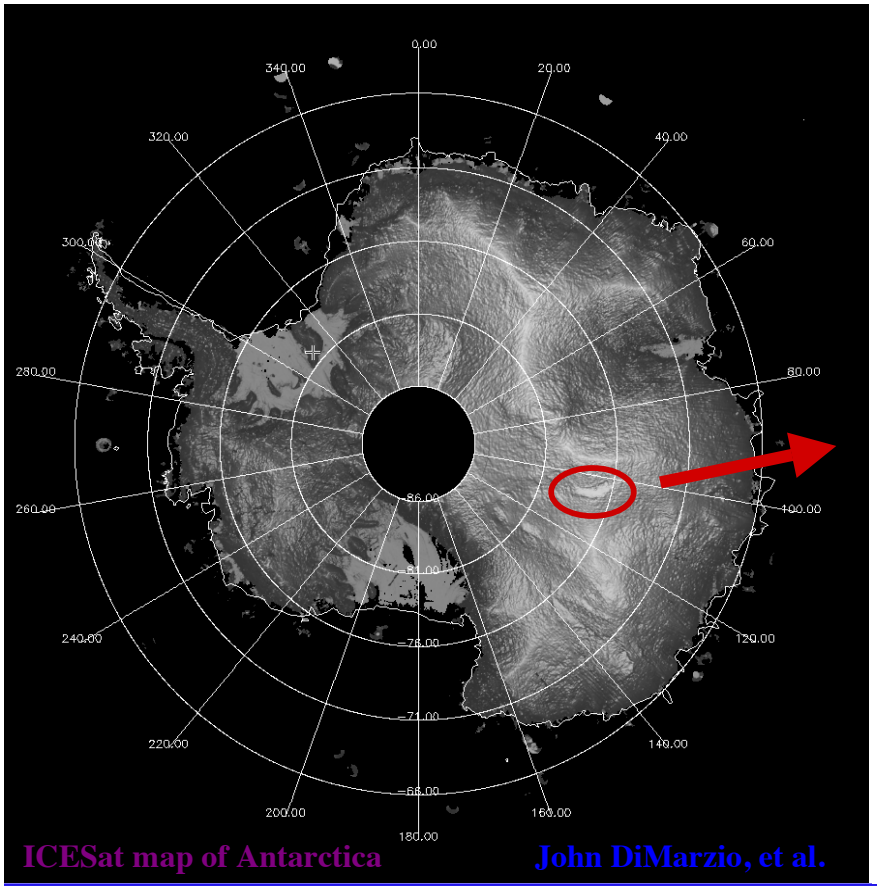

ICESat map of Antarctica John DiMarzio, et al.

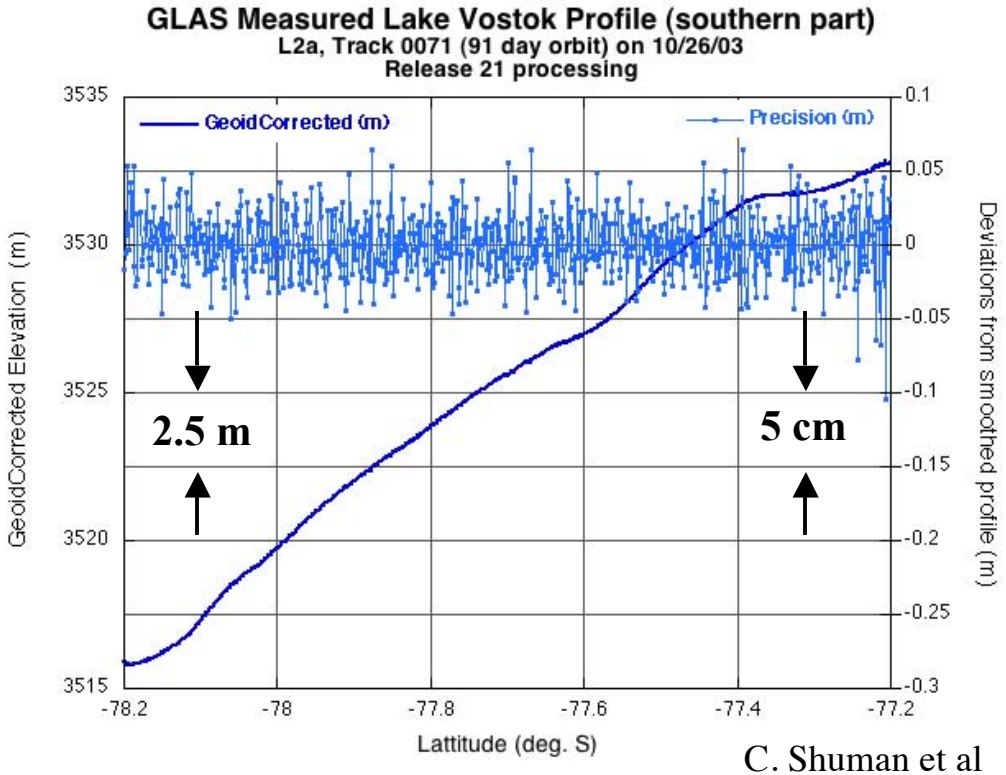

C. Shuman et al

Antarctica - Ross Ice Shelf Elevations from ICESat (one operating campaign)

ICESat elevation profiles overlayed on MODIS Image

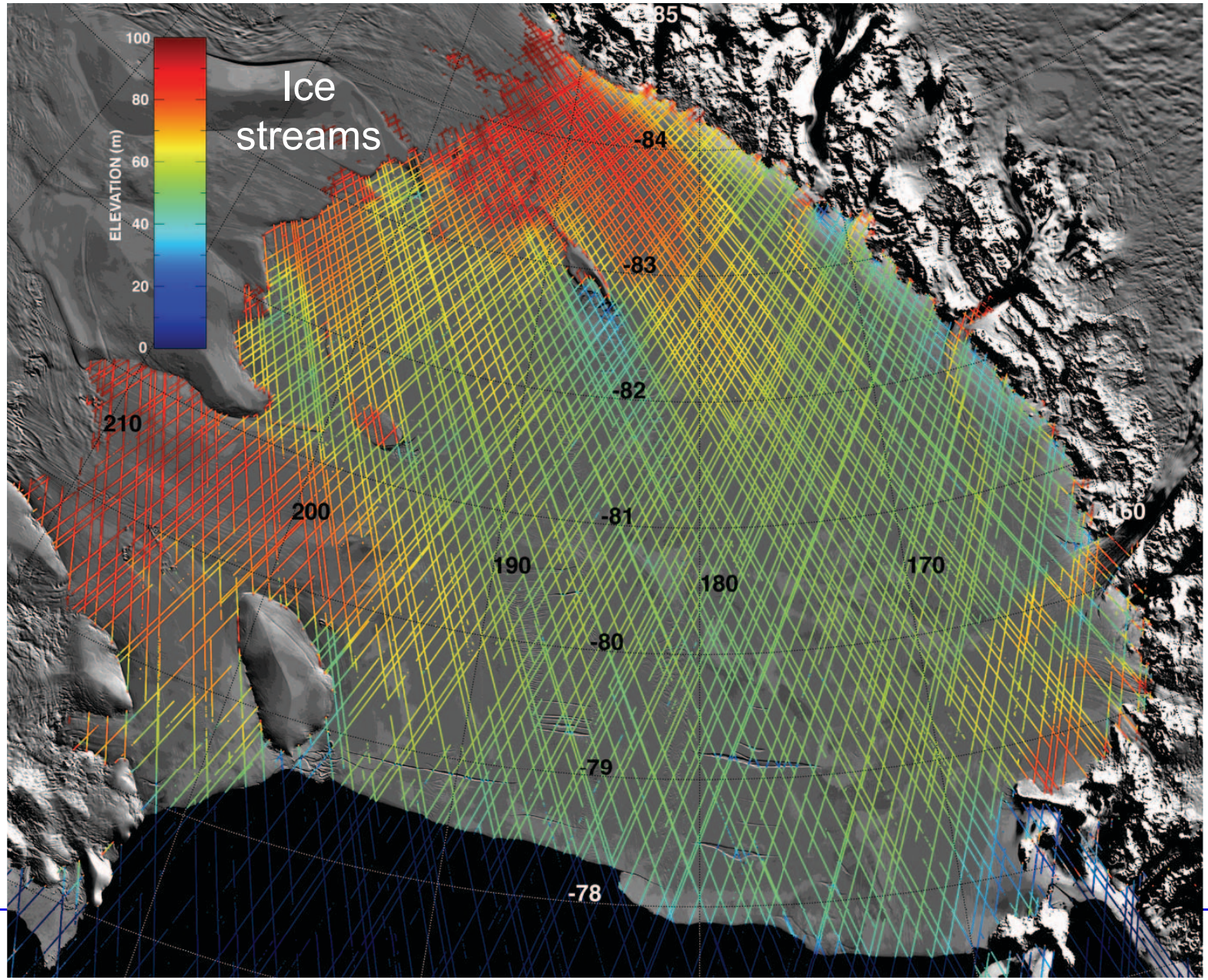

Example of measuring elevation change rate of West Antarctic Ice Sheet (B. Smith)

Rate of elevation change for the West Antarctic ice sheet from analysis of ICESat tracks, repeated by spacecraft pointing

Feb-March, 2005
Feb-March, 2006

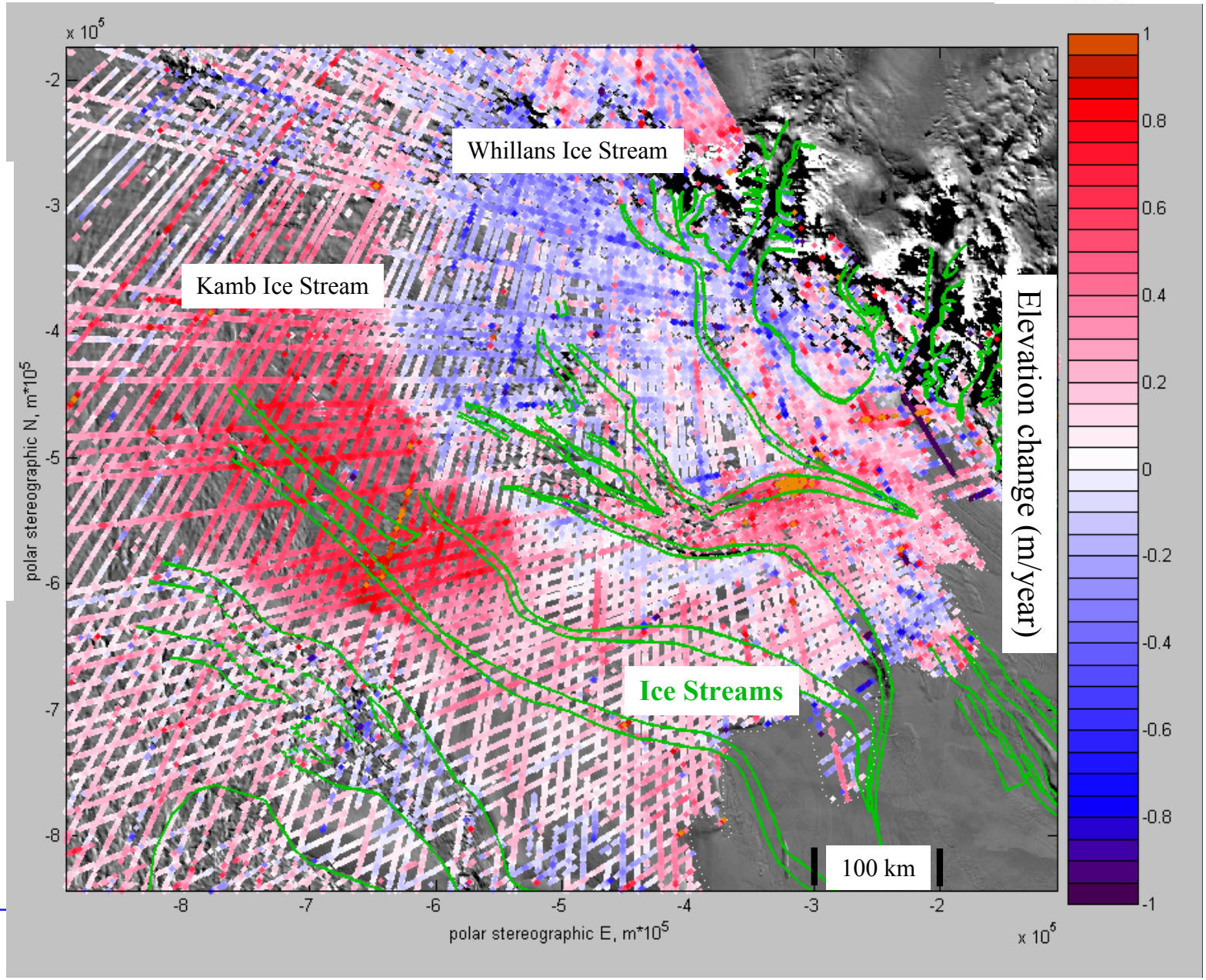

Active lakes under ice streams

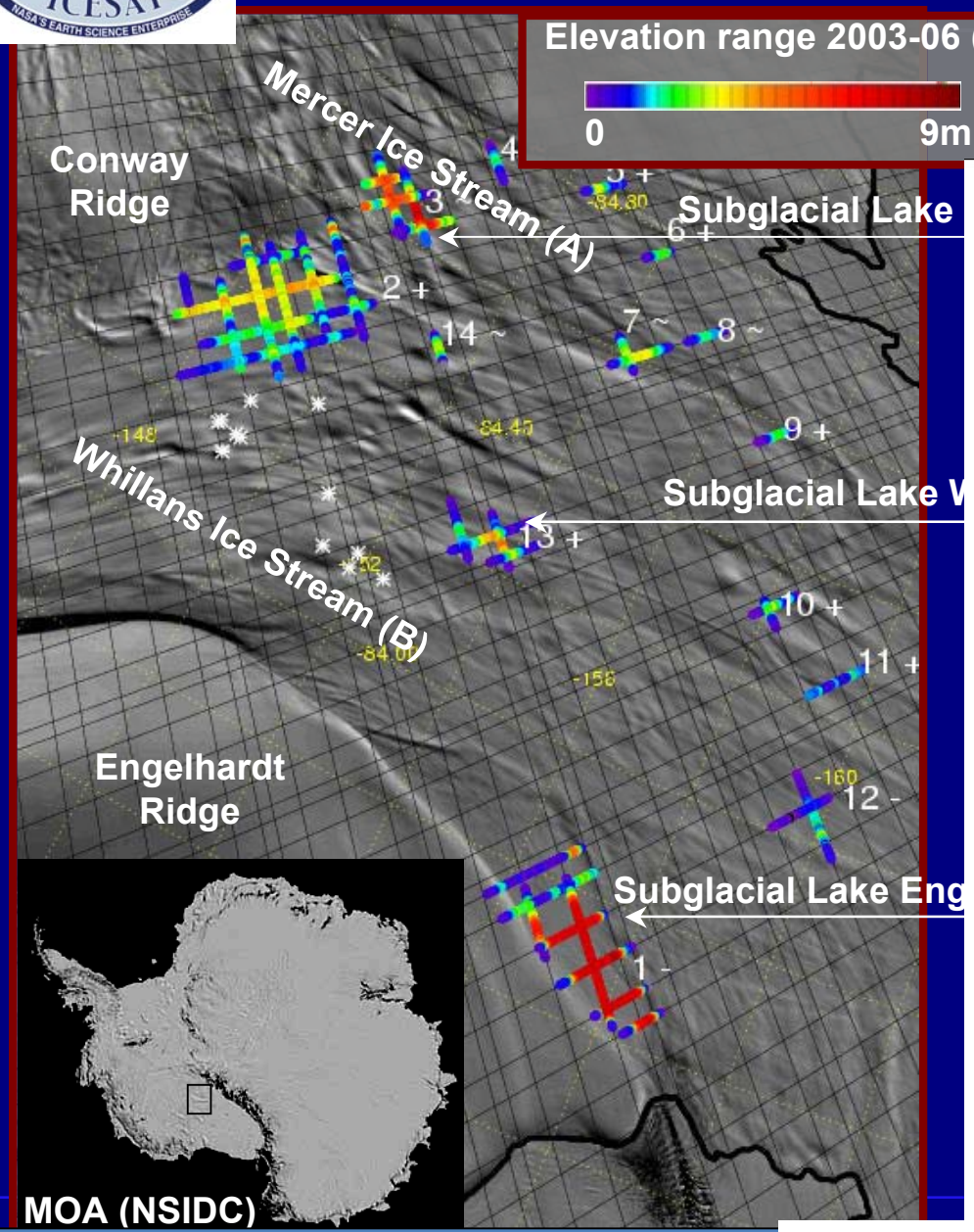

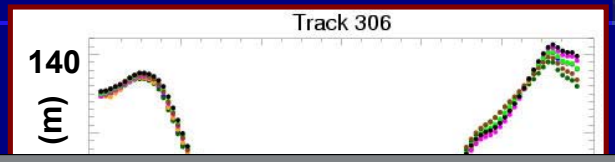

RESEARCH ARTICLES

An Active Subglacial Water System in West Antarctica Mapped from Space

Helen Amanda Fricker,[1]* Ted Scambos,[2] Robert Bindschadler,[3] Laurie Padman[4]

Satellite laser altimeter elevation profiles from 2003 to 2006 collected over the lower parts of Whillans and Mercer ice streams, West Antarctica, reveal 14 regions of temporally varying elevation, which we interpret as the surface expression of subglacial water movement. Vertical motion and spatial extent of two of the largest regions are confirmed by satellite image differencing. A major, previously unknown subglacial lake near the grounding line of Whillans Ice Stream is observed to drain 2.0 cubic kilometers of water into the ocean over ~3 years, while elsewhere a similar volume of water is being stored subglacially. These observations reveal a widespread, dynamic subglacial water system that may exert an important control on ice flow and mass balance.

At least 145 subglacial lakes have been mapped beneath the Antarctic Ice Sheet (*1*). Recent pivotal studies based on satellite data have demonstrated that Antarctic subglacial water can move in large volumes between lakes, on short time scales and over long distances (*2*, *3*). Large outbursts of subglacial water have been observed in coastal regions (*4*), but it is not known how frequently these occur, nor the total amount of water involved continent-wide. Water beneath an ice stream, acting as a lubricant either between the ice and subglacial bed or between grains of a subglacial till, affects ice flow rates (*5*). Subglacial lakes have recently been linked to the broad onset of faster flow of the Recovery Ice Stream (*6*) and are located at the heads of other Antarctic ice stream tributaries (*7*). The drastic deceleration (a "shutdown") ~150 years ago of Kamb Ice Stream has been attributed to a decrease in subglacial water supply (*8*). Thus, knowledge of subglacial water movement is fundamental to understanding Antarctic ice stream dynamics and to predicting future Antarctic ice sheet behavior and sea-level contribution.

Subglacial water systems are pressurized to near the weight of the overlying ice (*9*), so movement of water can cause an elevation change of the ice surface that can be detected by satellites. Past observations interpreted to be Antarctic sub-

[1]Institute of Geophysics and Planetary Physics, Scripps Institution of Oceanography, University of California, San Diego, La Jolla, CA 92093, USA. [2]National Snow and Ice Data Center, University of Colorado, Boulder, CO 80302, USA. [3]NASA Goddard Space Flight Center, Greenbelt, MD 20771, USA. [4]Earth & Space Research, Corvallis, OR 97333, USA.
*To whom correspondence should be addressed. E-mail: hafricker@ucsd.edu

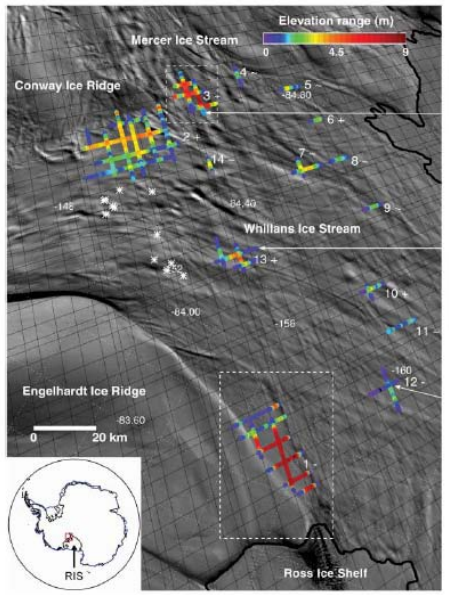

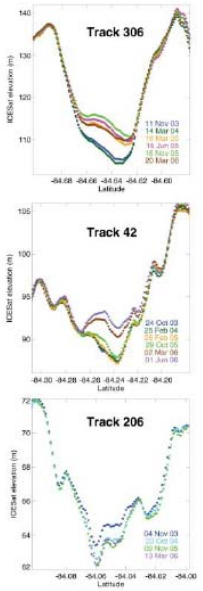

Fig. 1. (**Left**) Locations of elevation-change events identified through ICESat repeat-track analysis on lower WIS and MIS (2003 to 2006). Straight black lines show the ICESat reference ground tracks. Colored track segments represent range in elevation amplitude for each elevation-change event. Events cluster into 14 elevation-change regions, which are either rising (+), falling (–), or oscillating (~). Ice flow is from top left to lower right. Background image is MODIS Mosaic of Antarctica (MOA) (*30*), and inset map shows its location in Antarctica. Bold black line indicates the break-in-slope associated with the grounding zone of the Ross Ice Shelf (RIS). White dashed boxes show regions covered in Fig. 2. White asterisks indicate locations of small surface-collapse features observed on WIS in 1987–1988 (fig. S4). (**Right**) Repeat ICESat elevation profiles along track segments that cross each type of region (~, +, –). Arrows point to the location of each track segment on the image.

Fricker et al./Scripps

ICESat/GLAS Lidar Coverage

ICESat Laser 2a Global Elevations: 9/25 to 11/19/03 (~45 days)

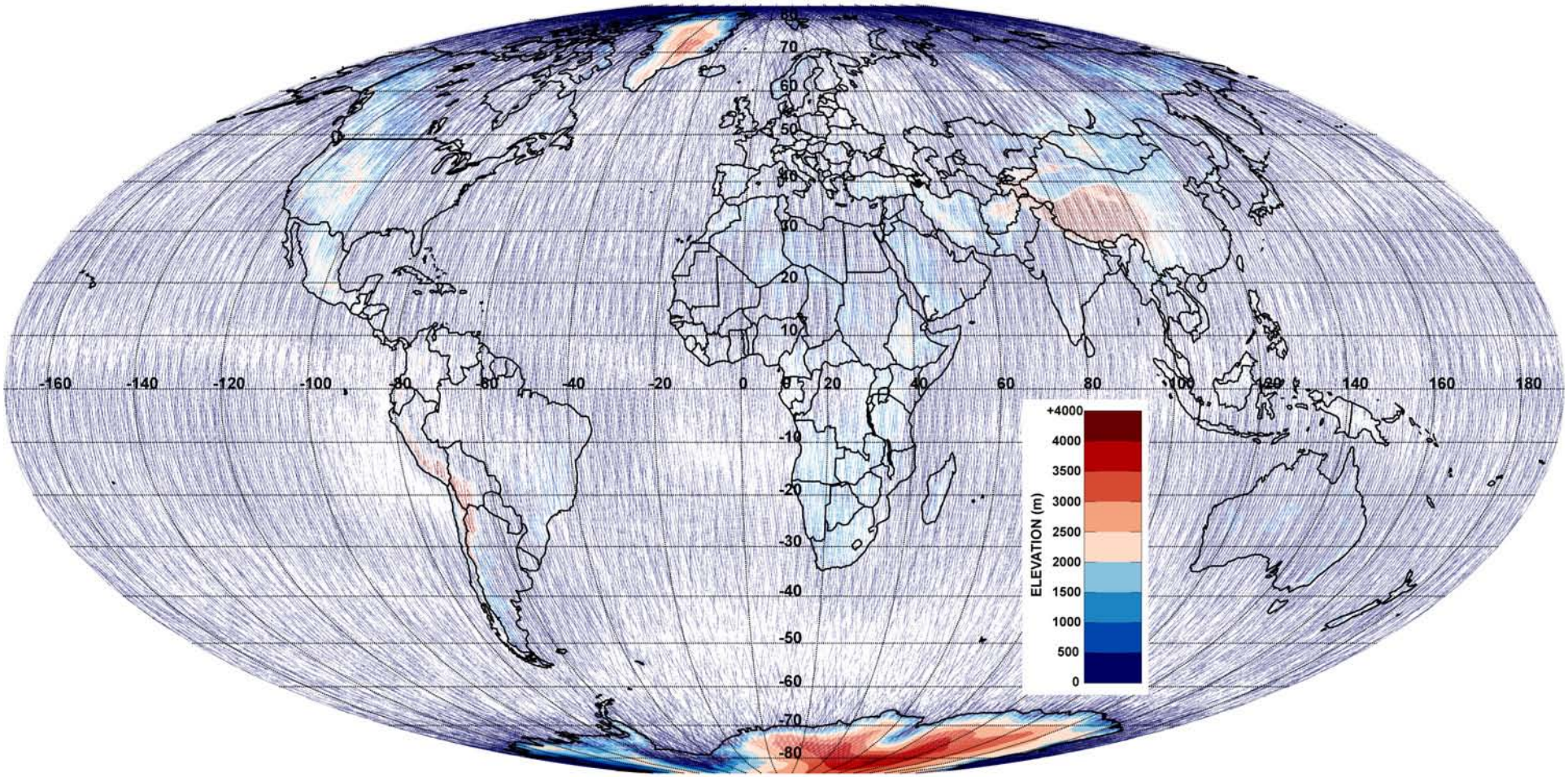

ICESat/GLAS total lidar observations: 1.98 Billion (13 times denser)

GLAS Measurement of Echo pulse from Trees

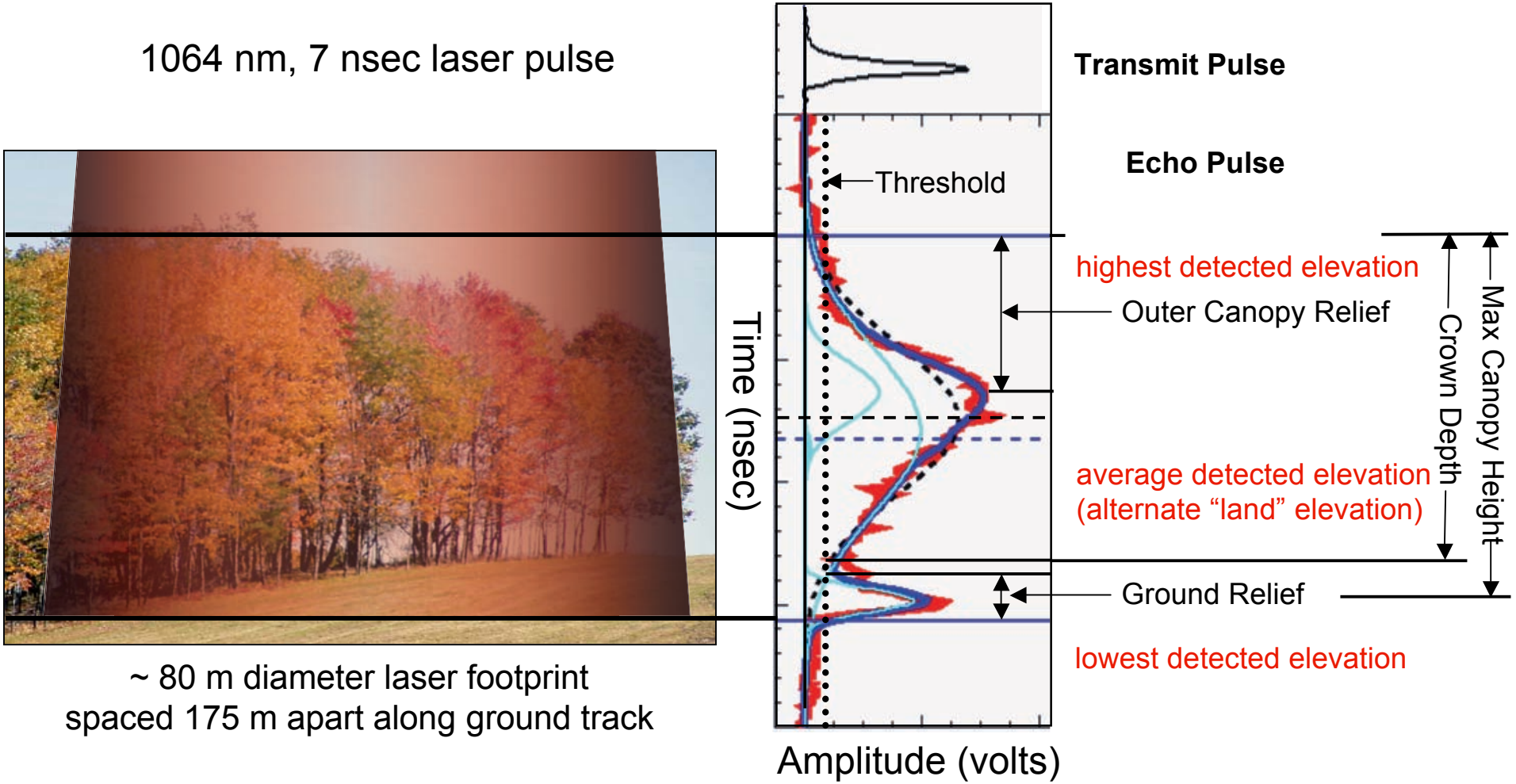

Height Distribution of Reflected Laser power with 15 cm Vertical Sampling

Harding/NASA- GSFC

Global Forest Canopy Height Map from ICESat/GLAS (M. Lefsky, GRL, 2010)

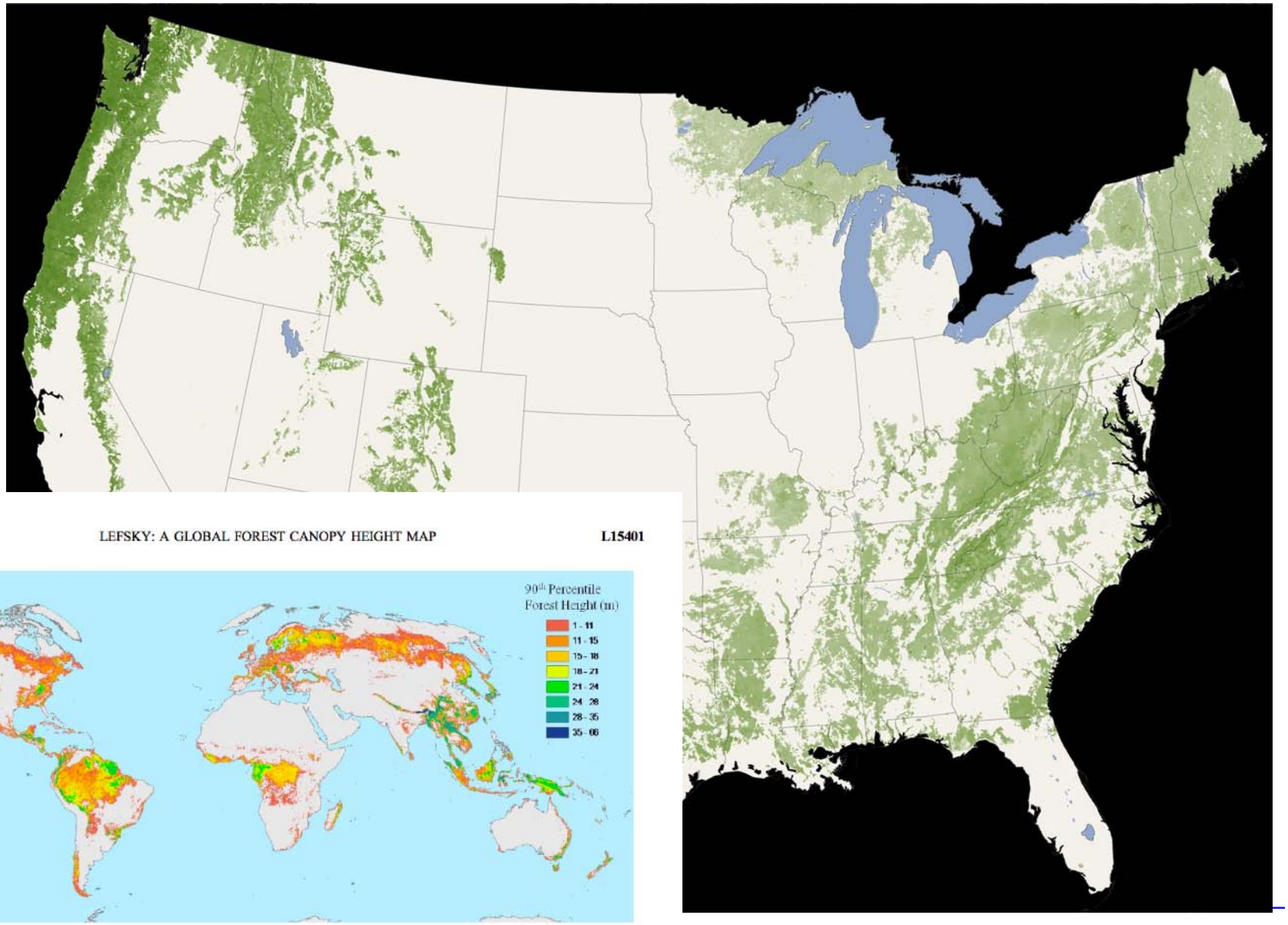

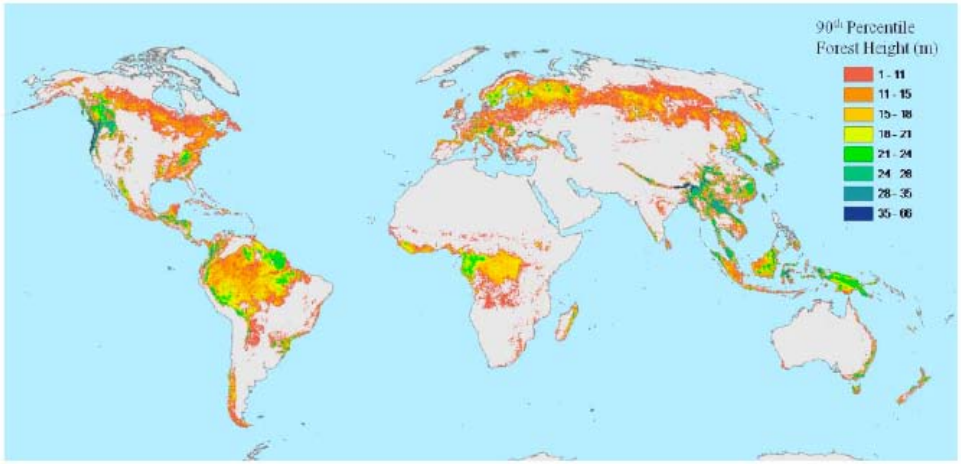

Figure 1. Global forest height map. Heights are the 90th percentile of GLAS height observations within a patch.

Overview and Some results from ICESat/GLAS

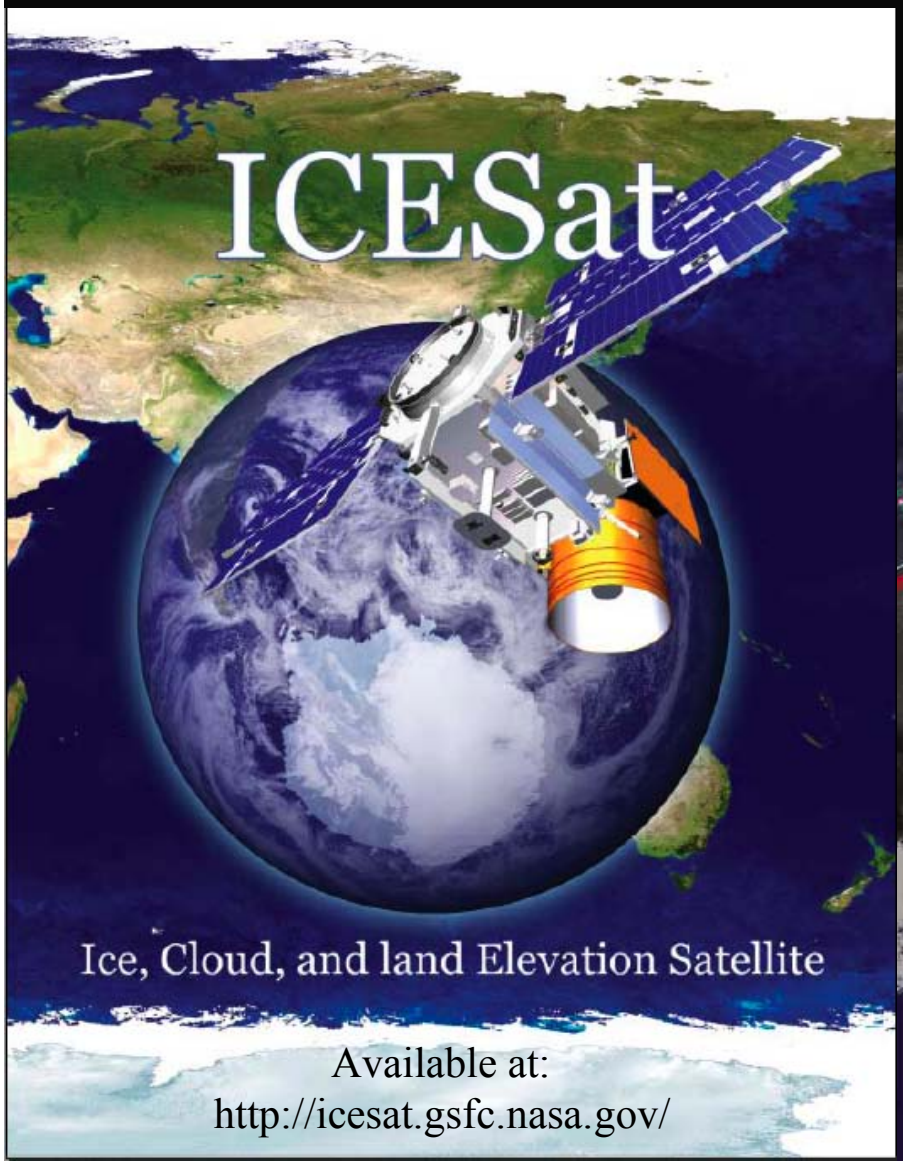

Available at:
http://icesat.gsfc.nasa.gov/

GLAS Laser Approach:
was adapted to other missions

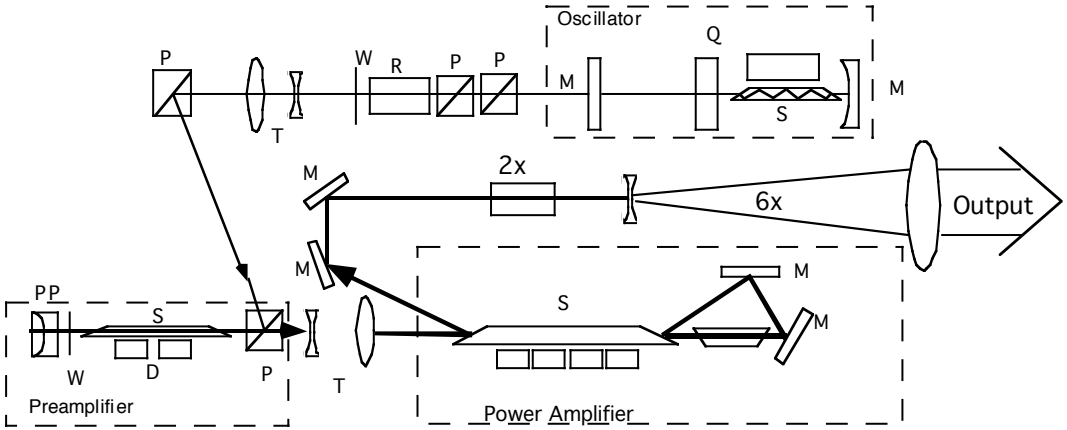

D	= Diode Pump	Q	= Q-switch
DP	= Dove Prism	R	= Faraday Rotator
M	= Mirror	S	= Nd:YAG zig-zag slab
P	= Polarizer	T	= 2x Telescope
PP	= Porro Prism	W	= Waveplate
2x	= Doubler	6x	= 6x Beam Expander

GLAS laser was designed and built at GSFC following MOLA.

- To meet the systems requirement, a MOPA architecture was chosen.
  - master oscillator (~2.2 mJ)
  - pre-amplifier (~10X -> ~22 mJ)
  - power amplifier (~5X -> ~110 mJ).
- Cr^{4+}:YAG passive Q-switch
- LBO for frequency doubling
- 6X achromatic telescope to meet beam divergence requirement

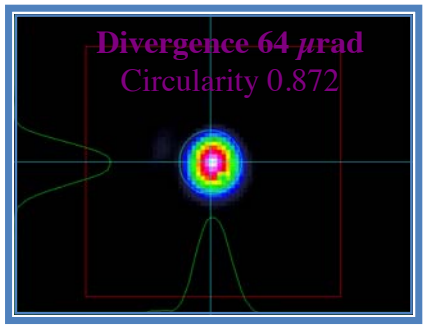

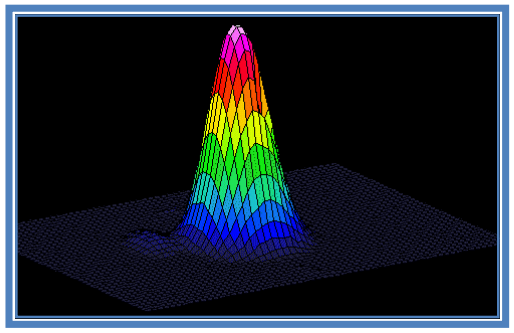

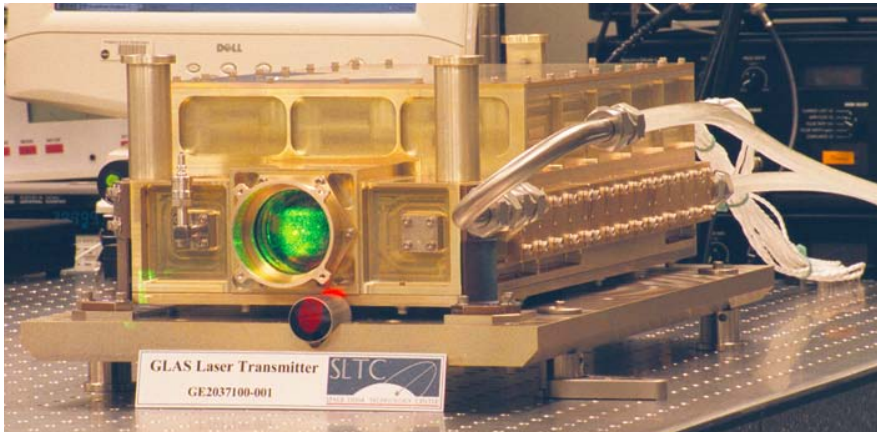

Lunar Reconnaissance Orbiter (LRO) and LOLA

GSFC/ Lunar Orbit

- LOLA is one of the 7 payload instruments on LRO
- Objectives are to measure lunar surface topography and to establish a global lunar geodetic coordinate system.

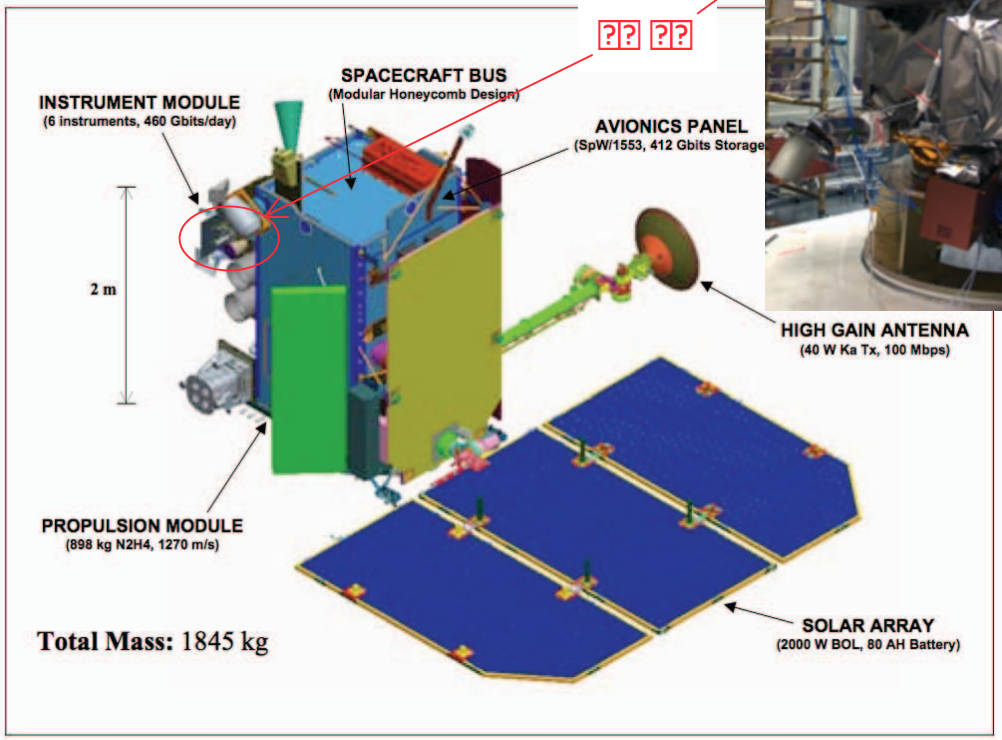

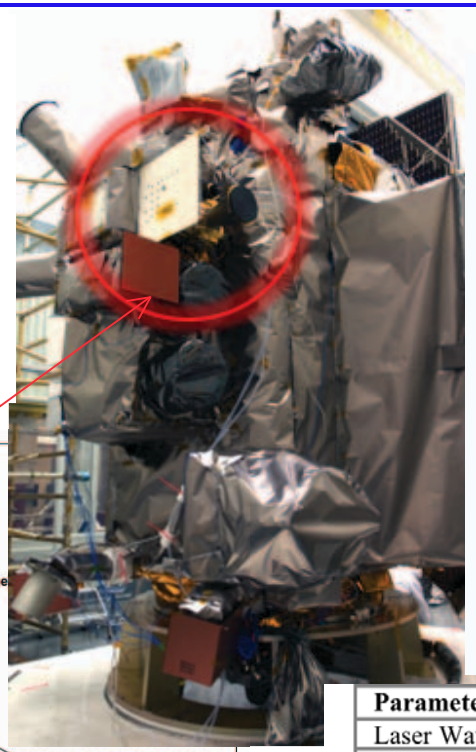

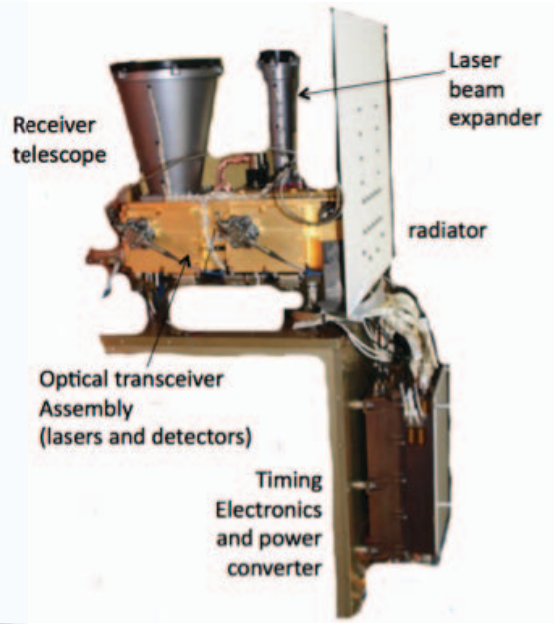

Parameter	Value
Laser Wavelength	1064.4 nm
Pulse Energy	2.7/3.2 mJ (laser1/laser2)
Pulse Width	~ 5 ns
Pulse Rate	28 ± 0.1 Hz
Beam Divergence	100 ± 10 µrad
Beam Separation	500 ± 20 µrad
Receiver Aperture Diameter	0.14 m
Receiver Field of View	400 ± 20 µrad
Receiver Bandpass Filter	0.8 nm
Detector responsivity	300 kV/W
Detector active area diameter	0.7 mm
Detector electrical bandwidth	46 ± 5 MHz
Timing Resolution	0.5 ns

Smith et al., *Space Science Reviews*, 2010

LOLA - 1st Multi-beam Space Lidar

- Use of a diffractive optical elements (DOE) to split the laser to illuminate five spots on ground
- Use of an optical fiber array to direct each spot into a separate receiver channel
- Make five measurements from a single laser shot to give range, slope and direction

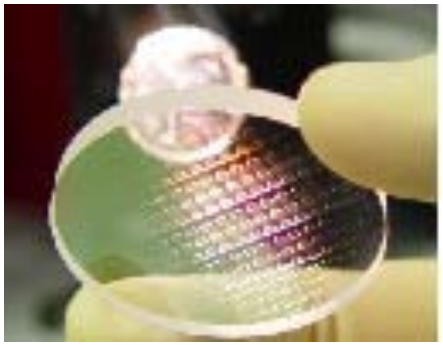

DOE and the optical fiber array

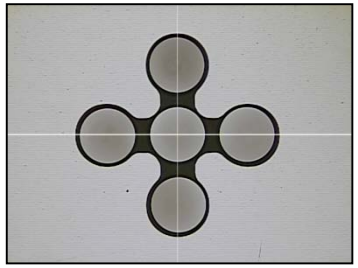

Fiber Pattern at telescope focal plane

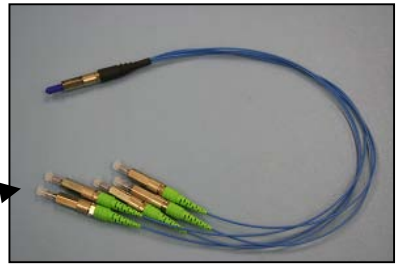

Each fiber couples to a separate Si APD detector

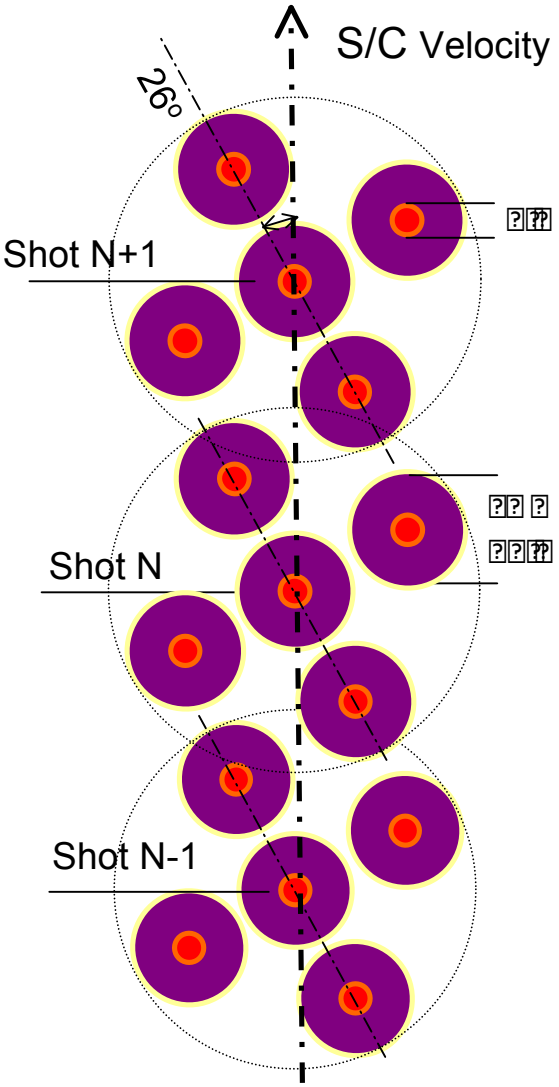

Lunar Topography Map From LOLA Measurements

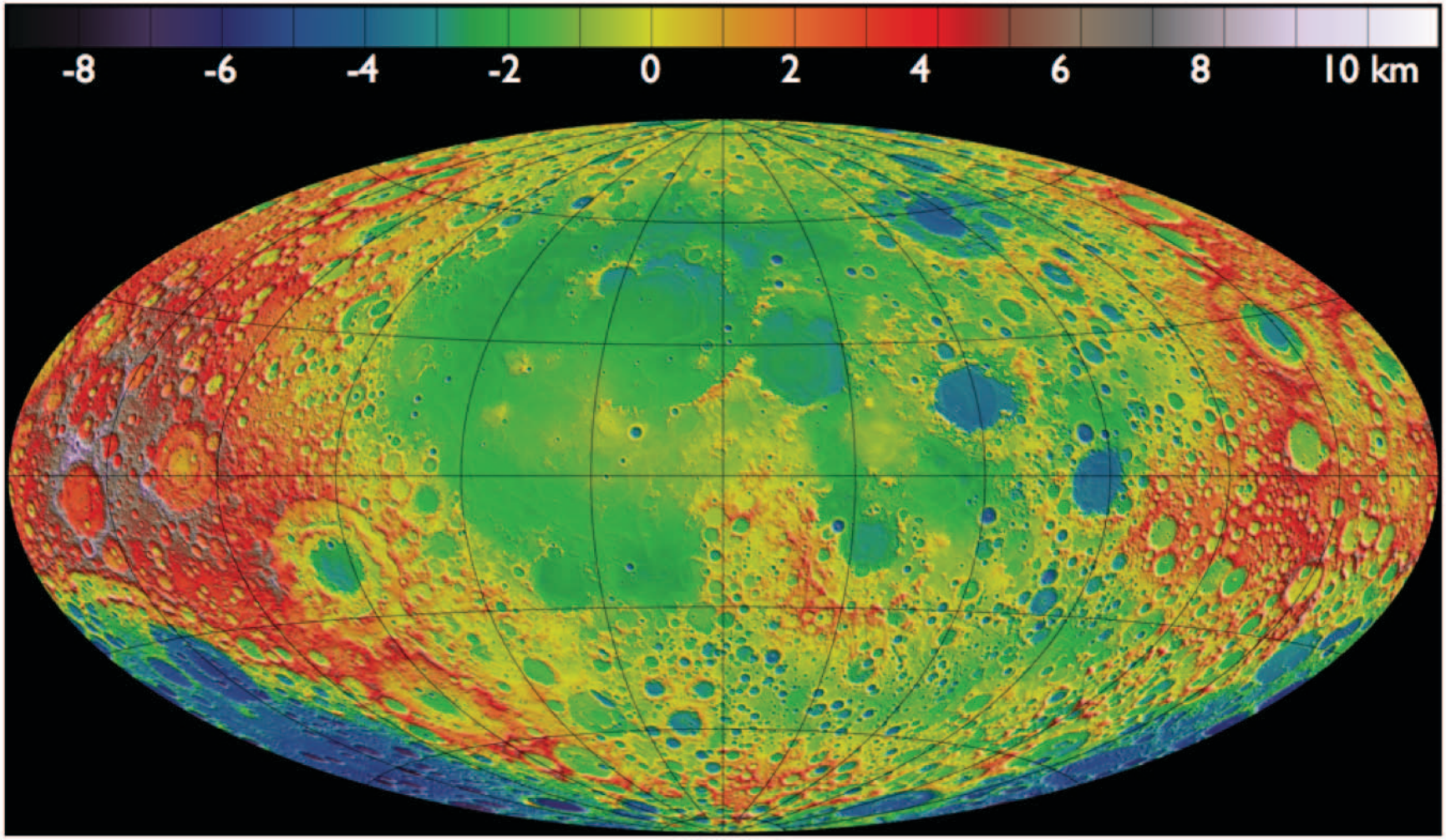

Equal-Area projection of lunar topography developed from1 billion LOLA measurements
Resolution: N/S ~20m; E/W ~0.1 deg (4.5km at equator, 200m at >85 Lat)

LOLA - Recent Results

REPORTS

Global Distribution of Large Lunar Craters: Implications for Resurfacing and Impactor Populations

James W. Head III,[1]* Caleb I. Fassett,[1] Seth J. Kadish,[1] David E. Smith,[2,3] Maria T. Zuber,[2,3] Gregory A. Neumann,[3] Erwan Mazarico[2,3]

By using high-resolution altimetric measurements of the Moon, we produced a catalog of all impact craters ≥20 kilometers in diameter on the lunar surface and analyzed their distribution and population characteristics. The most-densely cratered portion of the highlands reached a state of saturation equilibrium. Large impact events, such as Orientale Basin, locally modified the prebasin crater population to ~2 basin radii from the basin center. Basins such as Imbrium, Orientale, and Nectaris, which are important stratigraphic markers in lunar history, are temporally distinguishable on the basis of crater statistics. The characteristics of pre- and postmare crater populations support the hypothesis that there were two populations of impactors in early solar system history and that the transition occurred near the time of the Orientale Basin event.

The record of impact craters on the surface of the Moon, particularly the size-frequency distribution (SFD) and spatial density of craters, has long been used to infer information about the age of surfaces and the sequence of geological events (*1*). Unfortunately, uneven areal coverage, different image resolutions, and a wide range of solar illumination geometries from previous spacecraft mission data have precluded the compilation of a consistent global data set of the impact crater population. In the past year, the Lunar Orbiter Laser Altimeter (LOLA) (*2*), an instrument on board the Lunar Reconnaissance Orbiter (LRO) spacecraft, has acquired globally distributed, high-precision measurements of the topography of the Moon, which enable the creation of a 64-pixels-per-degree digital terrain model (DTM) and a shaded relief model of the surface (*3*). These data provide a view of the global distribution of impact craters without the observational uncertainties that arose from measurement of craters on images of heterogeneous illumination condition and uneven coverage and quality. We used this data set to produce a global compilation of the distribution of impact craters ≥20 km in diameter.

We mapped craters on the Moon by overlaying a 20-km reference grid on the topography and hillshade and by systematically measuring across the lunar surface (*4*) with the CraterTools extension to ArcMap (*5*) to make diameter measurements of craters. All craters with a measureable rim and central depression were cataloged, regardless of their degradation states or whether they were embayed or buried by younger surface

[1]Department of Geological Sciences, Brown University, Providence, RI 02912, USA. [2]Department of Earth, Atmospheric and Planetary Sciences, Massachusetts Institute of Technology, Cambridge, MA 02129, USA. [3]Solar System Exploration Division, NASA Goddard Space Flight Center, Greenbelt, MD 20771, USA.

*To whom correspondence should be addressed. E-mail: james_head@brown.edu

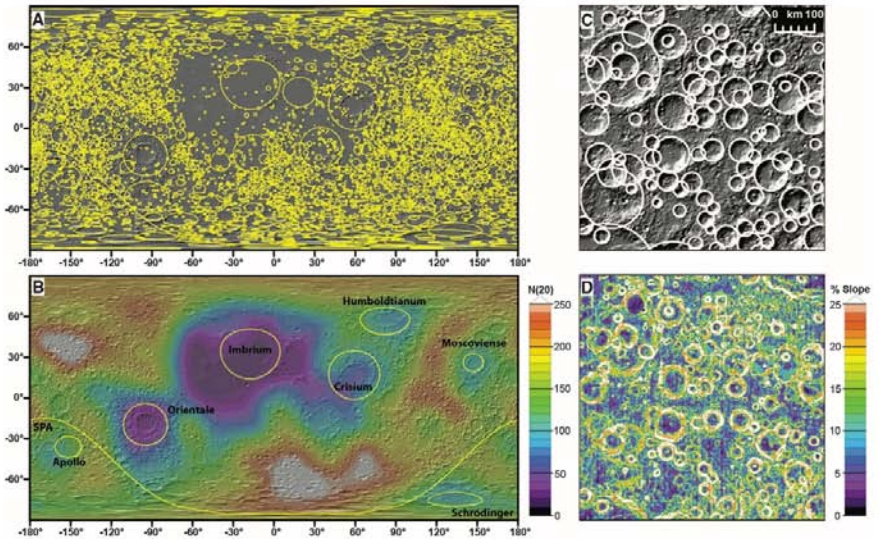

Fig. 1. **(A)** An outline of the craters mapped on the surface of the Moon from LOLA data superposed on a hillshade rendering of LOLA topography (*2*, *3*). **(B)** Crater densities on the Moon for craters ≥20 km in diameter, calculated in neighborhoods of radius 500 km. **(C** and **D)** Central far-side highlands (centered at −7°N, 130°E), one of the most densely cratered areas of the Moon. (C) Craters superposed on a LOLA hillshade base map. (D) Slope map of area in (C) showing the lack of smooth intercrater plains such as those found on Mercury (*11*).

Downloaded from www.sciencemag.org on September 20, 2010

MESSENGER Spacecraft & Science Payloads (JHU/APL, Mercury Orbit)

MESSENGER - MErcury Surface, Space ENvironment, GEochemestry, and Ranging
MLA – Mercury Laser Altimeter

- The first spacecraft to orbit Mercury
- Developed by JHU/APL, under NASA's Discovery Program
- Launched on 8/3/2004 from KSC
- Mercury orbit insertion: March 2011

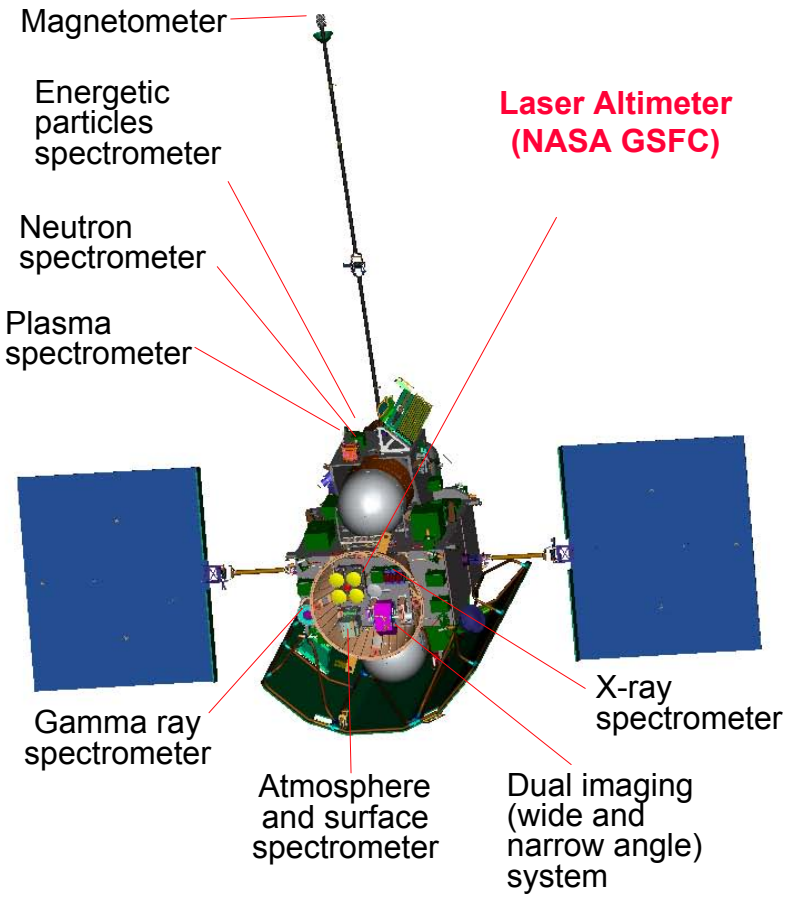

Messenger Laser Altimeter (MLA)

Laser pulse energy	***20 mJ***
Pulse rate	***8 Hz***
Pulse width	***6 ns FWHM***
Wavelength	***1064.30 ±0.05 nm***
Beam divergence	***80 µrad (TEM00)***
Receiver aperture	***11.5 cm diameter, X4***
Receiver field of view	***400 µrad***
Receiver optics transmission	***77%***
Receiver optical bandwidth	***0.7 nm FWHM***
Detector quantum efficiency	***>35%***
Receiver dark noise equivalent power (NEP)	***200 pW (over 33 MHz Noise BW)***
Receiver timing electronics	***6 channel event timers***
Receiver timing accuracy	***<1 ns***
Operation duty cycle and lifetime	***30 min/12 hour orbit, for 365 earth days***
Data rate while in operation	***2.4 kbits/s***
Weight	***7.4 kg***
Size	***30x30x30 cm***
Electrical power consumption while in operation	***23 W***

Electro-Optics & timing electronics assembly

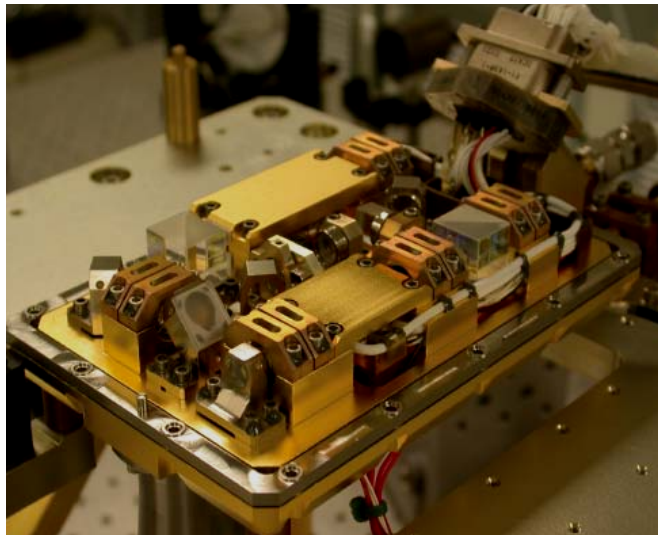

2 stage laser transmitter

MESSENGER Orbit Trajectory and Timeline

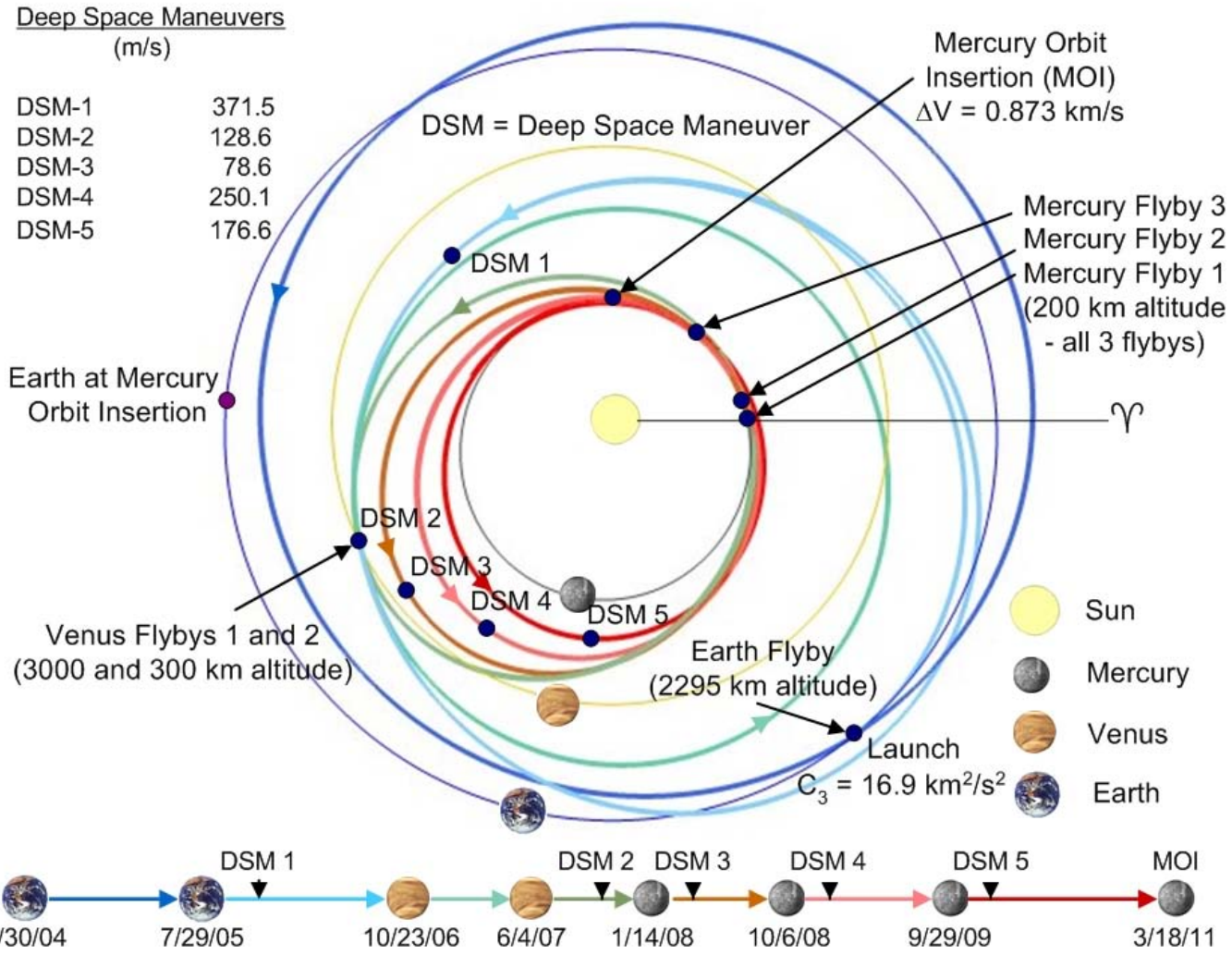

Planetary flybys:

- Earth, July 2005
  2-way laser ranging over 24 million km

-Venus-1, Oct. 2006
Instrument off due to solar conjunction

-Venus-2, June 2007
Attempted to range to Venus cloud decks

-Mercury-1, Jan. 2008
First successful laser ranging to Mercury

-Mercury-2, Oct. 2008
Second successful laser ranging to Mercury

-Mercury-3, Sept. 2009
To repeat laser ranging to Mercury

Mercury Flyby on Jan. 14, 2008

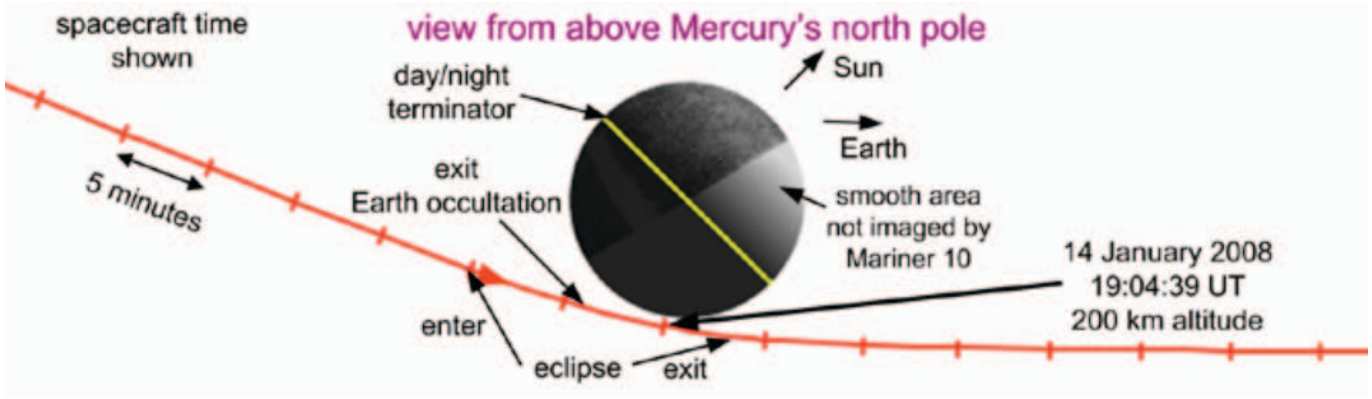

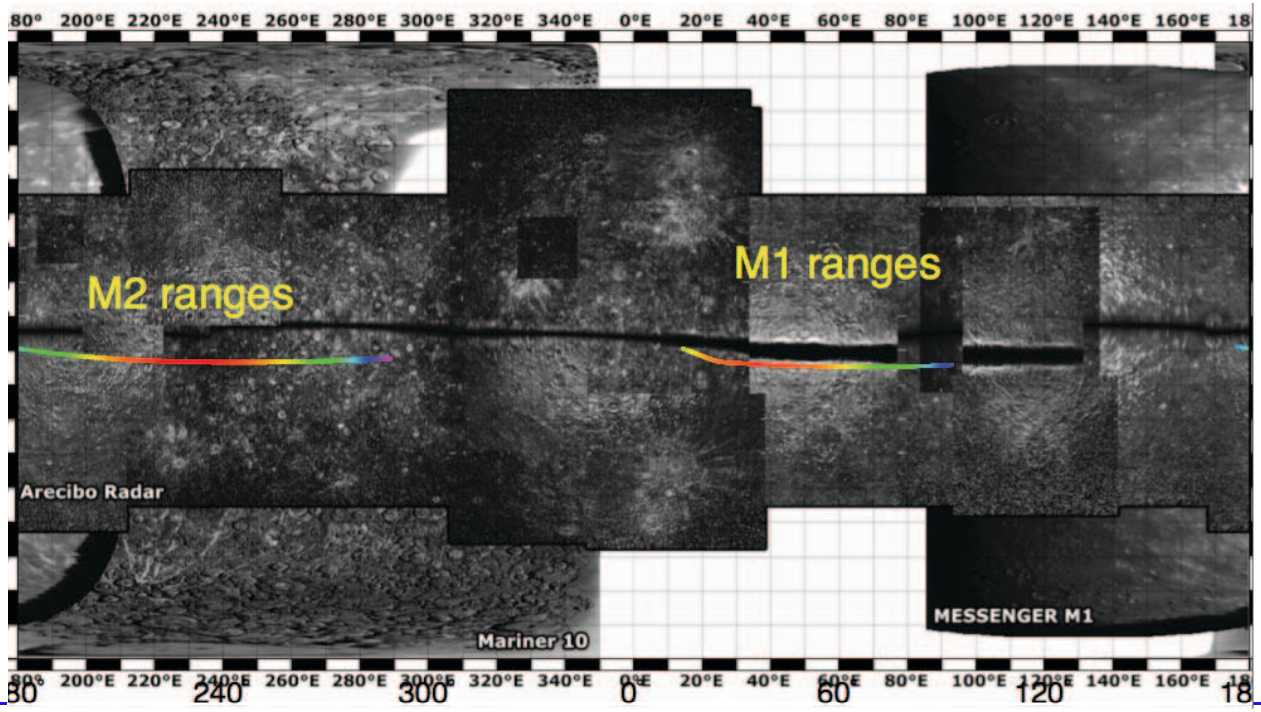

MLA was pointed to Mercury for about 10 minutes about the closest approach

2nd Mercury Flyby on Oct. 6, 2008

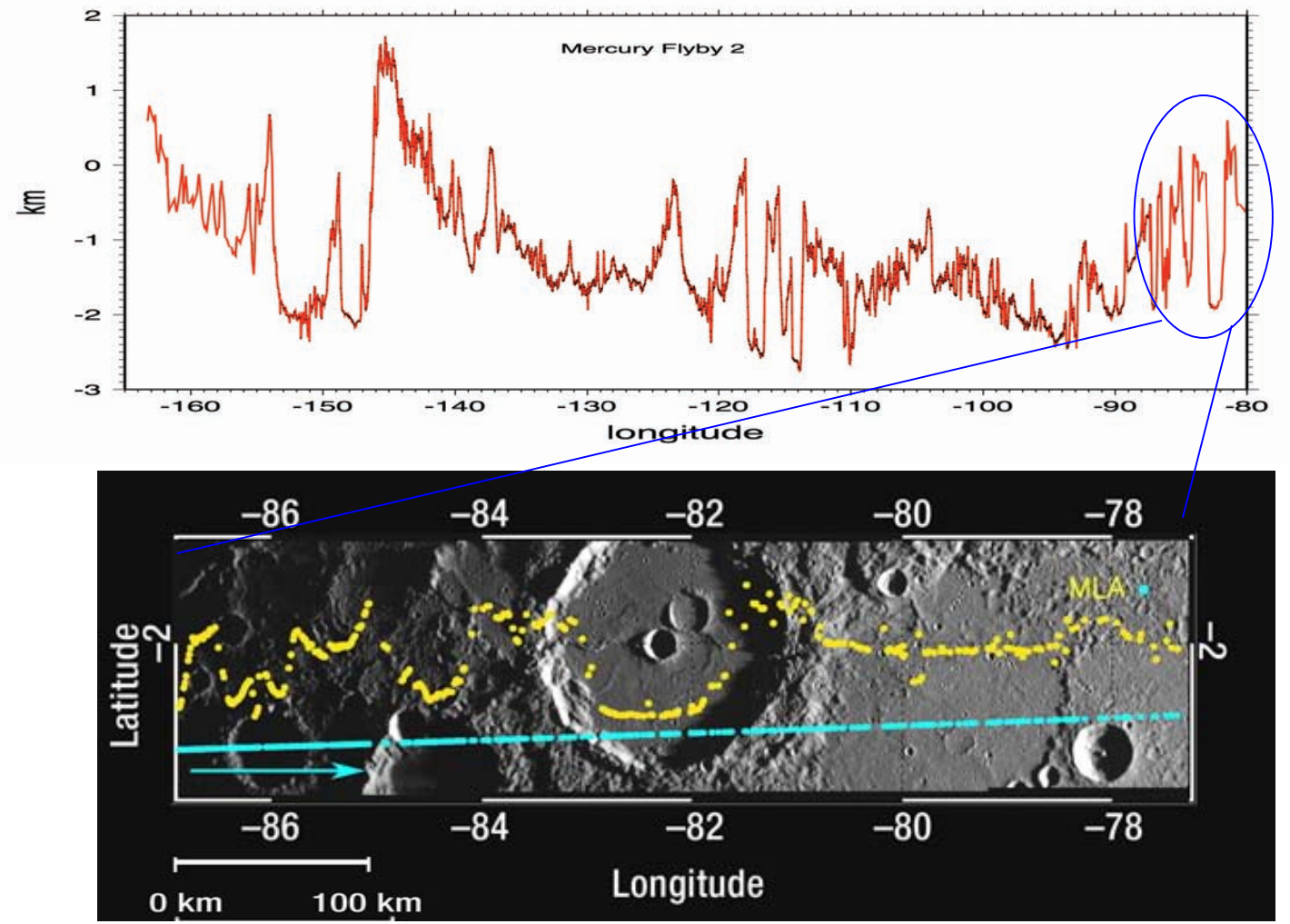

Mercury surface elevation profile measured by MLA during the second flyby.

Elevation profile measured by MLA superimposed on the MESSENGER Narrow Angle Camera (NAC) mosaic.

MLA- 1st two Measurements in Mercury Orbit (will be making 2 profiles/day)

GSFC

Measured Last week !

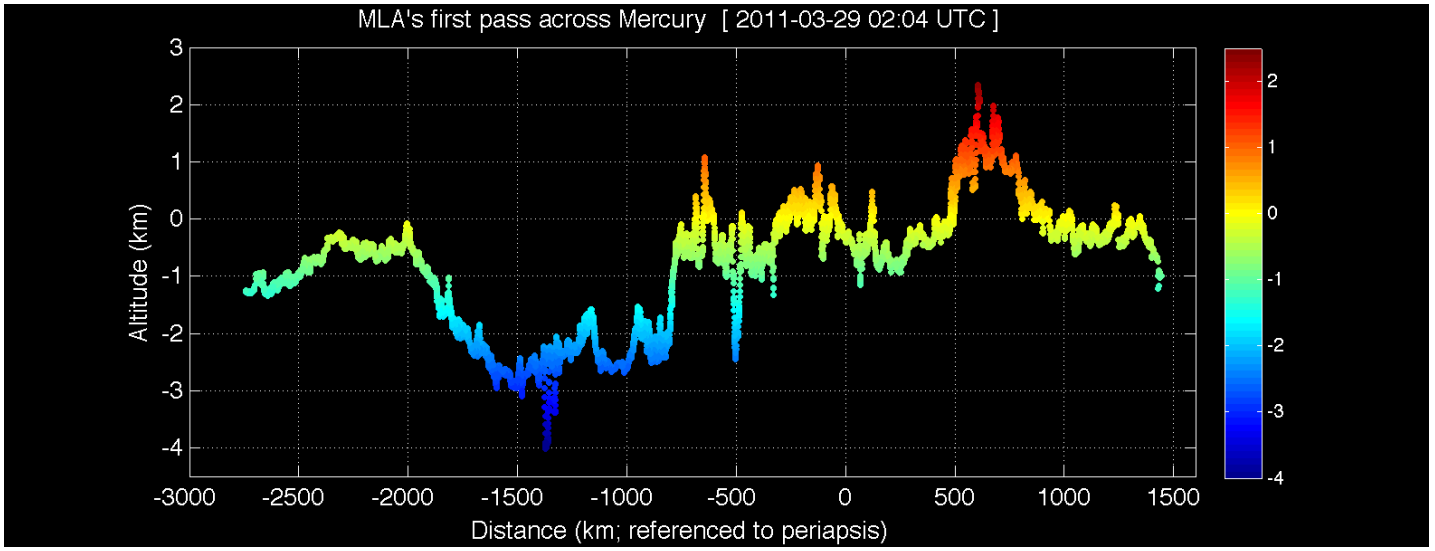

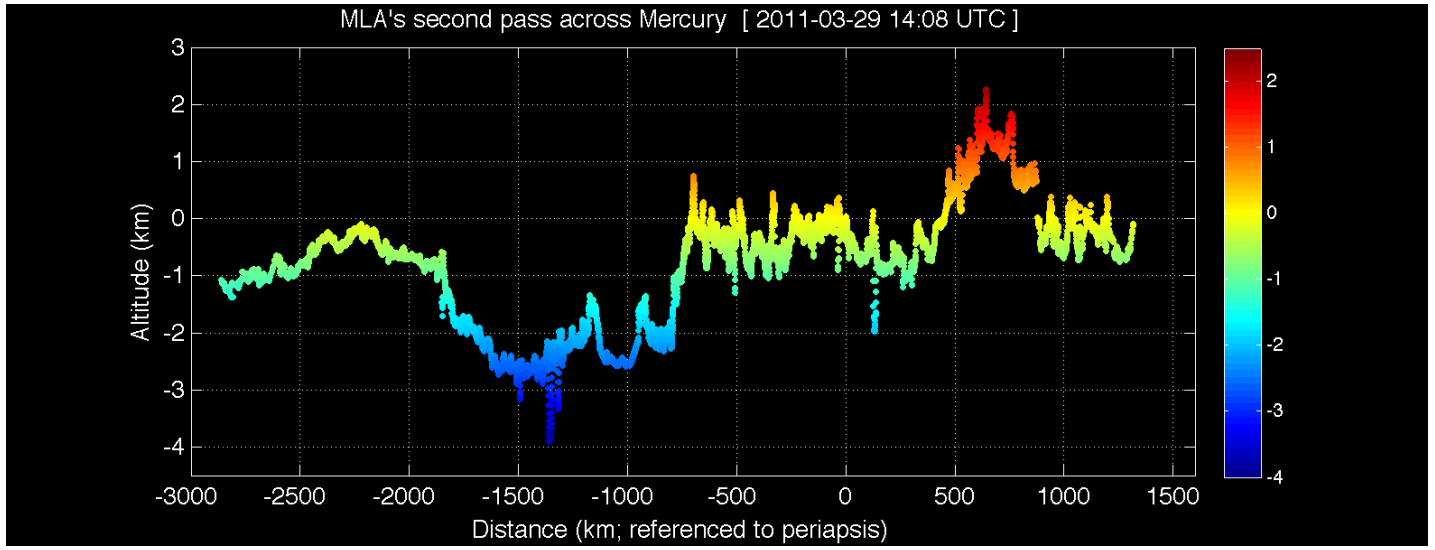

Space Lidar History to date
(LITE & SLA experiments not shown)

Apollo, - Moon
NASA (1971-1972)
Ruby laser,
5,000 shots

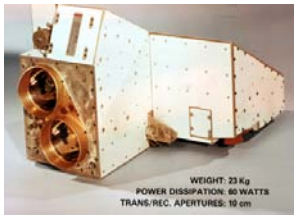

Clementine - Moon
LLNL/NRL (1994)
Nd:YAG laser,
~72,000 shots

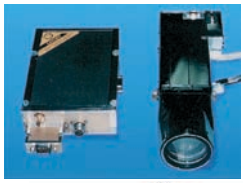

SELENE/LALT - Moon
Japan (2007-present)
Nd:YAG laser,

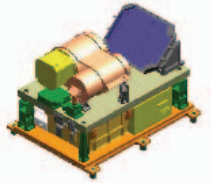

Chang'E - Moon
China (2007-present)
Nd:YAG laser

LRO/LOLA - Moon
NASA GSFC (2008-now)
Nd:YAG laser,
>1 Billion shots

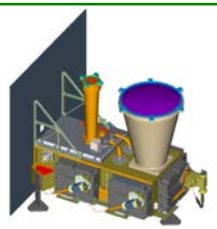

MGS/MOLA - Mars
NASA GSFC (1992, 1996 -2000)
Nd:YAG laser,
670 Million shots

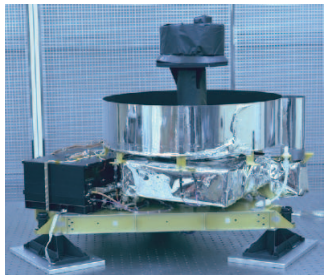

NEAR/NLR - Eros
JHU/APL (96-2001)
Nd:YAG laser,
11 Million shots

MESSENGER/MLA -
Mercury
NASA GSFC (2004-2012)
Nd:YAG laser,
12M shots (planned)

Green:
Operating Now

ICESat/GLAS - Earth
NASA GSFC (2003-2009)
3 Nd:YAG lasers
1.98 Billion shots

CALIPSO/CALIOP - Earth
NASA LaRC/ Ball Aerospace
(2006-present)
2 Nd:YAG lasers,
> 2B shots to date

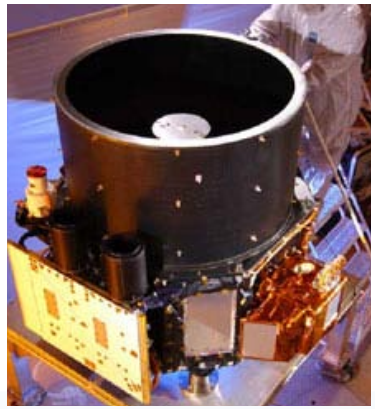

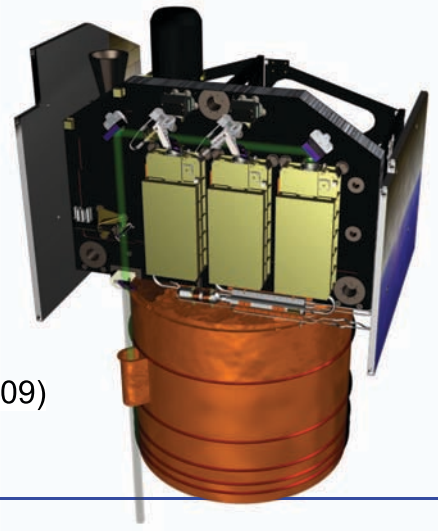

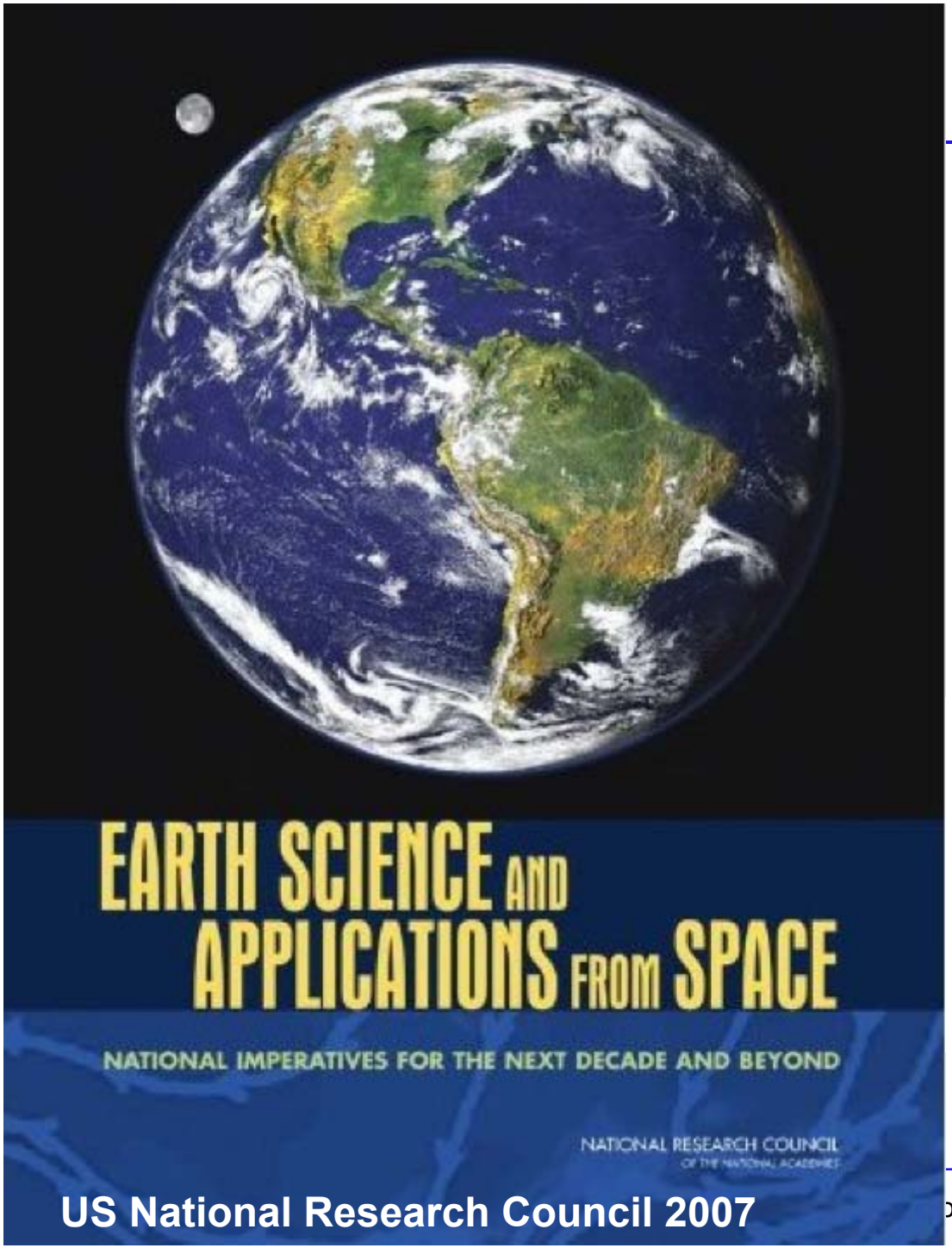

US National Research Council 2007

GSFC

NASA's Charter & Roadmap for New Earth Science Orbital Missions

Committee on Earth Science and Applications from Space:
A Community Assessment and Strategy for the Future

Space Studies Board
Division on Engineering and Physical Sciences

NATIONAL RESEARCH COUNCIL
OF THE NATIONAL ACADEMIES

6 new lidar-based missions

NASA Earth Science Topographic Lidar Mission Plans

GSFC

Earth Science Surface Lidar Mission Evolution

NRC Earth Science Decadal Survey Missions

ICESat
Single Beam Profiler

Ice Bridge (ice) & LVIS (trees)
Airborne Swath Mapping

ICESat-2
6-Beam Profiles 532 nm

DESDynI lidar InSAR +
5-Beam Profiles analog

LIST global topography 1000 beams 1 um Photon counting

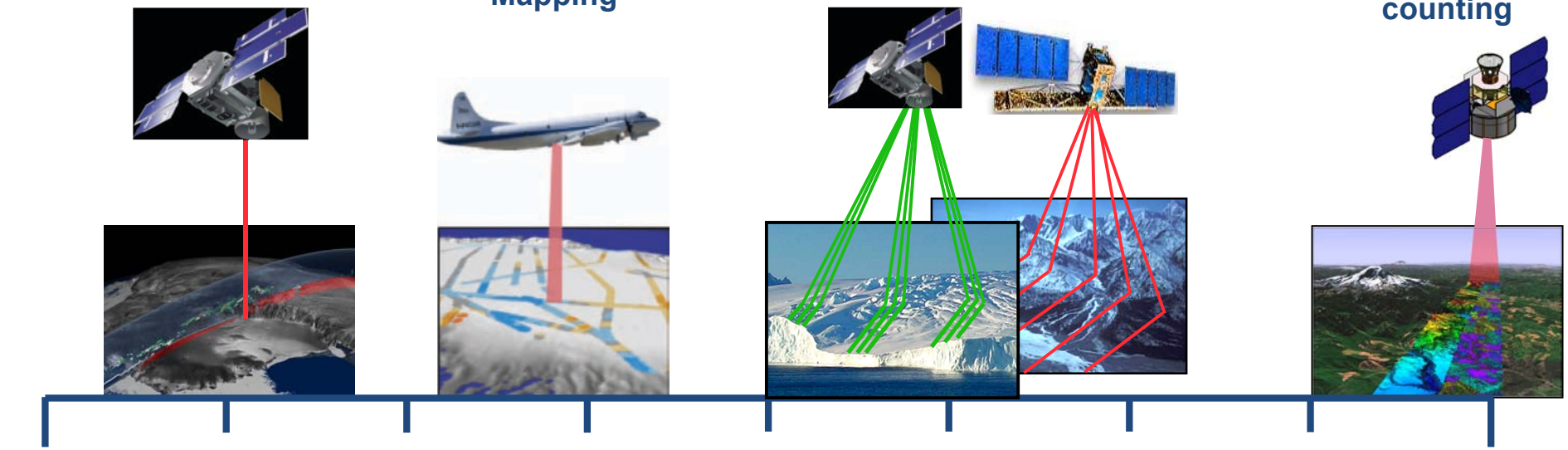

2005 2010 2015 2020 2025

ASCENDS
(Atm CO_2 concentrations)

Lidar Surface Topography Mission (LIST)

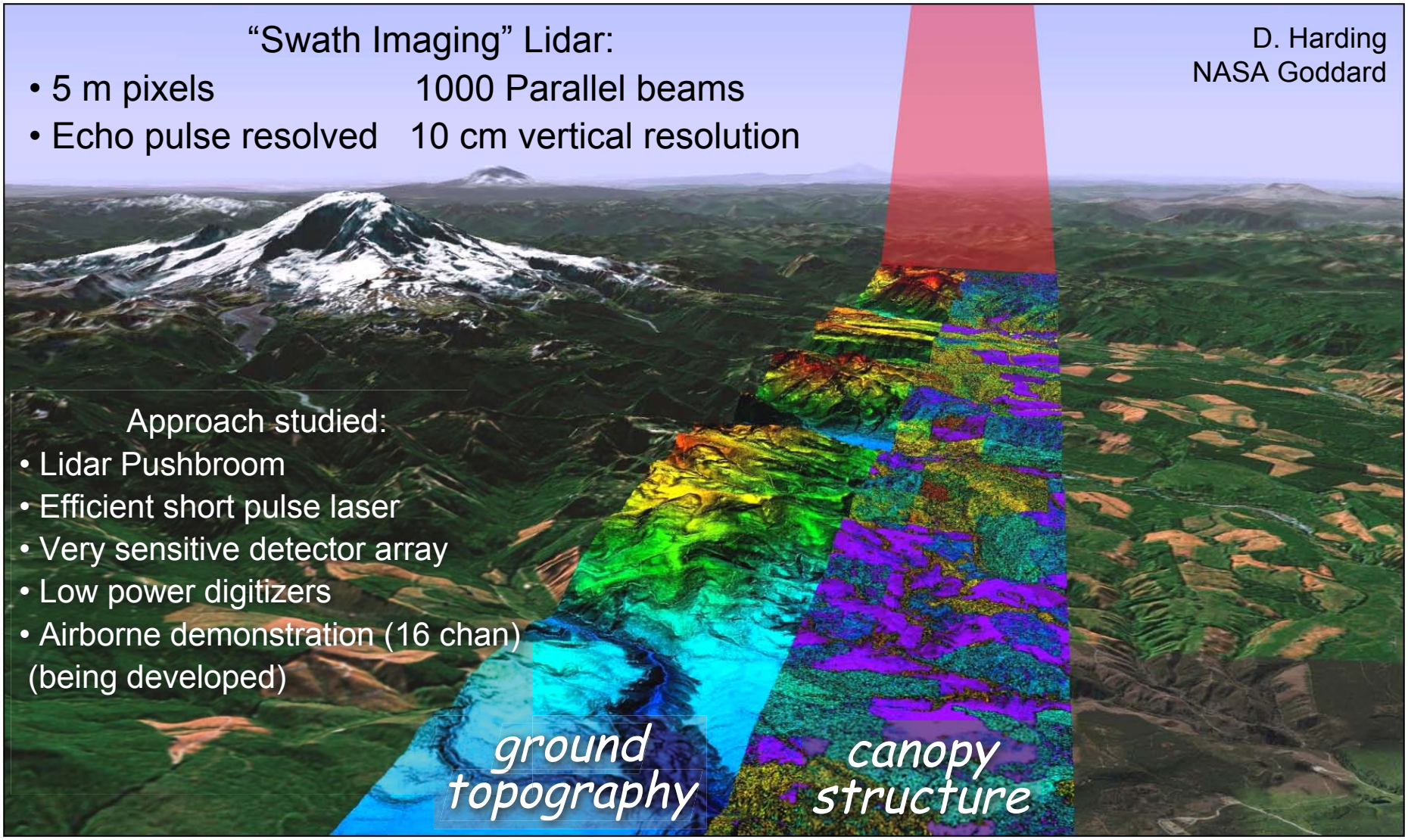

ASCENDS Mission & Laser Sounder Approach

Earth Orbit, Column CO2 concentration

GSFC

Simultaneous laser measurements:

1. CO2 lower tropospheric column
   One line near 1572 nm
2. O2 total column (surface pressure)
   Measure 2 lines near 765 nm
3. Altimetry & atmospheric backscatter profile from CO2 signal:

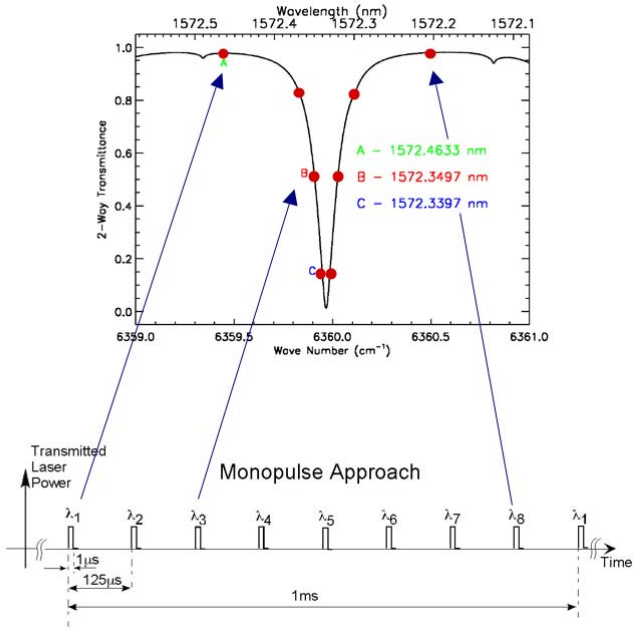

Measures:
- CO2 tropospheric column
- O2 tropospheric column
- Cloud backscattering profile

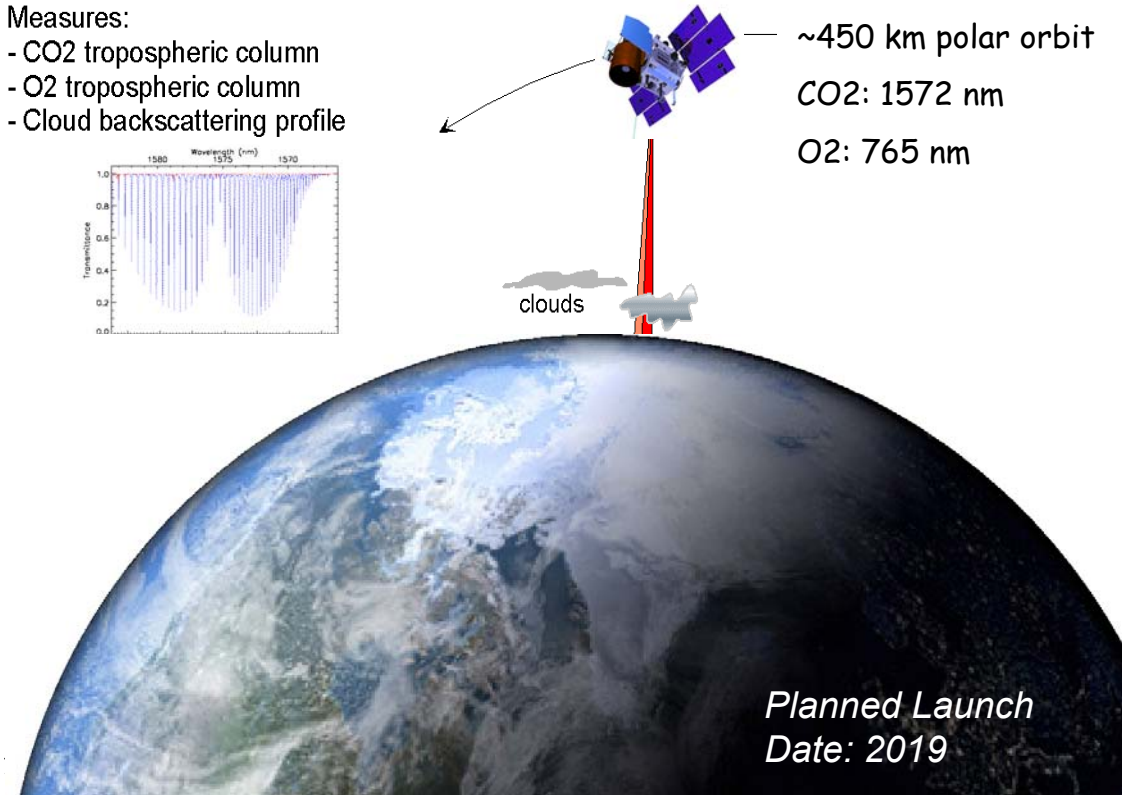

Measurements use:

- Single frequency tunable pulsed lasers
- 8-10 KHZ pulse rates
- Time gated Photon counting receiver
- High SNRs (~ 1000 in 10 sec)

Summary

Space Lidar Missions as of 2011

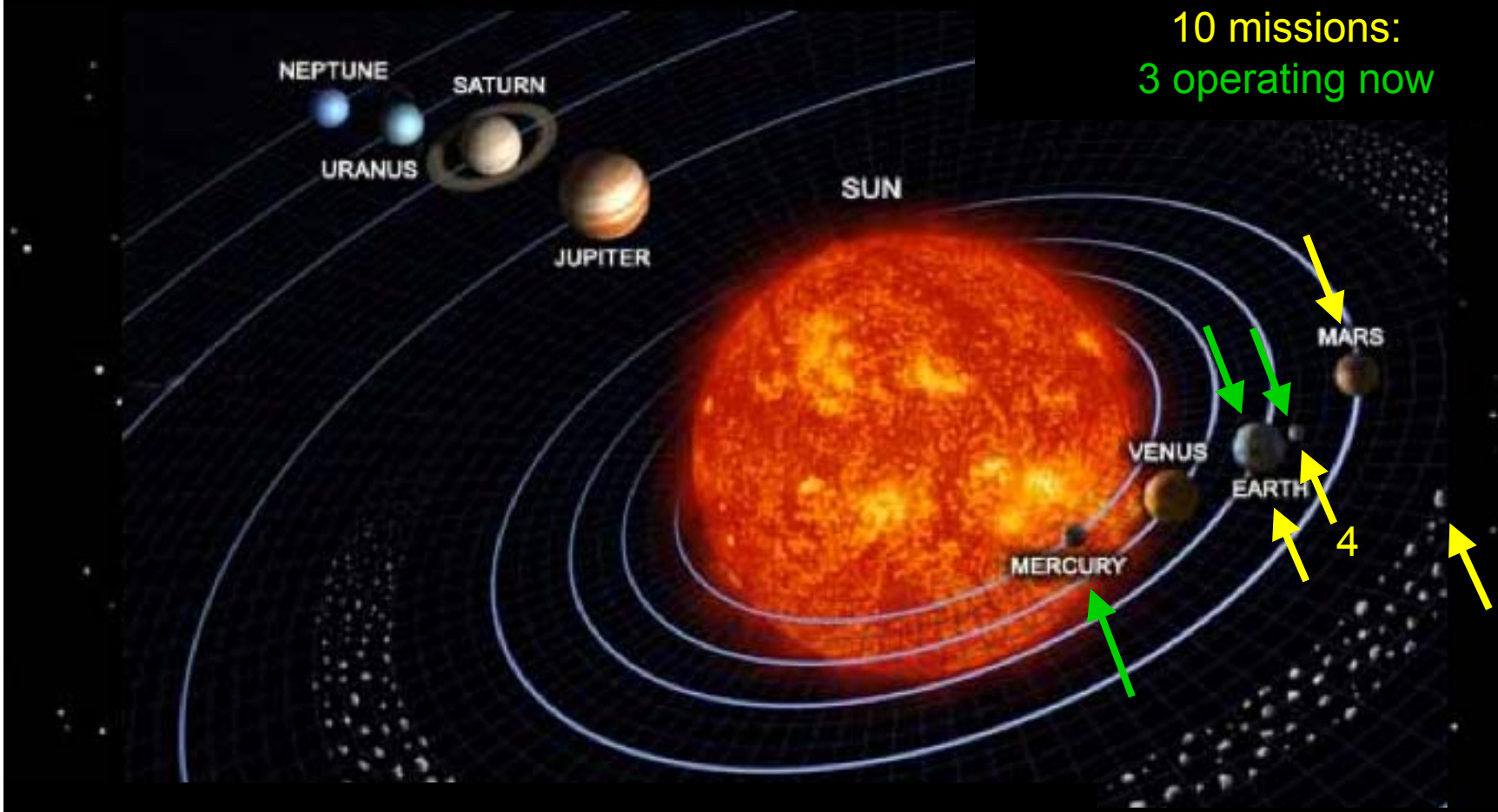

- Started 40 years ago
- Dramatic progress since the early 1990s
- Enabled new geophysical science & discoveries !